POLITECNICO DI TORINO

Dipartimento di Ingegneria Meccanica e Aerospaziale

Corso di Laurea Magistrale
in Ingegneria Meccanica

Tesi di Laurea Magistrale

Input-output and output-only modal analysis in the frequency domain: a comparison.

Tutor

Professor Alessandro Fasana

Candidate

Tahir Batuhan
Çebi

October 2021

“Bu tezi aileme, dostlarıma ve
tez yazma bahanesi ile ektiğim
tüm buluşmalara adıyorum”

“Dedicated to my family, friends
and all the hangouts I ditched
in order to write this thesis”

Abstract

Vibrations are an omnipresent phenomena and generally their presence is sought to be limited since they may cause malfunction, noise, wear, discomfort and destruction. In the last century, methods and technologies regarding to dynamic analysis developed significantly. Modal analysis constitutes an important section of these developments and all the numerous approaches it has can be grouped in two major categories: Experimental Modal Analysis (EMA) and Operational Modal Analysis. Because of the sheer number of modal analysis approaches and them being constantly developed it is hard to come by up-to-date comparisons of different methodologies under different circumstances. In this thesis, modal parameter extraction method Rational Fraction Polynomials method in z-domain (RFP-z) is elaborated and evaluated by creating a numerical model to run digital simulations. Other than a comparison of EMA and OMA accuracy, different parameters and their effect on accuracy are contrasted as well since the performance of the extraction may change depending on factors such as noise, excitation typology and frequency. Results indicate with numerical evidence that EMA is significantly more accurate and should be utilized if possible, especially for the analysis of critical parts. The effect of the presence of noise can be mitigated for well-separated modes by increasing the model order of RFP-z, but it affects the extraction accuracy of closely placed modes in a critical and unsalvageable way. Results also highlight that RFP-z method works much more accurately when the excitation applied to the structure is arbitrary in nature, rather than harmonic. In case of hybrid excitations, the "random" contribution should dominate the load behaviour. Another finding is that if of steep peaks are present in the frequency response function (FRF), it should be estimated with a higher number of spectral lines, otherwise the low resolution causes a loss of information ergo an inaccurate modal parameter extraction. The effect of RFP-z maximum model order is very situational and a general conclusion cannot be reached in that regard.

Acknowledgements

I would like to acknowledge the great support of my supervisor Prof. Alessandro Fasana for his attention throughout the preparation of this final project and the great opportunity he has given to me to develop myself in this interesting field of expertise.

I would also like to thank my dear friends in Torino who had been there in my times of needs and did not make me feel far away from home in another country. Without them years of study would not have been memorable.

Finally, I would like to thank my family for always motivating and supporting me in all my academic career. I got through all my personal and academic hardships thanks to their faith in me which I will always be grateful.

Table of Contents

1. Introduction **1**

Motivation 2

Outline of the Thesis 3

2. Outline of the RFP -Z Method **5**

2.1 Additional Considerations due to Z-Transform 8

2.2 Elimination of the Spurious Modes 10

2.3 Output of the RFP-z Algorithm 11

3. Experiment Simulation **12**

3.1 Simulating the Time Domain Data 12

3.1 Obtaining the FRF of Experiment Simulation 15

3.1.1 Experimental Modal Analysis (EMA) Approach 15

3.1.2 Operational Modal Analysis (OMA) Approach 17

4. Verification Procedure **18**

4.1 Computation of the FRFs 19

4.2 Computation of MAC 21

5. Evaluation of RFP-z in Output-Only Case **22**

5.1 Random Excitation 24

5.1.1 %3 Noise in Output 24

5.1.2 %10 Noise in Output 31

5.2 Harmonic Excitation 35

5.2.1 %3 Noise in Output 35

5.3 Harmonic Excitation with Random Contribution 44

5.3.1 Excitation Close to an Eigenfrequency 44

5.3.2 Excitation Far from an Eigenfrequency 47

5.3.2 High Excitation Frequency with High Output Noise 49

5.4 Inaccuracies Related to Spectral Line Density 51

5.5 Final Remarks 55

6. Evaluation of RFP-z in the Input-Output Case **57**
6.1 Random Excitation 58
6.1.1 %3 Noise in Output..... 58
6.1.2 %3 Noise in Input and Output 62
6.1.3 %10 Noise in Input and Output 65
6.2 Harmonic Excitation 70
6.3 Harmonic Excitation with Random Contribution..... 76
6.3.1 %3 Noise in Output..... 76
6.3.2 %3 Noise in Input and Output 85
6.3.3 %10 Noise in Input and Output 87
7. Conclusion **91**
7.1 FRF Estimation Method 91
7.2 Noise Level 93
7.3 Force Typology 95
7.4 Harmonic Excitation Frequency 97
7.5 Spectral Line Density 99
7.6 Utilizing Automatic Selection Algorithm 101

Appendix A – Calculation of Unknown Vectors **107**
Appendix B – Calculation of Normalized Residues **108**
Appendix C – Main MATLAB Verification Code **109**
Appendix D – Auxiliary MATLAB Functions **113**

Bibliographic References **114**

List of Abbreviations

SDOF	Single Degree of Freedom
MDOF	Multi Degree of Freedom
SISO	Single Input - Single Output
SIMO	Single Input - Multiple Output
MIMO	Multiple Input - Multiple Output
RFP-z	Rational Fraction Polynomials in z-Domain
FRF	Frequency Response Function
NFRF	Number of Frequency Response Functions
MAC	Modal Assurance Criterion
EMA	Experimental Modal Analysis
OMA	Operational Modal Analysis
ODS	Operational Deflection Shapes
LTI	Linear Time Invariant
CPSD	Cross Power Spectral Density
SLD	Spectral Line Density

List of Symbols

$h(t)$	Time domain response function
$H(i\Omega)$	Frequency response function
ω_r , f_r	Natural frequency of the r-th mode
ζ_r	Damping ratio of the r-th mode
s_r	Generic pole of the r-th mode
A_r	Residue of the r-th mode of a specific FRF
$\bar{A}_r$	Normalized residue of the r-th mode of a specific FRF
ϑ_r	r-th Mode shape
$[\alpha_{jk}(\omega)]$	Receptance
μ	Mean
σ	Standard Deviation
$[\mathbf{M}]$	Mass Matrix
$[\mathbf{K}]$	Stiffness Matrix
$[\mathbf{C}]$	Damping Matrix
$[\boldsymbol{\mathcal{A}}]$	Dynamic Matrix
$[\boldsymbol{\mathcal{B}}]$	Input Gain Matrix
$[\boldsymbol{\mathcal{C}}]$	Output Gain Matrix
$[\boldsymbol{\mathcal{D}}]$	Direct Influence Matrix
$[\mathbf{A}]$	Duncan Matrix A
$[\mathbf{B}]$	Duncan Matrix B
$[\ ]^{-1}$	Matrix Inverse
$[\ ]^{T}$	Matrix Transpose
$[\ ]^{H}$	Hermitian Transpose

1. Introduction

In many branches of industry and engineering there comes the need to study the vibrational response and the overall dynamic behaviour of certain components, because vibration can cause a plethora of undesired effects including fatigue, abrasion, noise, discomforts to human body such as nausea and even destruction of the machine or the structure. A very powerful approach to study the dynamic behaviour is 'modal analysis'[1][2] which has its roots in around 1940 and, thanks to the developments in dynamic testing, spectrum analyser availability and signal processing is developing further with new methods ever since. In modal analysis a components response to vibration is assumed as a combination of different modes, each with its own parameters such as natural frequency, mode shape and damping ratio (figure 1.1). Even though in real life every component has an infinite amount of modes, simulating the component as a lumped model and taking only a finite amount of significant modes gives very accurate results, given that the modal parameters of the component to be studied is known beforehand.

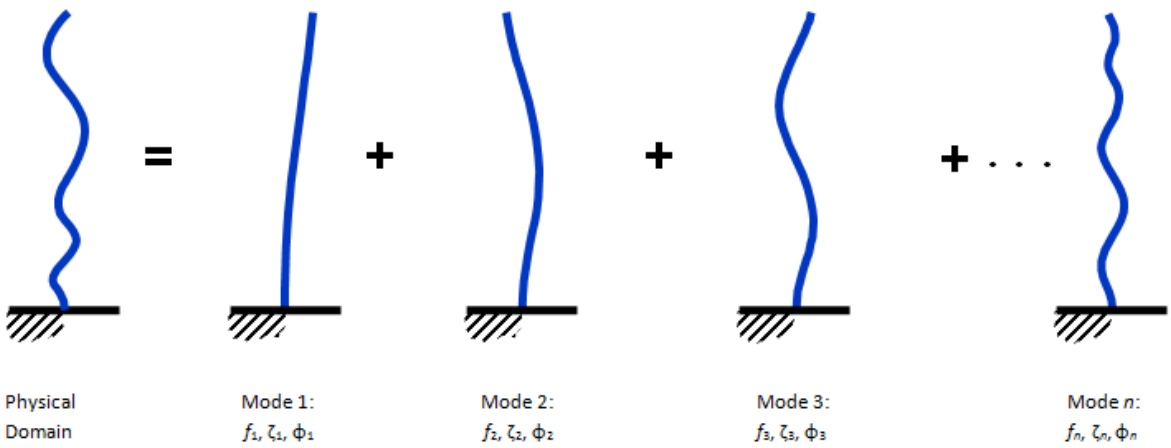

Figure 1.1: Modal Decomposition (Structural Vibration Solutions)

In practice, engineers usually do not know the modal parameters of the component which they work with. If the component has a simple shape and the material is known then it is possible to calculate the parameters without much trouble. Even the parameters of more complex parts can be identified with simple experimental ways such as the logarithmic decrement method, as long as the component can be modelled as a single degree of freedom (SDOF) system. But most of components an engineer will face in practice is a more complex assembly of different parts consisting of maybe more than one material. They can only be modelled as multiple degree of freedom systems (MDOF) where even small structural changes can alter the modal parameters significantly.

Therefore, one of the most fundamental areas in modal analysis is the 'Modal Parameter Extraction' or 'Modal Parameter Identification'. As the name suggests this area consists of methods to find out the modal parameters of a component via experimentation. This is an area with utmost engineering and academic interest, new methods of extraction are constantly

invented and developed, each having advantages and disadvantages on particular conditions. There are different ways to classify among these extraction methods. One of the most common property of an extraction method is in which domain is the data it uses. The excitation and response in an experiment or calculation can be either in time domain or frequency domain. Another crucial property is whether we have only the output data or if the output data (response) is supplemented with the input data (excitation). The output only case gives less accurate results but it still might be required in some cases since the excitation cannot always be precisely measured, for instance in the case of a bridge excited by the wind.

Also depending on the input and output data sets we can classify the extraction data further into single input single output (SISO), singe input multiple output (SIMO), multiple input single output (MISO) or multiple input multiple output (MIMO) methods. This is usually decided in the conduction of the experiment and the extraction method may vary greatly passing from one way to another. Also, another very basic method classification is whether if the system is SDOF or MDOF. A selection of common extraction methods can be seen in the figure 1.2 below.

1.1 Motivation

The extraction method which will be studied and elaborated in this thesis is the 'RFP-Z method' [3]. The details of this method will be elaborated in the following chapter, but for an introduction it models the system in the same manner as the 'Rational Fraction Polynomials (RFP) method'[4][5] which was developed in the 1980s. The main difference of RFP -Z method from the RFP method is that it transforms the experimental data from the time domain to the z domain, which introduces some numerical advantages.

The primary aim of this thesis is to verify the RFP -Z method on changing conditions such as different noise levels and different excitation types. Also, different numerical methods of creating a frequency response function (FRF) from the experimental data will be discussed, elaborated and compared using the modal assurance criterion (MAC). The reader of this thesis will gain an idea about the RFP -Z method in general and also about the accuracy of the extracted modal parameters via this method under different conditions.

Also, a proper code will be developed on MATLAB in order to automatically verify the RFP -Z method under different conditions.

1.2 Outline of the Thesis

In chapter 2 of this thesis there will be an overview of the RFP -Z method so that the reader can understand the principal idea of how to extract the modal parameters from experimental time-domain data with this method. In chapter 3 the system on which we will perform the numerical experiment will be described. The way to get the time-domain data on matlab will also be discussed in brief, and different ways to transform data into the frequency domain will be outlined. These data in frequency domain will be our starting point of the data extraction with RFP -Z method.

Chapter 4 will outline the methods used in the verification process. Procedure stated here will be important in comparing the results of different simulations under several circumstances.

In the remaining chapters the RFP -Z method will be verified under different conditions such as different noise levels, different excitation types (random, harmonic or hybrid excitations), and different ways to compute the initial FRF.

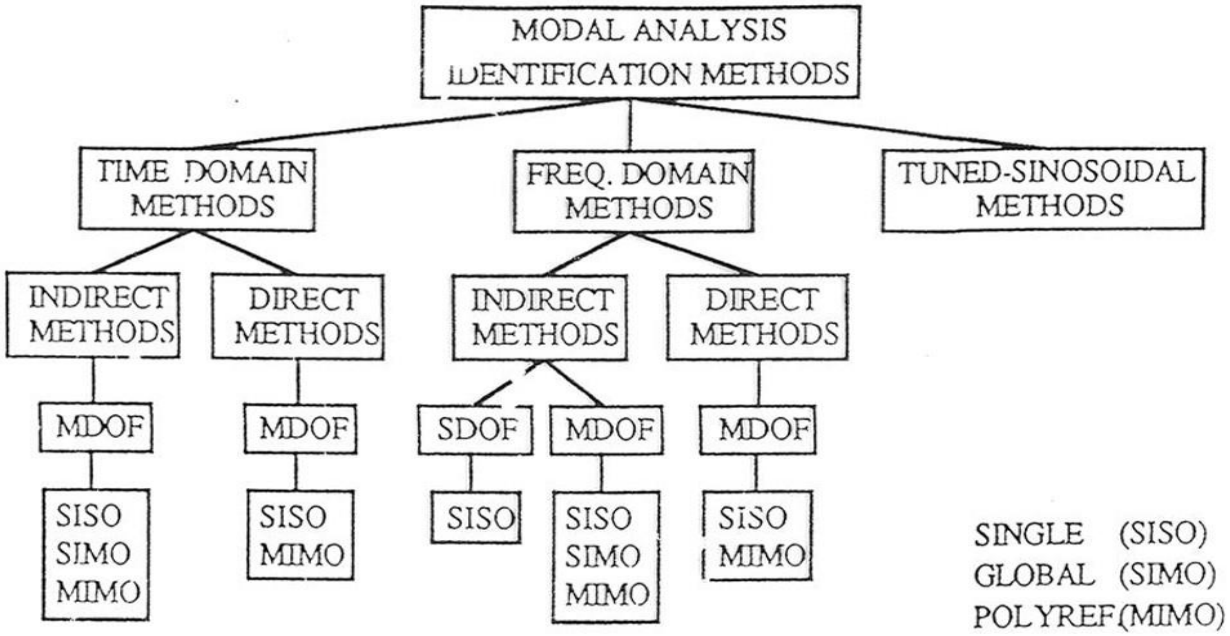

(a)

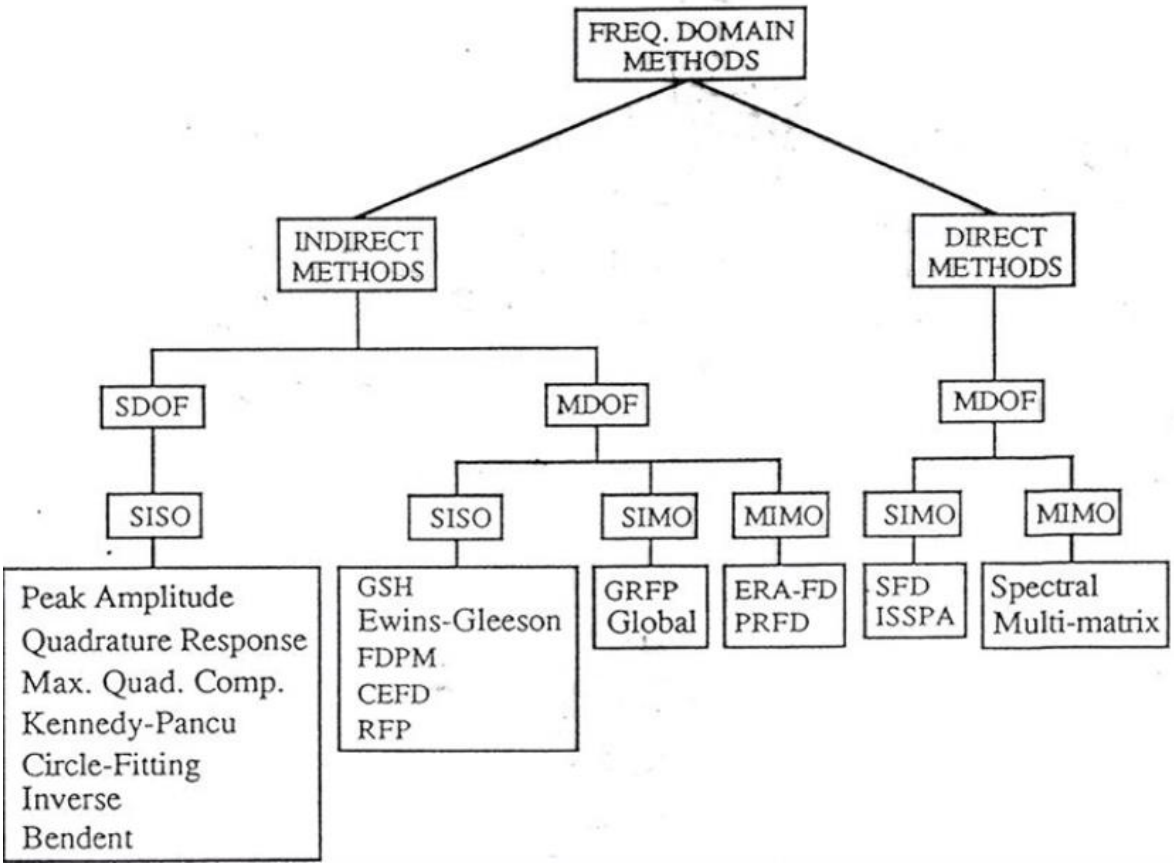

(b)

Figure 1.2: (a) Modal analysis identification method classification (b) Frequency domain identification method classification. (Maia, Nuno M.M. and Silva, Julio M.M. (1997), Theoretical and Experimental Modal Analysis, Chapter 4)

2. Outline of the RFP -Z Method

The main part of this thesis will be about the verification of the RFP -Z method under varying conditions, so it makes sense to describe the method itself beforehand. The reader is highly encouraged to read its original paper [3]. Although the exact paper version of the method is viable, in 10 years numerically more efficient modifications have been introduced on the method and they will be described in this chapter.

To use the RFP -Z method, firstly we must consider the experimental signal received to be from a linear time invariant (LTI) system. In this description "linear" underlines that the signal can be considered as a sum of different signals, according to the superposition principle. "Time invariant" implies that the considered structure does not change in time, i.e. its mass, stiffness and damping are constant.

The fact that our system is a LTI system ensures that it also has a transfer function, which we call the response function. If it is in the time domain, it generally has the symbol ***h(t)*** and is called the impulse response function. When Fourier transformed, we obtain the frequency response function, notated as ***H(ω),*** which is a complex function and has the information of the magnitude and the phase of response of a point to a harmonic excitation with frequency ω.

Another a priori assumption is the damping model of the system. Damping is an inherent characteristic of every real-life system, since it models the dissipation of energy which is negligible at best. Since there are lots of different energy dissipation mechanisms in the system it is hard to accurately describe them all with a simple model. There are two common damping models; the viscous model, which is linear and analogous to a real viscous dashpot, and the hysteretic or the structural model, which is analogous to a viscoelastic solid and is independent on the frequency. Viscous damping is the simplest model to use and since the system we will use in this thesis is a theoretic system generated in MATLAB we will proceed with the viscous damping model.

The impulse response function of a LTI system with *n* degrees of freedom (dof) can be expressed as:

$$h(t) = \sum_{r=1}^{2n} A_r e^{s_r t} \tag{2.1}$$

We can take the Fourier transform of the impulse function to obtain the frequency response function (FRF):

$$H(i\Omega) = \sum_{r=1}^{2n} \frac{A_r}{i\Omega - s_r} \tag{2.2}$$

In these equations r denotes the mode number. Any n dof system has n modes which often occur in complex conjugate pairs, hence there are a total of 2n contributions. Equation (2.2) is just a more compact form to write the same equation in another way as:

$$H(i\Omega) = \sum_{r=1}^{n} \left(\frac{A_r}{i\Omega - s_r} + \frac{A_r^*}{i\Omega - s_r^*} \right) \tag{2.3}$$

In this thesis I will stick with the notation of equation (2.2) since it is more compact.

The element denoted as s_r is the r-th generic pole of the r-th mode shape. It is linked to the r-th natural frequency ω_r and damping ratio ζ_r as:

$$s_r = -\zeta_r \omega_r + i\omega_r \sqrt{1 - \zeta^2} \tag{2.4}$$

Since we are working with digital data, we cannot think of the frequency spectrum as a continuous band but rather a set of discrete frequencies. Therefore, moving to the Z-domain Eq. (2.2) would take the form:

$$H_k = \sum_{r=1}^{2n} \bar{A}_r \frac{z_k}{z_k - z_r} \tag{2.5}$$

In this notation H_k denotes the spectral line of the k-th generic frequency. A crucial point to underline is that the sampling frequency information is completely lost when we do the z-transform. It is as if we take the sampling frequency as 1 Hz and hence the sampling period as 1 s. Later, the calculated residues will be adjusted with this regard. Z coefficients are tied to the z-transformation, and they are expressed as:

$$z_r = e^{s_r \Delta t} \tag{2.6}$$

$$z_k = e^{-i(k-1)\Delta\Omega\Delta t} = e^{-\frac{i\pi(k-1)}{N-1}} \tag{2.7}$$

where N denotes the total number of spectral lines, Δt is the sampling period and $\Delta\Omega$ is the discretization step width for the frequency. To avoid confusion, it must be noted that Eq. (2.7) is slightly modified with respect to the original paper. The reason is that having a negative exponent in that case will give a more stable stabilization chart in the end.[6]

Z-transform maps a function into a unit circle in the Argand-Gauss plane. In this case we are interested only in the upper semicircle because we can only analyse the spectrum up to half the sampling frequency according to Shannon-Nyquist sampling theorem.[7]

To proceed with the parameter estimation Eq. (2.5) is written in the form:

$$H_k = \frac{b_1 z_k + \cdots + b_{2n} z_k^{2n}}{a_0 + a_1 z_k + \cdots + a_{2n-1} z_k^{2n-1} + z_k^{2n}} \tag{2.8}$$

It is worth noting that all the parameters a_i and b_i are real.

We can then expand Eq. (2.8) to N spectral lines using matrix notation.

$$\begin{bmatrix} H_1 & H_1 z_1 & \cdots & H_1 z_1^{2n-1} \\ H_2 & H_2 z_2 & \cdots & H_2 z_2^{2n-1} \\ \vdots & \vdots & \ddots & \vdots \\ H_N & H_N z_N & \cdots & H_N z_N^{2n-1} \end{bmatrix} \begin{Bmatrix} a_0 \\ a_1 \\ \vdots \\ a_{2n-1} \end{Bmatrix} - \begin{bmatrix} z_1 & z_1^2 & \cdots & z_1^{2n} \\ z_2 & z_2^2 & \cdots & z_2^{2n} \\ \vdots & \vdots & \ddots & \vdots \\ z_N & z_N^2 & \cdots & z_N^{2n} \end{bmatrix} \begin{Bmatrix} b_1 \\ b_2 \\ \vdots \\ b_{2n} \end{Bmatrix} = - \begin{Bmatrix} H_1 z_1^{2n} \\ H_2 z_2^{2n} \\ \vdots \\ H_N z_N^{2n} \end{Bmatrix} \quad (2.9)$$

When there are $N \geq 4n$ spectral lines Eq. (2.9) can be solved via Least Squares Method.

Eq. (2.9) consider only a single FRF with N spectral lines. We can expand the equation even further to include a total of NFRF frequency response functions. It can straightforwardly be observed that the first matrix of Eq. (2.9) will be subject to change from FRF to FRF while the second matrix is same for all the FRFs. Also, the first vector of coefficients a_i will be same for all FRFs while coefficients b_i are tied to residues and hence they vary.

$$\begin{bmatrix} \boldsymbol{A}_1 \\ \vdots \\ \boldsymbol{A}_{NFRF} \end{bmatrix} \boldsymbol{a} + \begin{bmatrix} -\boldsymbol{B} & \cdots & 0 \\ \vdots & \ddots & \vdots \\ 0 & \cdots & -\boldsymbol{B} \end{bmatrix} \begin{Bmatrix} \boldsymbol{b}_1 \\ \vdots \\ \boldsymbol{b}_{NFRF} \end{Bmatrix} = \begin{Bmatrix} \boldsymbol{w}_1 \\ \vdots \\ \boldsymbol{w}_{NFRF} \end{Bmatrix} \quad (2.10)$$

Eq. (2.10) can theoretically be solved with a least squares approach, but the matrices involved might be ill-conditioned and thus they may bring numerical errors. Also, when the number of N spectral lines and NFRF FRFs is large taking the inverse matrices is going to be very time consuming, especially when the number of modes n is not known a priori, and an iterative procedure is required to build the stabilization chart. These drawbacks are circumvented by a very interesting approach using matrix/vector calculus and minimizing the error. The steps of the procedure are described in the original paper (See Appendix A), and the result reached is:

$$\boldsymbol{Ra} = \boldsymbol{r} \quad (2.11)$$

Where the matrix $\boldsymbol{R}$ and the vector $\boldsymbol{r}$ are easily calculated via matrices $\boldsymbol{B}$ and $\boldsymbol{A}_m$ of each NFRF, and they are well-conditioned. After finding vector $\boldsymbol{a}$, the solution of the system can be found by the equation:

$$a_0 + a_1 z + \cdots + a_{2n-1} z^{2n-1} + z^{2n} = 0 \quad (2.12)$$

Eq. (2.12) yields 2n zeros and they are utilized in order find the poles of the system:

$$s_r = \frac{\ln z_r}{\Delta t} \quad (2.13)$$

2.1 Additional Considerations due to Z-Transform

In this point it is worth reminding that the sampling period information was lost in Eq. (2.5), and it is considered as 1s. Therefore Eq. (2.13) can be written as:

$$s_r = \ln z_r = -\zeta_r \overline{\omega_r} + i\overline{\omega_r}\sqrt{1-\zeta_r^2} \tag{2.14}$$

We can exploit some mathematical properties to easily extract the following parameters:

$$|s_r| = \overline{\omega_r} = 2\pi \bar{f}_r \tag{2.15}$$

$$\zeta_r = \frac{Re(s_r)}{|s_r|} \tag{2.16}$$

In the above equations the frequency value $\bar{f}_r$ does not retain its absolute value but rather the relative value due to mapping. The mapping itself can be graphically visualized in figure (2.1).

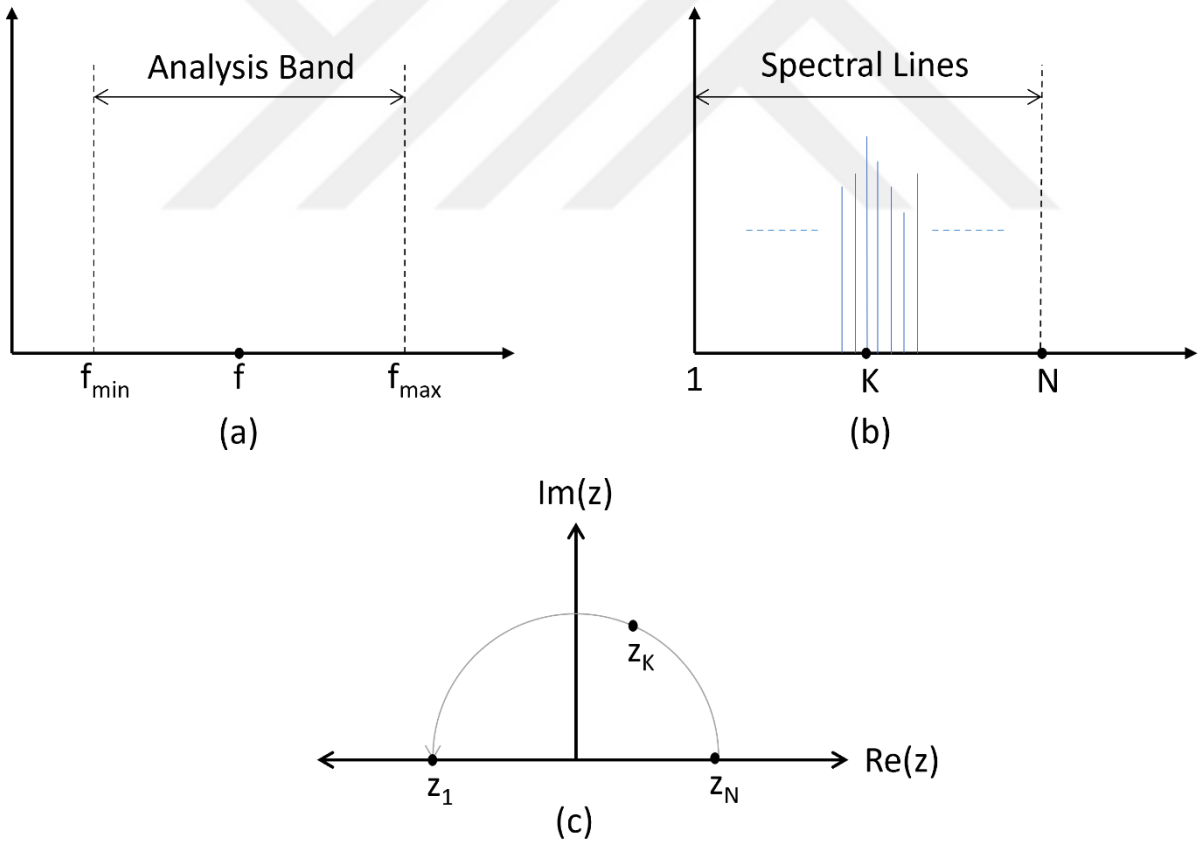

Figure 2.1: (a) Representation of the analysis band in the frequency domain. (b) How we numerically simulate the FRF of the analysis band using N discrete spectral lines (line 1 corresponds to fmin and N corresponds to fmax). (c) Z-transformation maps N discrete z values, as semicircle.

To avoid confusion, it is useful to make some remarks about figure (2.1.c). Z-transformation normally maps a given discrete set of values in the shape of a circle but due to the Shannon-Nyquist theorem we can only properly analyse up to half the sampling frequency and therefore the mapping is made so that the analysis band is fitted in a semicircle.

Another remark is that the same figure is drawn according to the Eq. (2.7) used as in the original paper. The version of the same equation in this thesis would generate a similar mapping, but with a semicircle in the 3rd and 4th quadrants.

Figure (2.2) and Eq. (2.17) summarizes the procedure to reach the correct absolute frequency value.

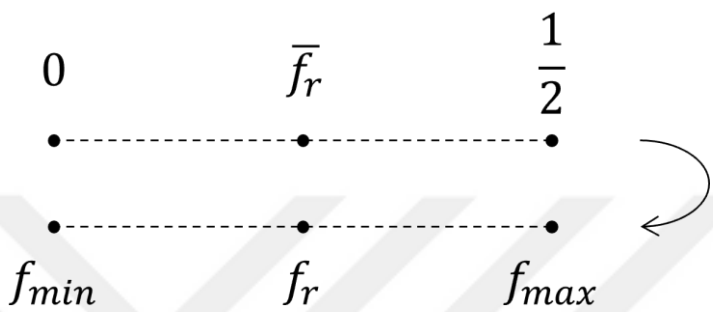

Figure 2.2: Reverting the frequency into the absolute term.

$$f_r = f_{min} + 2(f_{max} - f_{min}) * \overline{f_r} \tag{2.17}$$

Asides from the natural frequency and the damping ratio another crucial parameter to extract in order to build the FRF is the residues. For that purpose, we utilize the vectors b_m, which is calculated independently for every measured FRF. (See Appendix A for derivation of (2.18))

$$\boldsymbol{b}_m = (Re[\boldsymbol{B}^H \boldsymbol{B}])^{-1}(Re[\boldsymbol{B}^H \boldsymbol{A}_m]\boldsymbol{a} - Re[\boldsymbol{B}^H \boldsymbol{w}_m]) \tag{2.18}$$

With some smart manipulations, residues can hence be computed. (See Appendix B)

$$\overline{A_s} = \frac{b_1 z_s + \cdots + b_{2n} z_s^{2n}}{z_s * \prod_{r \neq s}(z_s - z_r)} \tag{2.19}$$

Since f_r and ζ_r are found using the vector $\boldsymbol{a}$ they will be shared across different FRFs while residues A_r are computed via vector $\boldsymbol{b}_m$ and they differ for each FRF, which represents a unique point of the structure.

2.2 Elimination of the Spurious Modes

Whichever modal parameter extraction method is put in use, there is always a common problem of deducing the number of modes. Modal analysis is based on modelling the important modes of a system which in theory has an infinite number of different modes. RFP -Z method analyses the experimental FRF via least squares approach and it identifies modal parameters by creating a best fitting. The model order n is not known a priori. While underestimating the model order yields inaccurate results, overestimating it might introduce unnecessary computational burden while potentially distorting the FRF outside the analysis band.

A simple and convenient procedure is to iteratively repeat the RFP-Z method assuming different model orders. It will be elaborated in the next chapter that the case study in this thesis is a system with 7 dof and the algorithm starts from assuming the model order to be $n = 5$ and iterates until it assumes model order to be $n = 30$. A complementary algorithm will be used to choose the model order with the best MAC matrix.

It can be expected that using a high model order will give more accurate results, due to numerical reasons, but it will also introduce spurious modes, which are modes that the structure does not physically possess but rather are the result of numerical approximations. An example of this issue can be seen in figure (2.3).

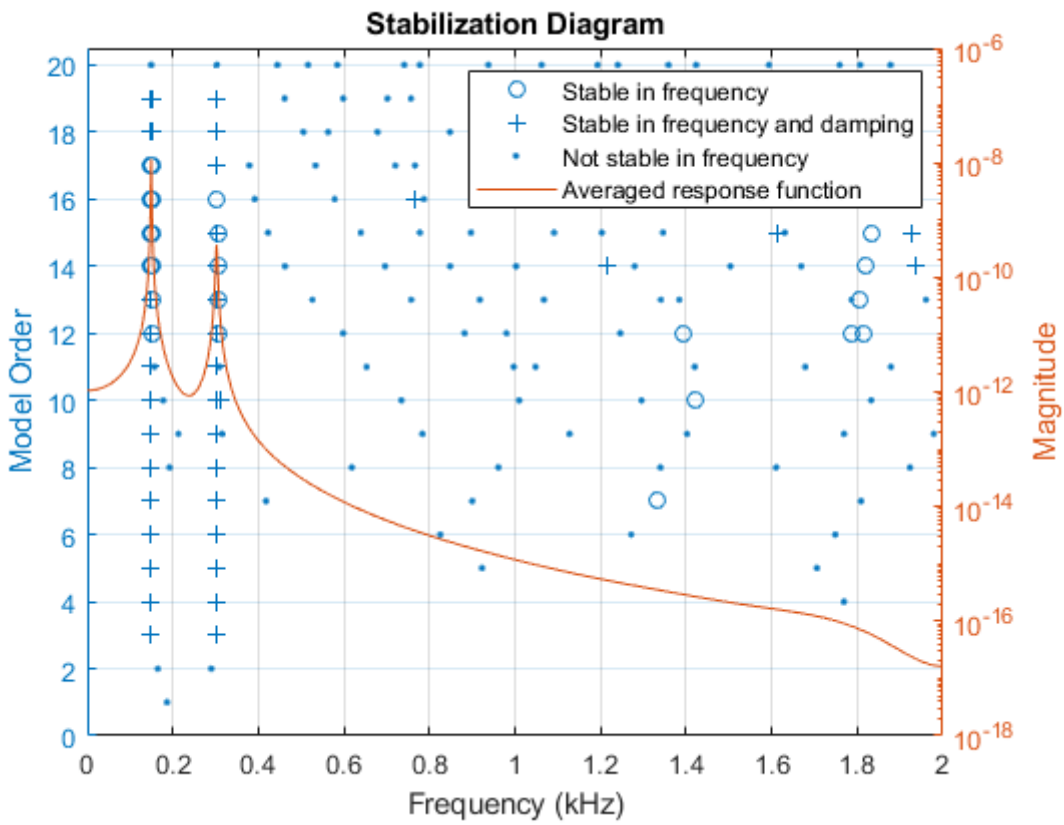

Figure 2.3: A stabilization chart. As the model order increases the stable frequencies get more accurate with occasional shifts, but also not stable spurious frequencies (or modes) are introduced. (With courtesy of MathWorks®).

In literature elimination of the spurious modes is a popular subject and there are some advanced methods available also for the RFP -Z algorithm.[8] However this topic is beyond the scope of this thesis so a much simpler but still effective method will be utilized.

RFP -Z algorithm will generate n complex conjugate pair of zeros, poles and thus modal parameters for each model order n. After each iteration it automatically checks the "quality" of modal parameters of every mode to whether delete them or not. First it checks if there is any mode with a negative or a too large damping ratio. Then it eliminates the modes with a natural frequency within %2 of the analysis band boundaries, since they are mathematically more prone to accumulate in that region . This simple filter lets less experienced technicians avoid inaccurate FRF models.

2.3 Output of the RFP -Z Algorithm

The MATLAB code of the RFP -Z method generates a matrix containing all the modal parameters as the output. The dimension of the matrix is $(2 + NFRF) * n \times n$. The column corresponds for the r-th mode. There are n vertical vectors of (2 + NFRF) elements in each column, one for each model order iteration, containing the information of the frequency, damping ratio and residue for each FRF of the j-th column mode. This matrix can be better explained visually:

$$\begin{bmatrix} f_1 & f_2 & & f_n \\ \zeta_1 & \zeta_2 & & \zeta_n \\ \bar{A}_{1,1} & \bar{A}_{1,2} & \cdots & \bar{A}_{1,n} \\ \vdots & \vdots & & \vdots \\ \bar{A}_{NFRF,1} & \bar{A}_{NFRF,2} & & \bar{A}_{NFRF,n} \\ \vdots & \vdots & \ddots & \vdots \\ f_1 & f_2 & & f_n \\ \zeta_1 & \zeta_2 & & \zeta_n \\ \bar{A}_{1,1} & \bar{A}_{1,2} & \cdots & \bar{A}_{1,n} \\ \vdots & \vdots & & \vdots \\ \bar{A}_{NFRF,1} & \bar{A}_{NFRF,2} & & \bar{A}_{NFRF,n} \end{bmatrix} \begin{matrix} \left.\begin{matrix} \\ \\ \\ \\ \\ \end{matrix}\right\} first\ model\ order \\ \\ \left.\begin{matrix} \\ \\ \\ \\ \\ \end{matrix}\right\} final\ model\ order \end{matrix} \tag{2.20}$$

It must be noted that natural frequencies, damping ratios and residues vary between each model order. Without the spurious mode elimination, this matrix would have been a quasi-triangular matrix (might not be triangular at all depending on the model order to begin the iterations). But thanks to the spurious mode filtering the latter columns are going to be mostly empty. This matrix does have all the necessary parameters to build a FRF.

One final remark should be made about the residues. As can be seen in Eq. (2.19) residues are calculated via z values which do not contain the frequency information. Thus, the residues in the output matrix, when used in order to build FRF, should be scaled as:

$$A_r = \overline{A_r} * 2 * (f_{max} - f_{min}) + f_{min} \tag{2.21}$$

3. Experiment Simulation

In this chapter the case study of this thesis will be presented. Instead of a laboratory experiment, a digital case study is numerically simulated on MATLAB. This approach welcomes the obvious advantage of easy reproducibility , especially when numerous iterations are required. Additionally, the verification of RFP -Z method will depend upon comparison of extracted parameters with real ones, and numerically generated "real" parameters will be stored in the system for quick and easy comparison.

3.1 Simulating the Time Domain Data

The system under study has 7 dof linked with 13 springs and 13 dampers. The topology of the elements can be seen in figure (3.1). In order to represent and simulate this system on MATLAB, it should be described with the mass, stiffness and damping matrices. Mass matrix is a simple diagonal matrix while the others are computed using local matrices.

$$\boldsymbol{M} = diag(\boldsymbol{m}) = diag(12, 15, 12, 15, 12, 15, 12)$$

$$\boldsymbol{K} = \begin{bmatrix} 1*10^6 & -2*10^5 & -3*10^5 & 0 & 0 & 0 & 0 \\ -2*10^5 & 9*10^5 & -4*10^5 & -1*10^5 & -2*10^5 & 0 & 0 \\ -3*10^5 & -4*10^5 & 1.5*10^6 & -3*10^5 & -5*10^5 & 0 & 0 \\ 0 & -1*10^5 & -3*10^5 & 9*10^5 & -2*10^5 & -3*10^5 & 0 \\ 0 & -2*10^5 & -5*10^5 & -2*10^5 & 1.4*10^6 & -4*10^5 & -1*10^5 \\ 0 & 0 & 0 & -3*10^5 & -4*10^5 & 9*10^5 & -2*10^5 \\ 0 & 0 & 0 & 0 & -1*10^5 & -2*10^5 & 3*10^5 \end{bmatrix}$$

$$\boldsymbol{C} = \begin{bmatrix} 75 & -15 & -10 & 0 & 0 & 0 & 0 \\ -15 & 120 & -50 & -50 & -5 & 0 & 0 \\ -10 & -50 & 120 & -10 & -50 & 0 & 0 \\ 0 & -50 & -10 & 85 & -15 & -10 & 0 \\ 0 & -5 & -50 & -15 & 170 & -50 & -50 \\ 0 & 0 & 0 & -10 & -50 & 65 & -5 \\ 0 & 0 & 0 & 0 & -50 & -5 & 55 \end{bmatrix} \tag{3.1}$$

The system is excited at the 3rd degree of freedom. The properties of the input force will change several times to verify the accuracy of the RFP -Z method under different conditions. Force typologies will be elaborated later, but in general it is a vector of normally distributed random numbers.

To compute the output of the system under given force the state space vectors are utilized.

$$\boldsymbol{z} = \begin{Bmatrix} \boldsymbol{x} \\ \dot{\boldsymbol{x}} \end{Bmatrix} \qquad \dot{\boldsymbol{z}} = \begin{Bmatrix} \dot{\boldsymbol{x}} \\ \ddot{\boldsymbol{x}} \end{Bmatrix} \tag{3.2}$$

With the use of state space variables, we can get an idea of both the current situation and the past history of the system. We can calculate and graph the response to the excitation by solving the following equations with system *quadruple*[9] :

$$\begin{cases} \dot{\boldsymbol{z}}(t) = \mathcal{A}\dot{\boldsymbol{z}}(t) + \mathcal{B}\boldsymbol{u}(t) \\ \boldsymbol{y}(t) = \mathcal{C}\boldsymbol{z}(t) + \mathcal{D}\boldsymbol{u}(t) \end{cases} \tag{3.3}$$

Where:

$$\boldsymbol{\mathcal{A}} = \begin{bmatrix} -\mathbf{M}^{-1}\mathbf{C} & -\mathbf{M}^{-1}\mathbf{K} \\ \mathbf{I} & \mathbf{0} \end{bmatrix} = Dynamic\ Matrix$$

$\boldsymbol{\mathcal{B}} =$ Input Gain Matrix

$\boldsymbol{\mathcal{C}} =$ Output Gain Matrix

$\boldsymbol{\mathcal{D}} =$ Direct Influence Matrix

$\boldsymbol{u}(t) = vector\ of\ inputs$

$\boldsymbol{y}(t) = vector\ of\ outputs$

The preceding set of differential equation are run on MATLAB and fourth order Runge-Kutta integration technique is implemented (ODE4). The force is simulated for 200 seconds. The input and output vectors have 102401 discrete values of force/response for each dof so a sampling period of $dt = \frac{1}{512}$ is mimicked.

After obtaining a set of input and output vectors to build a analytical FRF, a random noise is added to input and output vectors to simulate real-life experimental conditions. The noise is also generated as a normally distributed random vector and its amplitude is tied to the standard deviation of input and output values. Also, a custom parameter is set to increase and decrease the noise conditions at will, to test RFP -Z method's accuracy under varying signal qualities.

It is also required to compute and store the modes and poles of the system. In the upcoming chapters those data will be used to build the MAC matrix and compare the FRF based on real analytical values and the FRF built with extracted parameters. In order to do so it is convenient to introduce the Duncan Method matrices, since we cannot assume that the damping is proportional, and solve the eigenproblem.[10]

$$\begin{bmatrix} \mathbf{C} & \mathbf{M} \\ \mathbf{M} & \mathbf{0} \end{bmatrix} \begin{Bmatrix} \dot{\mathbf{x}} \\ \ddot{\mathbf{x}} \end{Bmatrix} + \begin{bmatrix} \mathbf{K} & \mathbf{0} \\ \mathbf{0} & -\mathbf{M} \end{bmatrix} \begin{Bmatrix} \mathbf{x} \\ \dot{\mathbf{x}} \end{Bmatrix} = \begin{Bmatrix} \mathbf{0} \\ \mathbf{0} \end{Bmatrix} \tag{3.4}$$

For rendering the future referencing of this formula simple, the compact form is written below.

$$[\boldsymbol{A}] \begin{Bmatrix} \dot{\mathbf{x}} \\ \ddot{\mathbf{x}} \end{Bmatrix} + [\boldsymbol{B}] \begin{Bmatrix} \mathbf{x} \\ \dot{\mathbf{x}} \end{Bmatrix} = \begin{Bmatrix} \mathbf{0} \\ \mathbf{0} \end{Bmatrix} \tag{3.5}$$

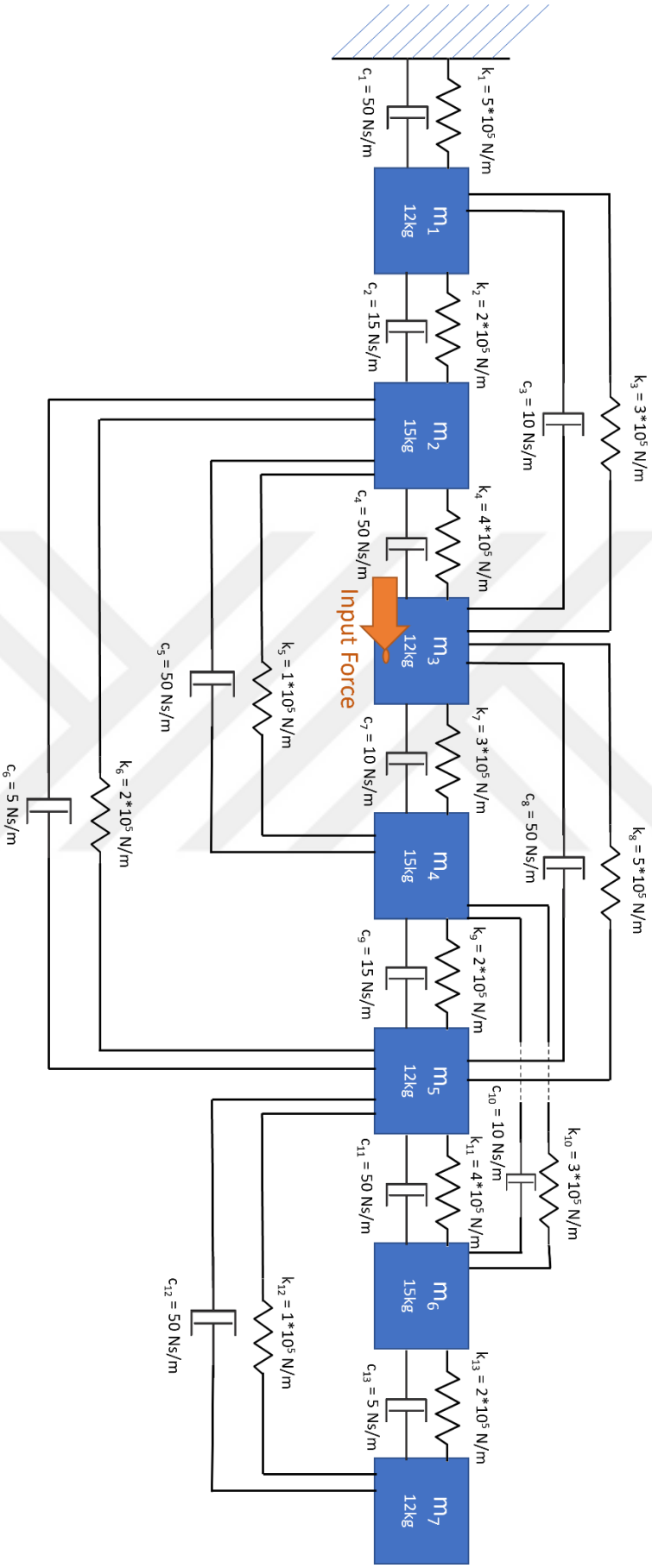

Figure 3.1: The 7dof system on which the simulations are made.

3.2 Obtaining the FRF of Experiment Simulation

To extract modal parameters from the system we need an established FRF. Simulated time domain data have to be Fourier Transformed into the frequency domain. In order to test the accuracy of RFP-Z method in different scenarios two different FRF generation approaches will be used; EMA (Experimental Modal Analysis) and OMA (Operational Modal Analysis).

The former uses the data of both the input (excitation) and the output (response). It is straightforward to think that it is more advantageous due to its higher number of information, but it should be noted that an engineer will encounter many situations where it is impossible to create a testing rig and provide laboratory conditions for some structures, especially for the big and heavy ones. Sometimes measuring the input will be outright impossible and sometimes due to high noise levels it will be unsatisfying. Also, sensors and shakers used to measure the input/outputs may alter the structure and thus the FRF result. Since there may be a limited number of sensors and/or data acquisition channels usually repeating test by changing the sensor positions are required and this may produce some inconsistent data.

OMA in the other hand is easier in the sense that it does not require the strict lab identification to perform the tests. It may also be referred as ODS (Operating Deflection Shapes). Often it is the only feasible option, but since it lacks the crucial input data it lacks the accuracy of EMA. There are many papers on how to optimize parameter extraction using OMA methods.[11][12]

The description of EMA and OMA method used in our case study is not in the scope of this thesis, but a basic elaboration of each method will be supplied to the reader in order to give context to the later chapters.

3.2.1 Experimental Modal Analysis (EMA) Approach

Instead of proceeding to compute FRF, it is more suitable to take use of a Welch Periodogram.[13] In essence, instead of Fourier transforming the whole time-domain signal at once we divide it into small sections with overlap (as seen in Fig. 3.2), Fourier transform the small portions one by one and take the average of spectral results. Although this might reduce the spectral precision the non-systematic noise is smoothed over.

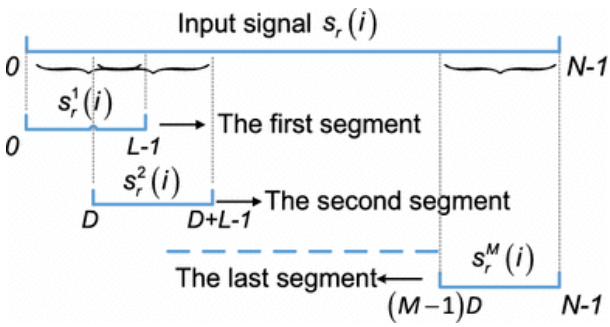

Figure 3.2: Overlapping intervals of a Welch Periodogram.

The percentage of overlap in our case is 67%. In the calculation of power spectral densities Hann window function is applied in each time window in order to reduce leakage caused by the non-periodicity of the original time data. The peak sidelobe relative to main-lobe amplitude of the Hann window is -31 dB. (Fig 3.3).

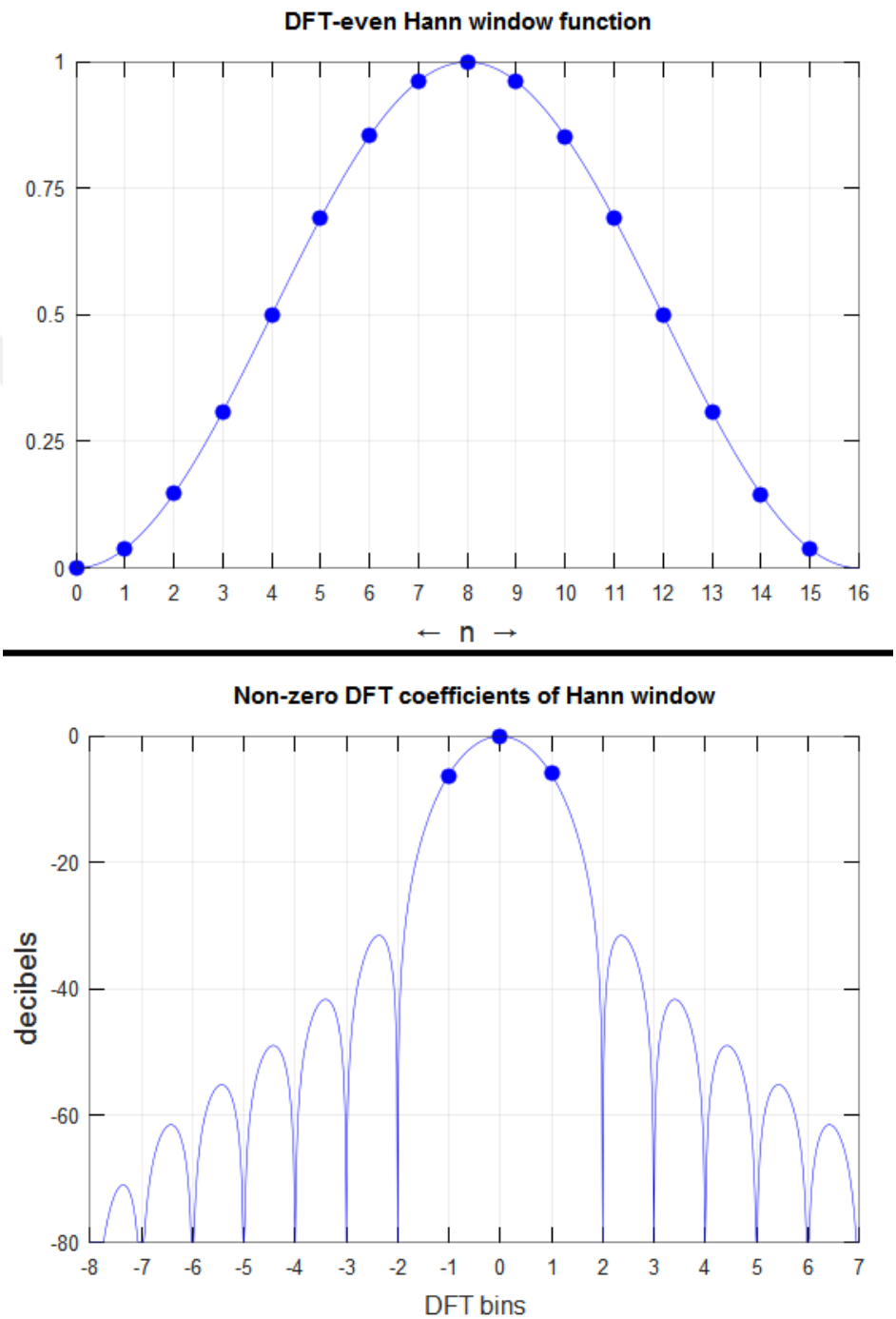

Figure 3.3: Hann Window. (With courtesy of Wikipedia).

Once the Power Spectral Densities (PSD) of both the input and output data are calculated different estimators can be used to build the FRF. The estimator applied in this case study is the maximum likelihood (ML) estimator.[14] The reason we have selected this estimator is the fact that we are numerically generating a random noise which can be considered as a white noise, and it is unbiased. The ratio of the spectra of the measurement noises $\kappa(f)$ is assumed to be unity and thus is omitted in the following equation.

$$H_v(f) = \frac{\tilde{S}_{y_m y_m}(f) - \tilde{S}_{x_m x_m}(f) + \sqrt{\left[\tilde{S}_{x_m x_m}(f) - \tilde{S}_{y_m y_m}(f)\right]^2 + 4\left|\tilde{S}_{x_m y_m}(f)\right|^2}}{2\tilde{S}_{y_m x_m}(f)} \tag{3.6}$$

Where S stands for cross PSD and auto PSD.

3.2.2 Operational Modal Analysis (OMA) Approach

While OMA approach is not essentially different from EMA there is a massive contrast; the input data is lacking. In OMA, an output channel is selected as a "reference channel" and it is treated as the input channel. In order to do so, some requirements are to be met. Obviously there has to be more than one output channel. Also, it is important that the different output data is simultaneously acquired, or at least the measurements are repeatable.

In case of using different sets of data not taken simultaneously the phase of different sets should also be adjusted before the FRF estimation. Also, the amplitude of different sets may vary due to repeating the experiment and thus a scale factor might be appropriate to use.

In our case we have the advantage of simulating the experiment digitally and thus we have the ability to measure every FRF simultaneously. Still, some consideration is required in selecting an output channel as the reference output. There are some papers in the literature addressing this (see ref. [12]) but this topic is beyond the scope of this thesis. Since in our case there are only 7 output channels, different reference channel selections will be tested and contrasted in the following chapter.

Once the reference output is selected the FRF is estimated simply using the cross power spectral density (cpsd) included in the MATLAB's Signal Processing Toolbox.

4. Verification Procedure

The previous chapters serve as a foundation for the verification of RFP-Z method. Chapter 3 describes how to build the numerical system model and build its FRF. Chapter 2 outlines the steps of ideal RFP-Z method which extracts the modal parameters from the FRFs. Since we know the modal parameters of the system we can easily compute the MAC matrix[15] of the extraction.

In the following chapters FRFs will be addressed according to this nomenclature:

Analytical FRF is the "real" FRF of our simulated system. It is built numerically from the modal parameters which can be calculated from the known mass, stiffness and damping matrices. The only error that might be present in the Analytical FRF is the numerical errors due to the computational process.

Experimental FRF is the FRF obtained from the simulated experiment. It is calculated by the input (the simulated random force) and the response (the simulated excitation). The input and output data are affected by a random generated noise to simulate real-life experimental cases. Because of the noise and generated FRF accuracy (The algorithms presented in Chapter 3.2 is not 100% accurate, especially when the input data is missing.) the Experimental FRF is different from the Analytical FRF.

Extracted FRF is the FRF built with the extracted parameters via RFP-Z method on the experimental FRF. Along experimental FRFs already existent inaccuracy the extracted FRF may introduce new errors due to the method itself.

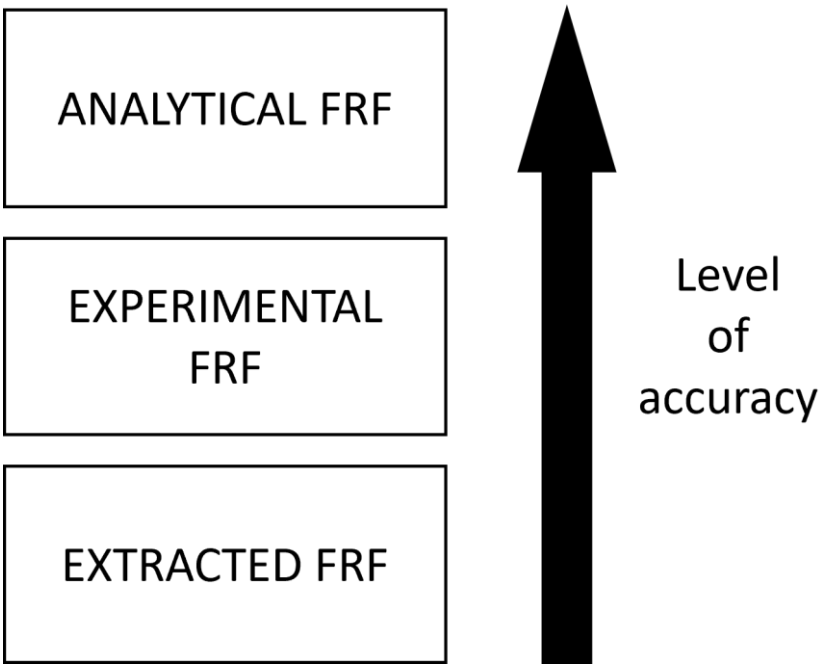

Figure 4.1: Accuracy level comparison of FRFs.

Contrasting the extracted FRF with the analytical FRF would show the accuracy of RFP-Z method considering also the errors related to estimation of the experimental FRF. In real-life structures the "real" modal parameters are never known because even they may be easily computable a small production defect of a part might influence the modal characteristics.

Comparing the extracted FRF with the experimental FRF shows only the accuracy contribution of the RFP-Z method. While the accuracy of the method might vary greatly with the noise level, the initial experimental FRF errors due to noise are overlooked in this comparison.

While the latter comparison seems more realistic I prefer to verify RFP-Z method with the former comparison because it is simply more conservative. The reduction of errors related to building the experimental FRF is a huge topic on its own and may seem unrelated to the RFP-Z method itself, but this thesis is aimed to control the "real" accuracy of RFP-Z method in conditions where the built FRF quality cannot be improved.

4.1 Computation of the FRFs

In this subchapter the methods used in finding the FRFs will be underlined. There is a different yet similar approach to compute the three different types of FRFs mentioned previously. All of these methods are also implemented in the MATLAB as a function of the main verification code. (See Appendix C for the main code and Appendix D for the related functions).

The first FRF to be computed is the **analytical FRF**. This is the easiest one due to the fact that we know all the variables beforehand. A very straightforward way to compute the response, or the receptance in the mdof case, is the following:

$$\left[\alpha_{jk}(\omega)\right] = \frac{\{\overline{\boldsymbol{X}}_j\}}{\{\boldsymbol{F}_k\}} = \left[[\boldsymbol{K}] - \omega^2[\boldsymbol{M}] + i\omega[\boldsymbol{C}]\right]^{-1} \tag{4.1}$$

Where:

$[\alpha(\omega)] = receptance$

$\{\boldsymbol{F}\} = force$

$\{\overline{\boldsymbol{X}}\} = displacement\ amplitude$

Although this is a theoretically very simple formula, numerically it might not be so simple. As the degree of freedoms of the system grows, the matrices grow larger and taking the inverse of the resulting matrix becomes a computational burden. Even though computers can handle this method for the 7dof system described in chapter 3, implementing it in the code would not be a good practice.

Numerically a more efficient method for computing the FRF exists.

$$\alpha_{jk}(\omega) = \frac{\{\overline{\boldsymbol{X}}_j\}}{\{\boldsymbol{F}_k\}} = \sum_{r=1}^{2n} \frac{\boldsymbol{\vartheta}_{jr}\boldsymbol{\vartheta}_{kr}}{b_r + i\omega a_r} \tag{4.2}$$

Where $\boldsymbol{\vartheta}$ are the eigenvectors of the Duncan eigenproblem. Constants a_r and b_r are computed in the following way:

$$diag(a_r) = \begin{bmatrix} \ddots & 0 & 0 \\ 0 & a_r & 0 \\ 0 & 0 & \ddots \end{bmatrix} = [\boldsymbol{\vartheta}]^T[\boldsymbol{A}][\boldsymbol{\vartheta}] \tag{4.3}$$

$$diag(b_r) = \begin{bmatrix} \ddots & 0 & 0 \\ 0 & b_r & 0 \\ 0 & 0 & \ddots \end{bmatrix} = [\boldsymbol{\vartheta}]^T[\boldsymbol{B}][\boldsymbol{\vartheta}] \tag{4.4}$$

Note that matrices A and B in the previous definitions are the Duncan matrices seen in Eq. (3.5). Eq. (4.2) is really simple especially with the fact that eigenvectors are known and modal constants are easily calculated without taking inverse of any matrix.

Calculating the **experimental FRF** is relatively more complex. A basic description which outlines the method is given in chapter 3.2.1 and chapter 3.2.2.

The **extracted FRF** is calculated in a way similar to the analytical one, but the parameters used are different. The parameters extracted from the RFP-Z algorithm, which are saved in the matrix of Eq. (2.20), are used in the following way:

$$[\alpha_{jk}(\omega)] = \frac{\{\overline{\boldsymbol{X}}_j\}}{\{\boldsymbol{F}_k\}} = \sum_{r=1}^{n} \left(\frac{{}_rA_{jk}}{i\omega - s_r} + \frac{{}_rA_{jk}^*}{i\omega - s_r^*} \right) \tag{4.5}$$

All variables in the equation above can be obtained from the output of RPF-Z. Poles s_r in the denominator can be computed from the Eq. (2.4). Residues ${}_rA_{jk}$ are obtained via Eq. (2.21).

As a small footnote it should be mentioned that while all the reported formulas use angular frequency, I will work with normal frequency in MATLAB. All the equations will be modified to convert frequency values as in $\omega = 2\pi f$.

4.2 Computation of MAC

Modal Assurance Criterion (MAC) is the most common tool in modal analysis to assess model similarity. Its greatest advantage is that the mode shapes are sufficient for its measurement. It is defined as follows:

$$MAC(r,s) = \frac{|\{\vartheta_r\}_{EXC}^H * \{\vartheta_s\}_{ANA}|^2}{(\{\vartheta_r\}_{EXC}^H * \{\vartheta_r\}_{EXC}) * (\{\vartheta_s\}_{ANA}^H * \{\vartheta_s\}_{ANA})} \tag{4.6}$$

Where:

$\{\vartheta_r\}_{EXC} = r - th\ extracted\ mode\ shape$

$\{\vartheta_s\}_{ANA} = s - th\ analytical\ mode\ shape$

It is worth noting that the nominator, as well as the two factors in the denominator are all real quantities. Since we are contrasting various mode shapes, a matrix called the MAC matrix will be obtained showing the coherence of a mode with every other one. The values are between 0 and 1. A highly accurate extraction would have high values on MAC's diagonal elements, showing correlation between modes, and low values on MAC's non-diagonal elements, showing that each mode is unique.

The analytical mode shapes are already calculated at this point. To find the extracted mode shapes, following relationship can be exploited:

$${}_rA_{pq} = \vartheta_{pr}\vartheta_{qr} \tag{4.7}$$

Where r is the mode, p is the output and q is the input reference. In our case a force is applied in 3rd degree of freedom so values of residues A with subtext $q = 3$ is what we have extracted. Thus the 3rd element of any mode shape r is given by:

$$\vartheta_{3r} = \sqrt{{}_rA_{33}} \tag{4.8}$$

Any other element of mode shape r can be found by the relation:

$$\vartheta_{pr} = \frac{{}_rA_{p3}}{\vartheta_{3r}} \tag{4.9}$$

It is evident that mode shapes are proportional to the residues. To computationally be more efficient, another approach in obtaining the MAC matrix can be used:

$$MAC(r,s) = \frac{|\{A_r\}_{EXC}^H * \{\vartheta_s\}_{ANA}|^2}{(\{A_r\}_{EXC}^H * \{A_r\}_{EXC}) * (\{\vartheta_s\}_{ANA}^H * \{\vartheta_s\}_{ANA})} \tag{4.10}$$

Where:

$\{A_r\}_{EXC} = Extracted\ residues\ of\ the\ r - th\ mode\ (input\ q = 3)$

5. Verification of RFP-z in Output-Only Case

In the previous chapters the basis of the RFP-Z and the verification process are described. That foundation will be exploited from now on in order to test the accuracy of this method. In this chapter our case study will be assumed as a structure which cannot be evaluated via EMA, thus its operational deflection shapes (ODS) will be used alternatively, or in other words OMA will be performed.

In real life the testing and performance conditions inevitably change. Vibrations, in most engineering fields, present a problem not only unavoidable, but in most cases also unpredictable. For this reason, assessing the accuracy of RFP-Z under differing circumstances is crucial.

The most significant characteristic remains without doubt the force itself. Since the vibrations the structure might encounter is largely unpredictable, different typologies of forces are to be expected. The following force types will be analysed in this chapter:

- Random force

- Harmonic force

- Harmonic force with an additional random force contribution

For the second case various excitation frequencies will be put under trial and for the last case, different circumstances with the magnitude of the additional random force relative to the harmonic force's amplitude will be tested.

It is reasonable to elaborate the randomness of the force. To make our tests more realistic the force will be random in a normally distributed way. The standard deviation will be defined in the code, and all the random values will be clustered around a mean of 0. The probability density function of the normal distribution is given below.

$$f(t) = \frac{1}{\sigma\sqrt{2\pi}} e^{-\frac{1}{2}\left(\frac{t-\mu}{\sigma}\right)^2} \tag{5.1}$$

Where:

$\mu = mean$

$\sigma = standard\ deviation$

To simulate a variety of different forces, standard deviation is going to be altered. This way also the impact of the standard deviation, if there is any, will be observed.

Another critical characteristic to test is the presence of noise. In an optimal case there would not be any noise but unfortunately this is never the case. Ergo, the response of the system under examination will always be contaminated with noise in the following tests.

The same problem is also present in the excitation itself as well. During experiments, the force transmitted by a shaker or an impact hammer can never exactly be known and this inaccuracy

can be mimicked by including noise in the generated force vector. The accuracy of the RFP-Z method will be measured where the noise is present only in the response, and in both input & output.

Finally, different noise levels will be applied in several tests in order to retain an opinion in every possible real-life case.

5.1 Random Excitation

5.1.1 3% Noise in Output

The first force typology to be put on trial is the simplest one, in the 3rd degree of freedom a normally distributed random force with a standard deviation $500N$ is inserted. Since our force typology is purely random mean value is not actually important. With the set of Eq. (3.3) the time history of the output, which is the displacement of seven dofs, can be calculated. The results can be seen in fig. 5.2 (a). Since the seven different time histories of each dof are all packed together and sometimes overlap, it is hard to see that fig. 5.2 (a) contains the displacement of each dof. To define a context, a close up of the same graph is given 5.2 (b).

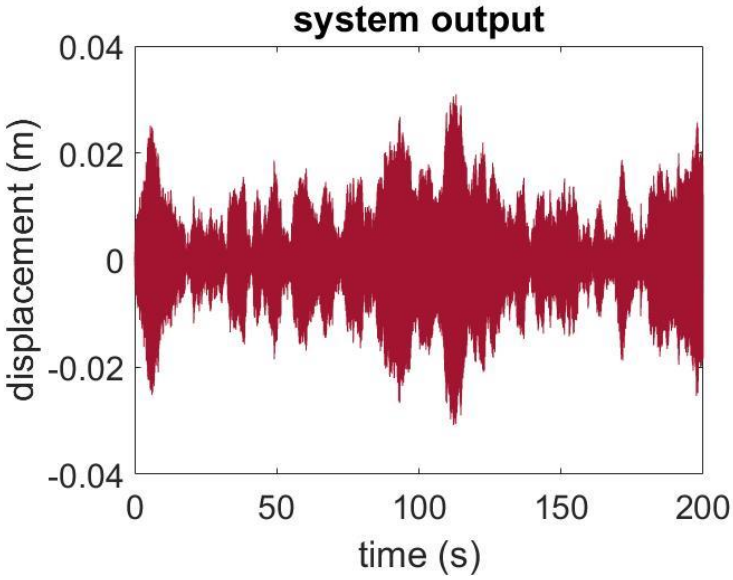

(a)

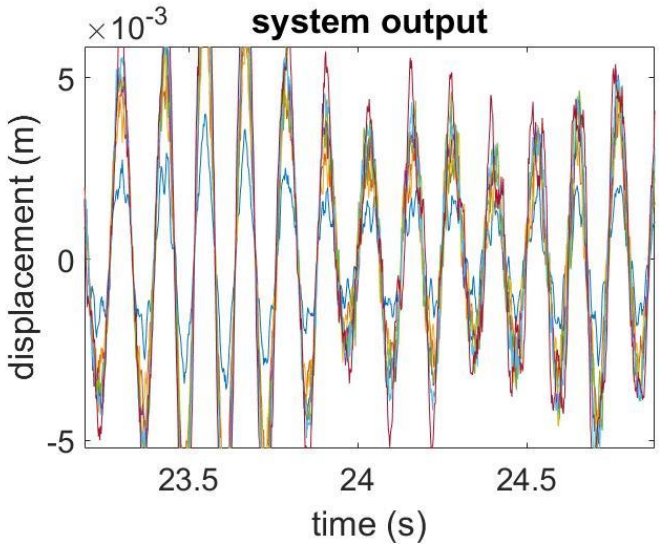

(b)

Figure 5.2: (a) Response of each degree of freedom to a random excitation of 200 seconds, with a 3% noise added in the output. (b) Zoomed in version of the same graph, highlighting that there is an output of every dof.

The seven different time histories will be cross correlated to build an FRF. Since this is the first case in which we adhere to the procedure described in chapter 3.2.2 we are obliged to determine the best dof to use as the reference response as well. As a side note it is possible that this reference dof will be different in various circumstances. The accuracy of the results will be assessed via their similarity to the analytical FRF of the structure. In figure 5.3, the sum of analytical FRFs of each dof can be observed. The more our experimental FRF resembles fig. 5.3 the more accurate it is.

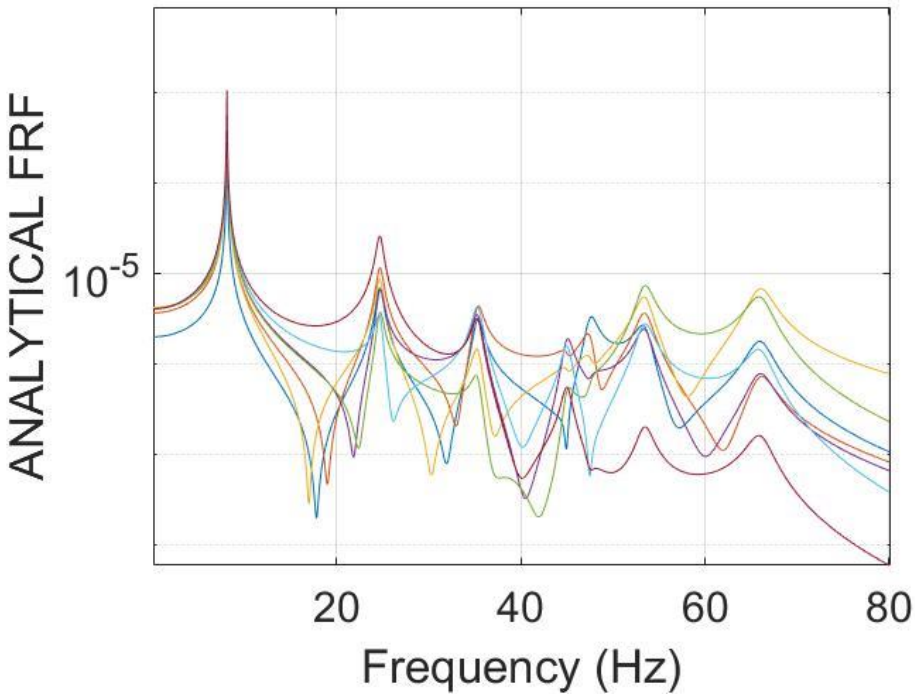

(a)

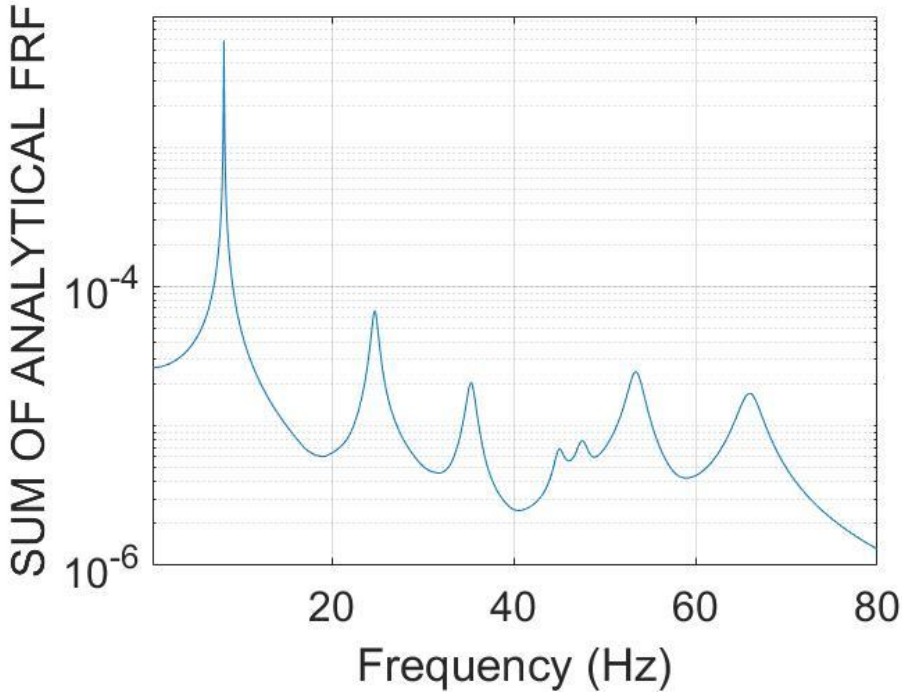

(b)

Figure 5.3: (a) Analytical FRF of 7 individual degrees of freedom. (b) Sum of all the analytical FRFs.

In fig. 5.3 there are 2 different representations of the FRF information. The first one possesses more information, it represents the FRF of every individual dof. The second represents essentially the sum of 7 individual FRFs. It contains less information but it is more concise and thus in the proceeding comparisons the second representation will be used.

The true natural frequencies and damping ratios of the system can be computed via Eq. (2.15) and (2.16). These values are reported in table 5.1 below.

MODE	1	2	3	4	5	6	7
f_n $[Hz]$	8.09	24.70	35.32	45.03	47.55	53.46	65.99
ζ	0.22%	1.44%	1.43%	1.15%	1.38%	1.61%	1.97%

Table 5.1: Analytical modal parameters of the 7-dof system.

It can be seen both by analysing fig. 5.3.b graphically or table 5.1 numerically the modes 1, 2, 3, 6 and 7 are properly separated. Modes 4 and 5 in the other hand are close to each other and weaker amplitude wise: Those two are going to pose the hardest challenge.

To deduce which dof has to be taken as the reference, the graphical results of FRF estimation using each dof as reference are given in fig. 5.4. It is lucid to the eye that the closest FRF estimation is when the reference dof is the 2nd one, as it is the solitary case in which 7 distinct modes are visually present. But running the RFP-Z algorithm on each of them separately highlights otherwise. The stabilization chart of the case where the reference dof is the 2nd one can be seen in fig. 5.5. It is apparent that the algorithm can estimate only 5/6 modes in the best case in a given model order. Increasing the model order iteration up to 80 has not proven any improvement in this regard.

Some further analysis on other cases makes it possible to deduce that either the 4th or the 6th dof is the most suitable as the reference. Their stabilisation charts can be seen in fig. 5.6 and fig. 5.8 respectively. A preliminary observation gives hints that 6th dof might be more suitable as it has more model orders containing 6 estimated modes, showing consistency, and the modal frequencies are more consistent with respect to those of the 4th dof. In both cases there no model order with 7 estimated modes so in any case one mode is lost. The lost mode is 5th analytical mode.

First the 4th dof is set as the reference. A least squares approximation suggests that 18th model order is the most accurate one. The FRF constructed using the parameters extracted from the estimated FRF is seen in fig. 5.7. The natural frequencies and the damping ratios of the extracted modes are reported in table 5.2. The natural frequency of each mode is quite accurate, all within an error margin of $\pm 0.4\%$. Regrettably, the same accuracy cannot be observed for the damping ratios, especially in the case of 1st and 4th modes. The fact that the first mode's damping ratio is loosely at least one order of magnitude lower than the rest causes it to dominate the dynamic response estimation of the system. The rest of the modes have lost their relevancy due to this wrong damping estimation.

MODE	1	2	3	4	6	7
f_n $[Hz]$	8.12	24.76	35.23	44.97	53.41	65.84
ζ	0.025%	1.32%	1.28%	0.18%	1.57%	1.54%

Table 5.2: Extracted modal parameters (reference dof:2 model order:24).

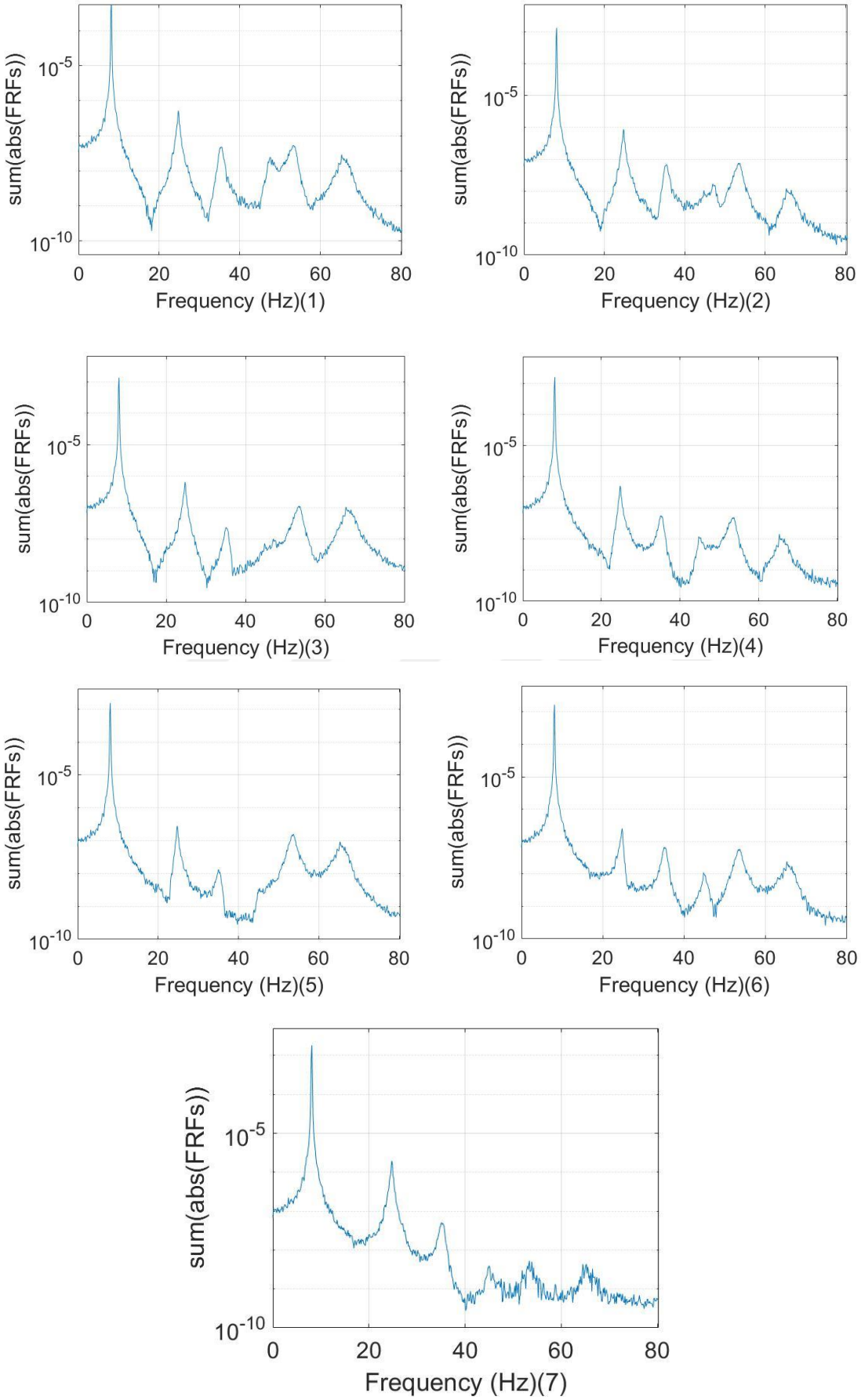

Figure 5.4: FRF Estimations having set each dof as the reference.

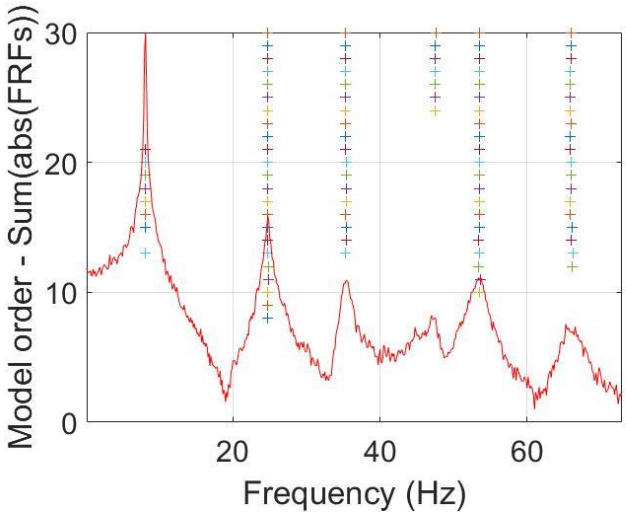

Figure 5.5: Stabilization chart of the case with the 2nd dof as the reference dof.

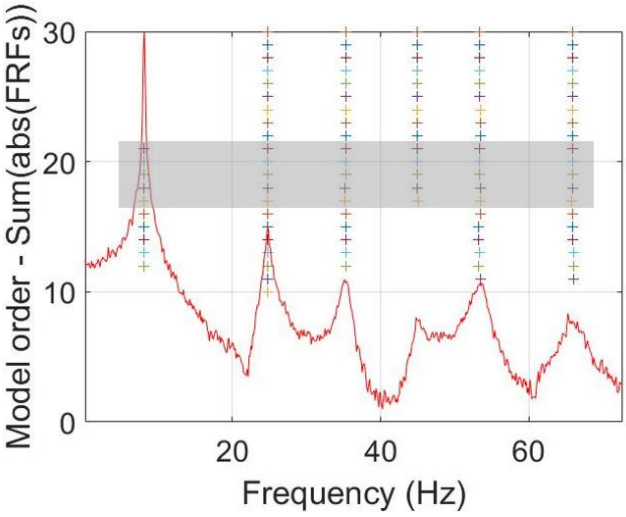

Figure 5.6: Stabilization chart of the case with 4th dof as the reference.

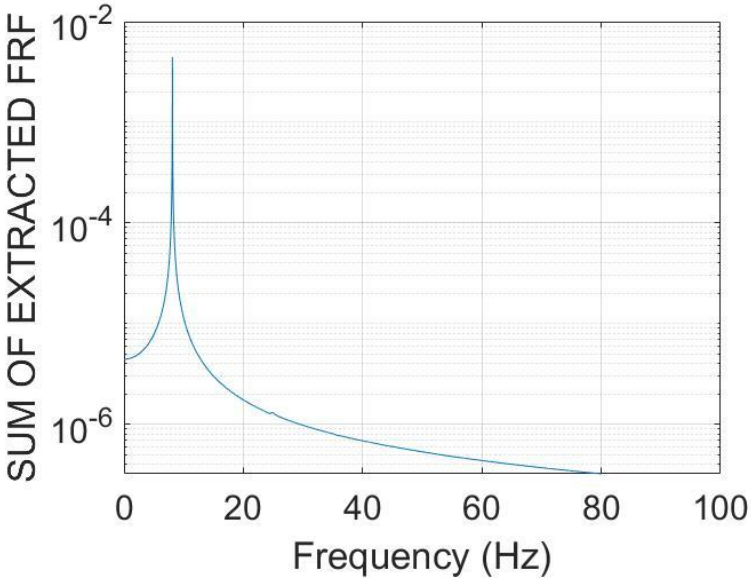

Figure 5.7: Constructed FRF using extracted modal parameters (reference dof:4 model order:18).

The mode shapes can be compared with the original ones via the MAC matrix reported in table 5.3. The analytical modes are represented as columns while the extracted ones correspond to the rows. It is observed that the original modes denoted with number 1, 2 ,3, 6 and 7 have their mode shapes extracted with an accuracy of at least ~ 90%. The analytical mode 5 is completely lost, while the analytical mode 4 is extracted in an inaccurate way. Its shape bears a nonnegligible similarity with respect to analytical modes 5, 6 and 7 respectively while being completely irrelevant to the actual 4th analytical mode.

	1	2	3	4	5	6	7
1	0.9906	0.0117	0.0028	8.7251e-04	0.0015	0.0064	8.2963e-04
2	0.0070	0.9920	0.0024	0.0024	0.0017	0.0014	0.0018
3	0.0161	0.0458	0.8977	0.0083	0.0099	0.0215	0.0148
4	0.0161	0.0197	0.0575	0.0063	0.2321	0.4462	0.1364
5	0.0082	0.0015	0.0018	9.8164e-04	0.0061	0.9540	0.0453
6	0.0020	0.0028	9.7220e-04	0.0020	6.4052e-04	0.0340	0.9718
7	NaN	NaN	NaN	NaN	NaN	NaN	NaN

Table 5.3: MAC Matrix of the case reference dof = #4, model order = #18.

To see if it yields a more accurate FRF estimation, 6th dof is set as the reference dof for another examination. Some preliminary analysis can be conducted by examining the stabilization chart in Fig. 5.8. This chart highlights that there are 7 different model orders, with the range 15-21, that extract 6 modes. The 5th analytical mode is lost also in this case. Additionally, a glance at fig. 5.9 shows that also in this trial the extracted damping ratio of the first mode is extremely low and thus it will dominate the FRF just like the previous case.

This is clearly an abnormal result, which sometimes may be observed in the first peaks. Throughout the following chapters the first damping ratio will persist being the biggest inaccuracy by an order of magnitude, and the source of it is not the related to the methods of cross-power spectral density or RFP-z but rather related to numerical reasons. Hence, that specific inaccuracy should be neglected until it and its remedy is explained in chapter 5.4.

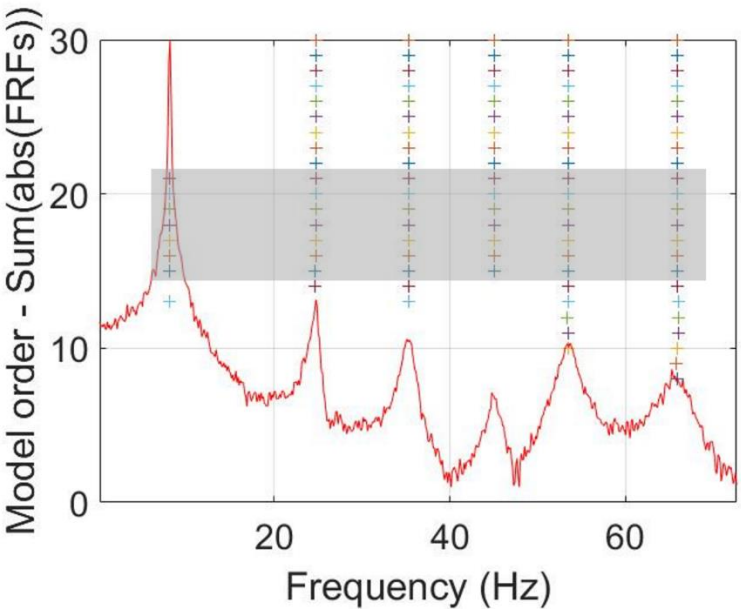

Figure 5.8: Stabilization chart of the case with the 6th dof as the reference dof.

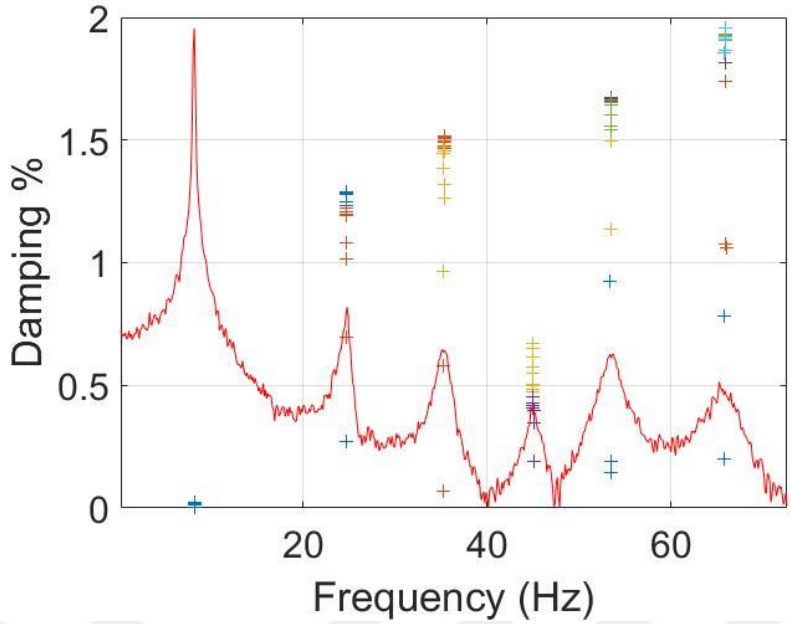

Figure 5.9: Damping ratio of each mode in several model orders.

Among the model orders noted above, #19 is the closest approximation to the analytical FRF in a least-squares sense so it will be used in further analysis. The estimated FRF in fig 5.10 is very similar to that in fig. 5.6. Due to the low damping estimation, the response is dominated by the first mode. The exact extracted parameters can be seen in table 5.4.

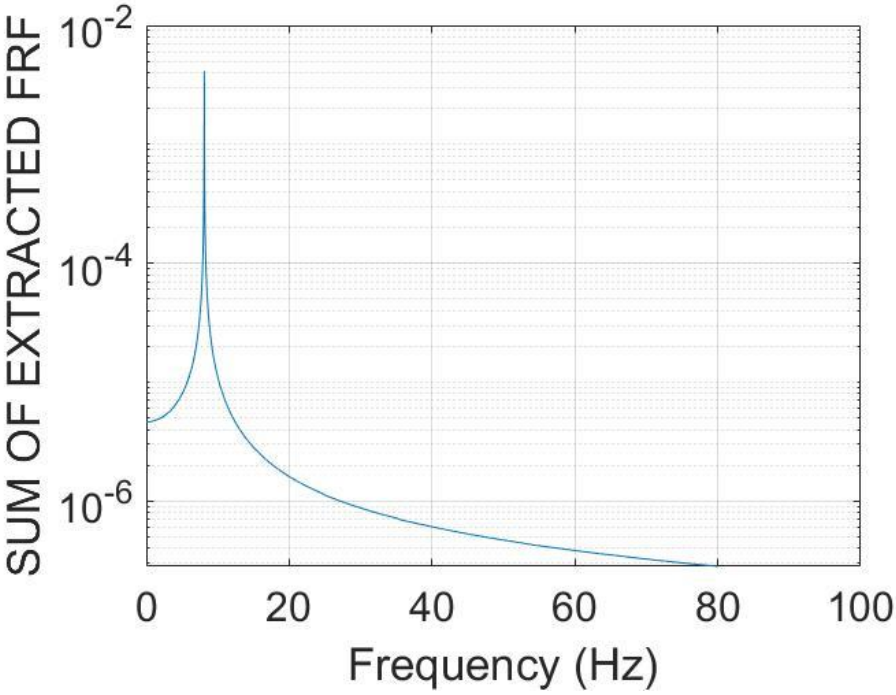

Figure 5.10: Constructed FRF using extracted modal parameters (reference dof:6 model order:19).

MODE	1	2	3	4	6	7
f_n $[Hz]$	8.1209	24.7137	35.2866	45.0220	53.4608	65.8821
ζ	0.016%	1.21%	1.44%	0.42%	1.64%	1.96%

Table 5.4: Extracted modal parameters (reference dof:6 model order:19).

The MAC matrix of this case is given below.

	1	2	3	4	5	6	7
1	0.9933	0.0105	0.0013	2.5088e-04	3.2801e-04	0.0099	3.3659e-04
2	0.0082	0.9922	0.0026	0.0025	0.0023	9.7482e-04	0.0012
3	0.0163	0.0427	0.9115	0.0041	0.0084	0.0153	0.0134
4	0.0206	0.0275	0.0399	0.0984	0.1654	0.4041	0.1456
5	0.0101	0.0021	0.0022	9.0785e-05	0.0048	0.9417	0.0604
6	0.0018	0.0030	8.4509e-04	0.0019	1.0335e-04	0.0425	0.9657
7	NaN	NaN	NaN	NaN	NaN	NaN	NaN

Table 5.5: MAC Matrix of the case reference dof = #6, model order = 19.

Shapes of the analytical modes 1, 2, 3, 6 and 7 show similar congruency levels to that of the previous instance. The 4th analytical mode shows a congruency of 10%, which is horrible.

The two previous situations demonstrate us that the Output-Only FRF Estimation can extract the natural frequencies with a excellent accuracy but is not reliable in damping ratio identification and this heavily distorts the constructed FRF. Mode shapes are identified with a satisfactory level of accuracy for fairly separated modes, but there is no accuracy for the case of twin modes. Another problem with this method is that when there are close modes, only one of them gets extracted and the other one is lost.

With both the 4th and the 6th as the reference, there is no crucial difference observed. They both confirm the same accuracy in extracting natural frequencies and inaccuracy in extracting the damping ratios. The mode shapes extracted with having the 6th dof as the reference are slight closer to the analytical model so the reference dof will be the 6th one in OMA method for the rest of this chapter.

5.1.2 <u>10% Noise in Output</u>

SNR or signal-to-noise ratio is a quantity used to describe the amount of noise present with respect to the original signal. This ratio should be bigger than 1, as in the previous subchapters, in order to yield a meaningful signal distinct from the noise. In this subchapter, a SNR level of 10, or in other words 10% noise is present in output.

The response graph can be seen in fig. 5.10. Since the excitation maintains a casual nature, the response graph is not unexpectedly random and it does not betray the higher noise level clearly. The graph of the excitation is not reported as a figure but it is subject to a noise in a similar fashion.

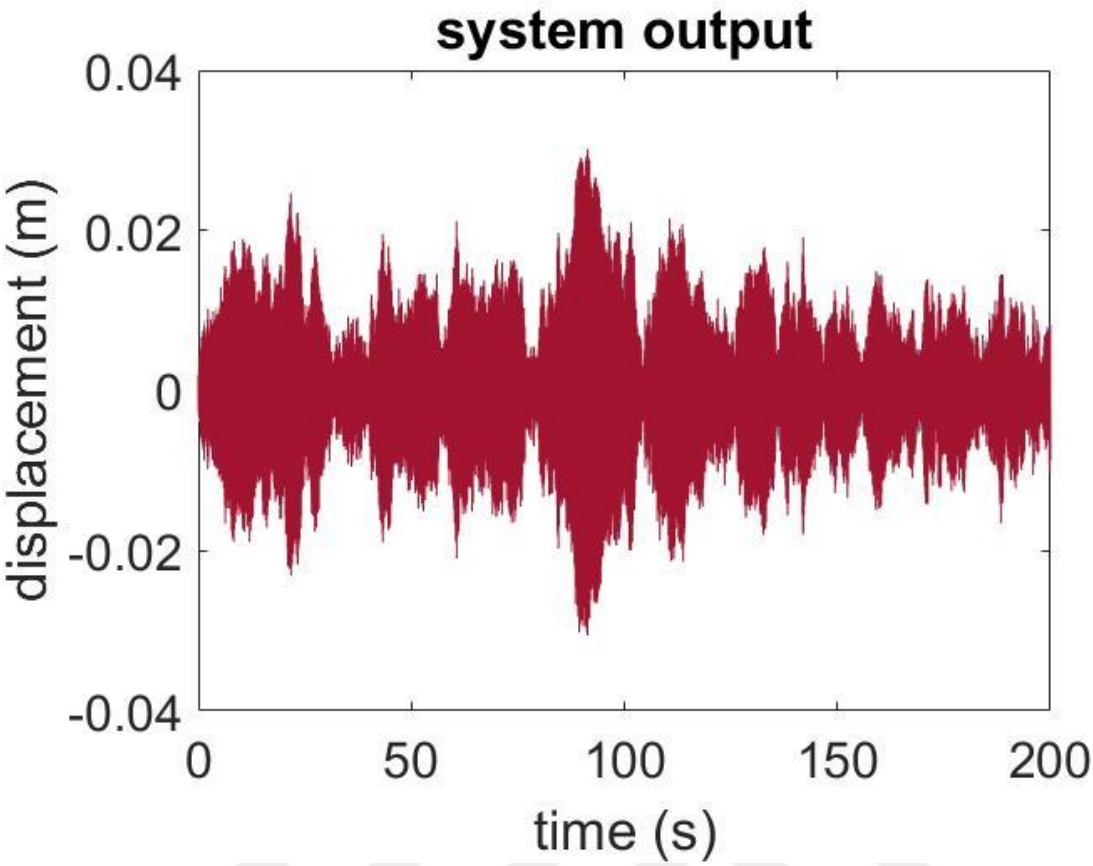

Figure 5.10: Response of each degree of freedom to a random excitation, with 10% noise in both input and output.

The estimated FRF using high-noise corrupted signals can be seen in the stabilization chart given in figure 5.11. The FRF, especially on frequencies not close to resonances, has ruggedness because of the higher noise in this simulation. In the FRF 6 modes can be detected visually, but the RFP-Z algorithm can extract only 5 of those. Trying different reference dofs for the OMA method does not improve this result. Model order #19 is selected because it has the highest damping ratio estimation for the first mode. The extracted modal parameters are reported in table 5.6. The constructed FRF is reported in fig. 5.12.

MODE	1	2	3	4	5
f_n $[Hz]$	8.1179	24.7263	35.2764	53.3680	65.8843
ζ	0.012%	0.41%	0.49%	1.08%	0.54%

Table 5.6: Extracted modal parameters (reference dof:6 model order:19).

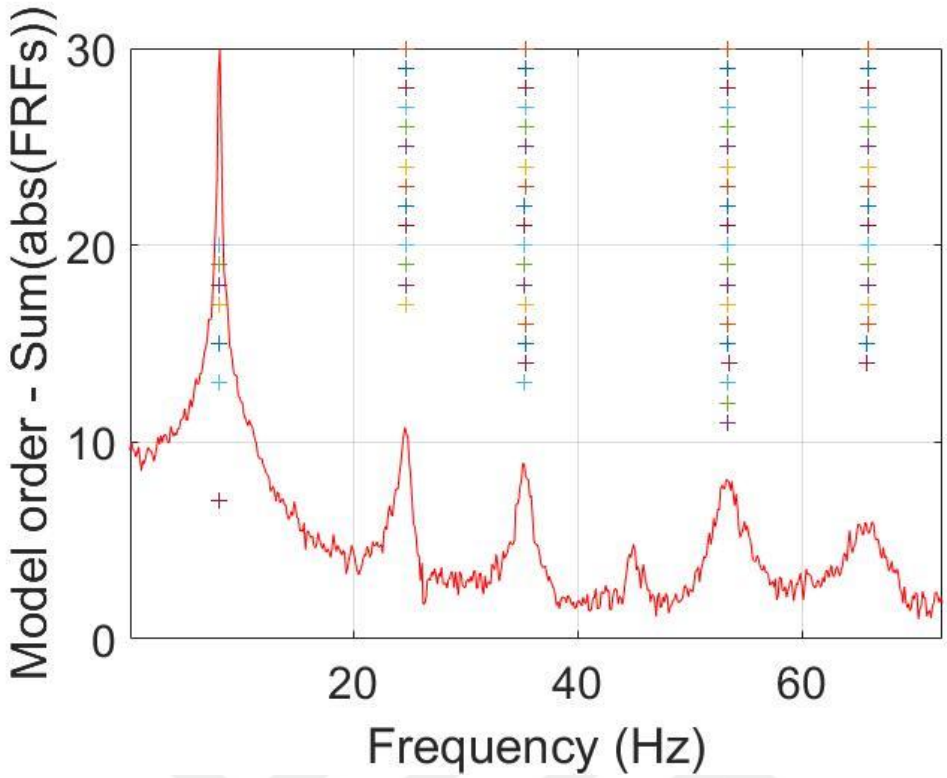

Figure 5.11: Stabilization chart in the case of randomly excited system with a 10% noise in input and output, with and operational modal analysis approach.

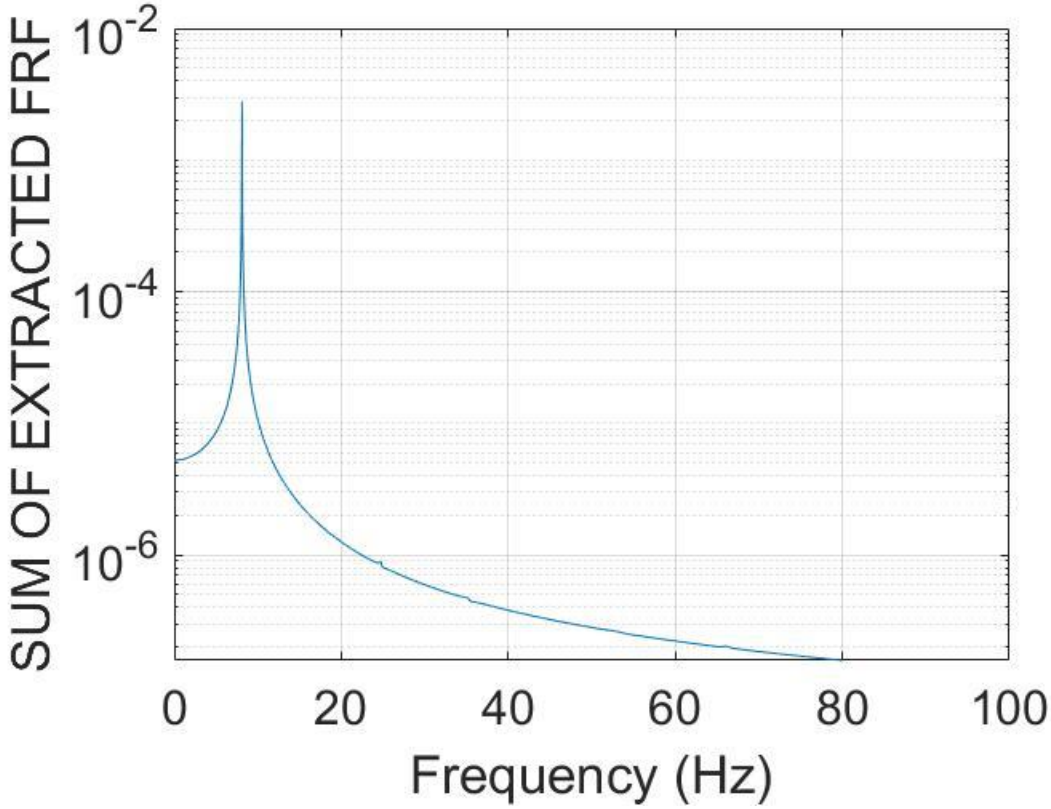

Figure 5.12: Constructed FRF using extracted modal parameters in table 5.8 (reference dof:6 model order:19).

The extracted parameters, although lacking a mode, show an acceptable accuracy level with regards to the natural frequency. A major difference from the previous cases is the damping ratios. All of the damping ratios are greatly underestimated. The first one is still at least an order of magnitude lower than the rest so it still dominates the constructed FRF, but at least some other modes are visually detectable in a narrow local resonance frequency band.

The mode shape closeness can be analysed via the MAC matrix in table 5.7. The twin modes and hence their mode shapes are completely lost. Shapes of the separate modes have accuracy levels slightly lower but still acceptable. The sole exception is the 3rd mode shape which has an accuracy of 87,6%. Although not very low, it is below the threshold of 90%. This amount of fall in the accuracy is in concordance with other papers about this topic in the literature such as [16].

	1	2	3	4	5	6	7
1	0.9967	0.0014	0.0029	4.0768e-04	0.0018	0.0063	0.0025
2	0.0102	0.9831	8.1415e-04	0.0021	0.0014	6.4704e-04	0.0077
3	0.0195	0.0563	0.8758	0.0065	0.0150	0.0148	0.0216
4	0.0098	0.0047	0.0024	4.6395e-04	0.0052	0.9353	0.0679
5	4.9873e-04	0.0032	0.0023	9.3913e-04	5.5189e-04	0.0608	0.9459
6	NaN	NaN	NaN	NaN	NaN	NaN	NaN
7	NaN	NaN	NaN	NaN	NaN	NaN	NaN

Table 5.7: MAC Matrix of the case with 10% noise in input and output.

This subchapter highlighted that the noise levels affect the accuracy of the RFP-Z method greatly. The natural frequencies are easier to extract and thus they are more resistant to noise levels. Identified mode shapes may remain within an acceptable margin of error given that the modes themselves are well separated. Damping ratios are the fundamental problem in modal parameter identification and the accuracy of their estimation is affected profoundly with the increasing noise levels. The RFP-Z method, when paired with OMA FRF estimation, would not yield good results in the case of a random excitation because of critically misidentified damping ratios.

5.2 Harmonic Excitation

In this chapter the previous testing procedure will be employed, but the typology of the force will be harmonic instead of a random force. Apart from different noise levels, different excitation frequencies will be tested as well in order to perceive the effects of exerting a force near to one of the natural frequencies.

5.2.1 3% Noise in Output

The first case to be put on trial is a harmonic force with an excitation frequency of $10Hz$. This frequency does not correspond to any natural frequency or their harmonics. A noise of 3% is present in the output signal. Response of this excitation in the time domain is seen in fig. 5.13. Unlike the previous random excitation, the response indicates a perpetual steady-state motion after the initial transient period. The transient section of the signal is usually not recorded in practical situations and therefore it must be cropped out for the analysis. A zoomed in section of the same time domain response indicates that the signal passes to steady state at around 30th second (fig. 5.13 b). Since the sampling frequency $f_s = 512\ Hz$, the first 15.360 samples will be neglected in every output signal.

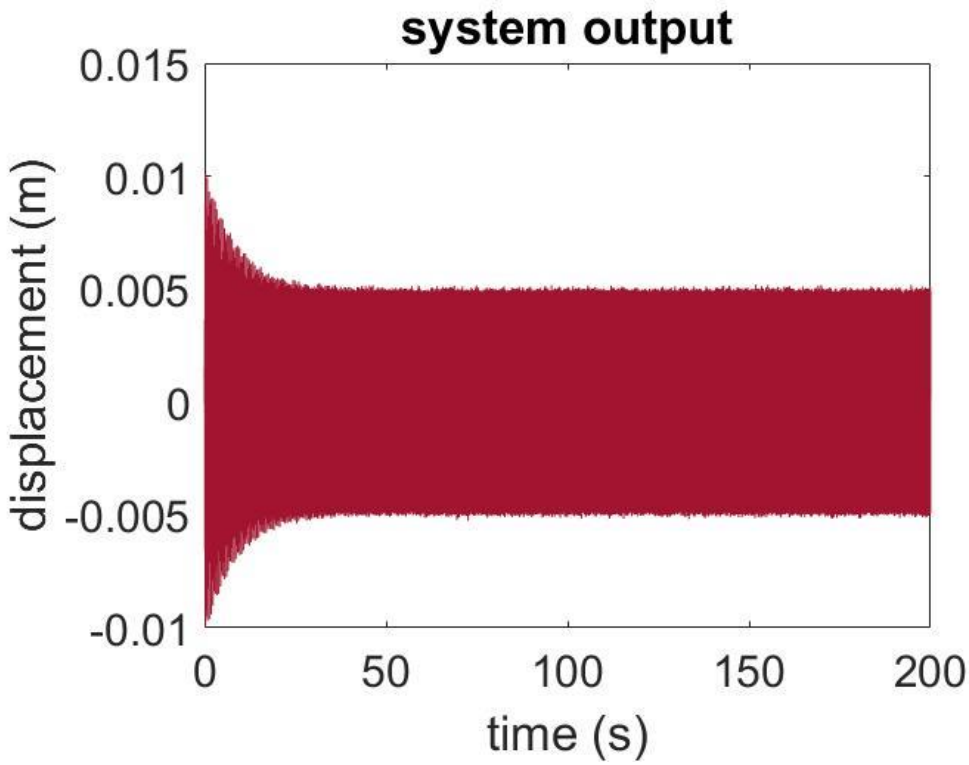

Figure 5.13a: Response of each degree of freedom to a harmonic excitation with a frequency of 10Hz, with 3% noise in output.

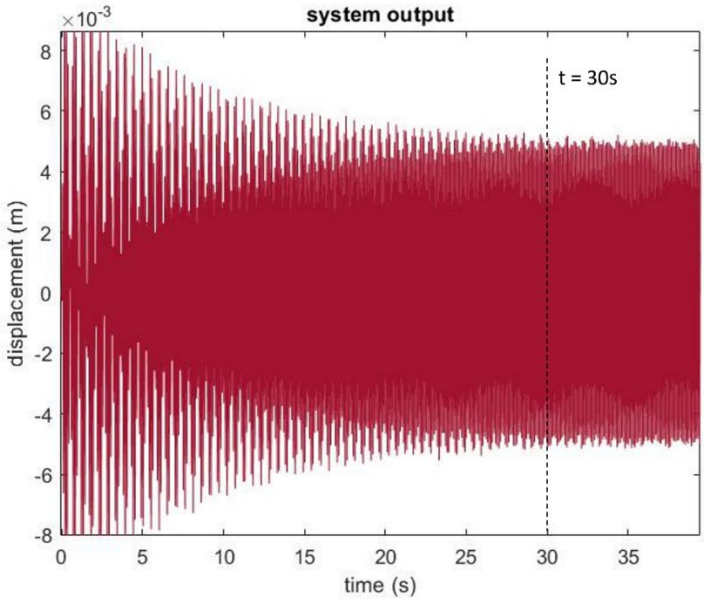

Figure 5.13b: Passing from transient to steady-state behaviour of the signal.

When the FRF is estimated from this response via the cross power spectral density method, the result is hopelessly inaccurate regardless of the reference dof chosen. As it can be observed in fig. 5.14, there are only 2 detected peaks. One of them is the first analytical mode and the other one is a non-existent virtual mode detected right in the excitation frequency. The damping ratio of the virtual mode is between the range of $1 - 2.1\%$ depending on the model order. This is an unexpected result which can be attributed to numerical reasons, similarly to the severe underestimation of the first mode. Due to the root of the problem being the same, this abnormal result will also be explained in chapter 5.4. Fig. 5.15 shows the FRF estimation in the case of not cropping the transient signal section. The change between 2 FRFs indicates limiting the analysis with steady state reduces the spectral leakage.

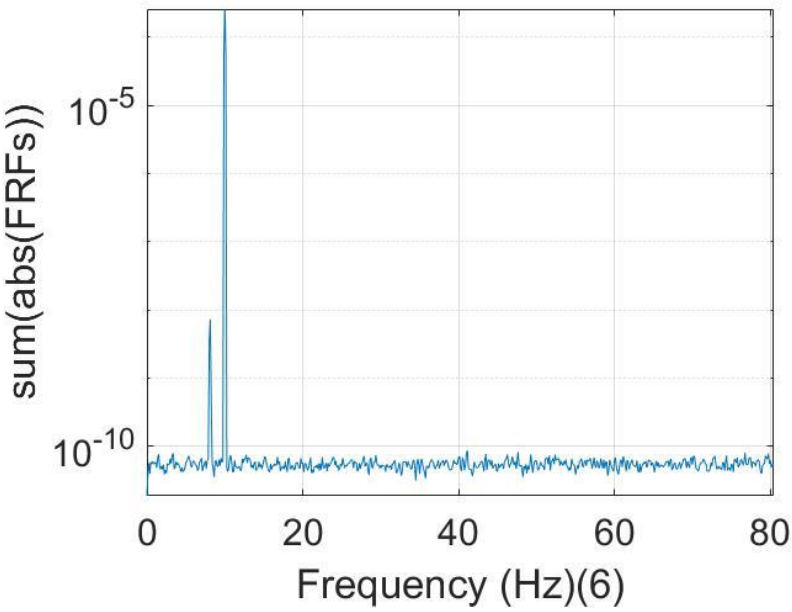

Figure 5.14: Sum of the FRF estimation of each dof with an excitation frequency of 10Hz. (Transient part excluded)

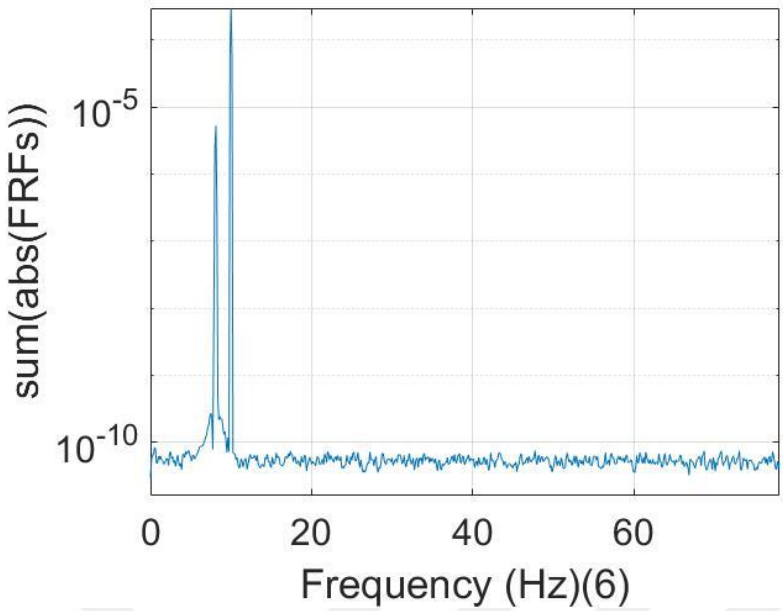

Figure 5.15: Sum of the FRF estimation of each dof with an excitation frequency of 10Hz. (Transient part included)

There is no point to test the extracted parameters and MAC matrix of this instance since the FRF estimation is completely irrelevant from the analytical FRF.

An interesting frequency to test is $24Hz$ because in its close proximity there is both the 2nd natural frequency and the 3rd harmonic of the 1st natural frequency. From fig. 5.16 it can clearly be seen that the response amplitude is twice that of the previous case. This behaviour is totally expected. In this case the transient response lasts merely 10 seconds so the first 5120 samples are to be neglected.

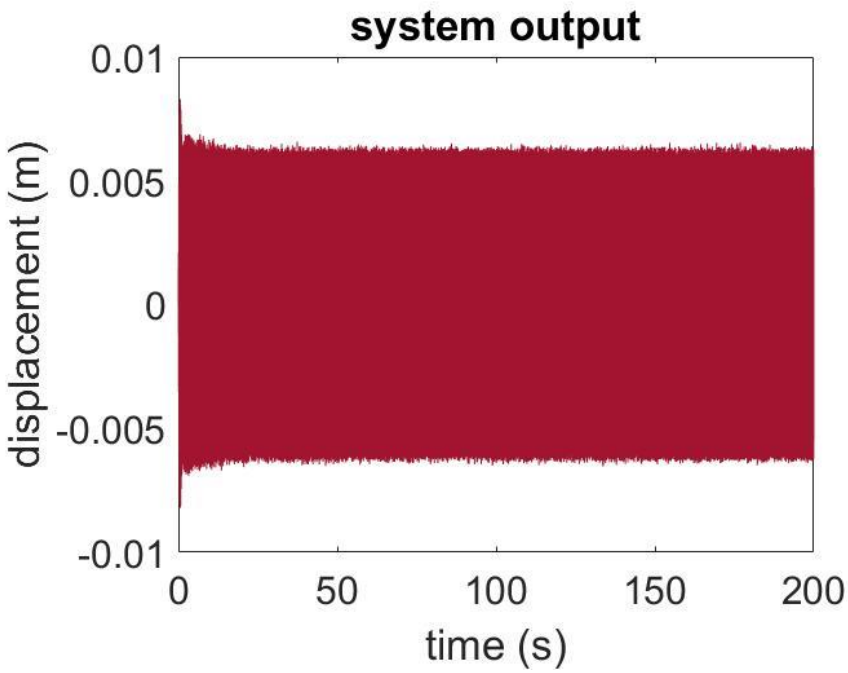

Figure 5.16: Response of each degree of freedom to a harmonic excitation with a frequency of 24Hz, with 3% noise in output.

The estimated FRF can be seen in fig. 5.17. Just like in the previous case the first analytical mode persists while all the other modes are failed to get estimated. The second mode seems to be present, but that is because of its superposition with the virtual mode in its natural frequency.

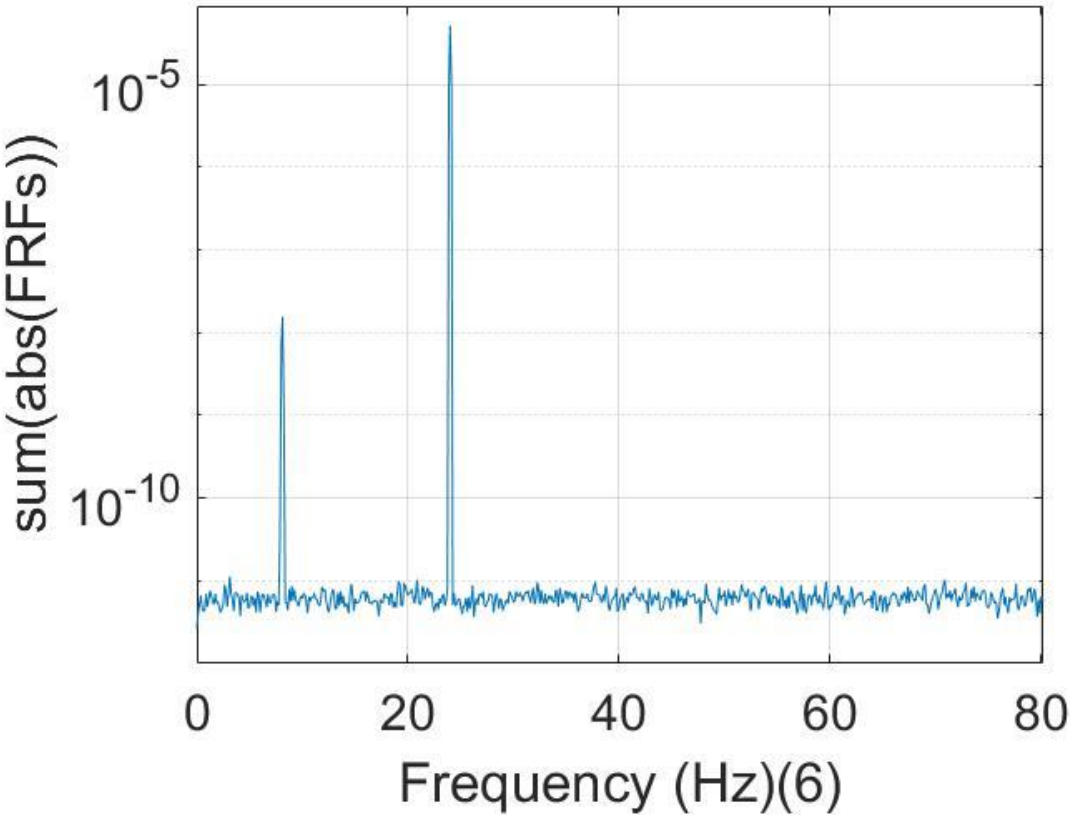

Figure 5.17: Sum of the FRF estimation of each dof with an excitation frequency of 24Hz.

Another interesting excitation frequency would be $40Hz$ because as seen in fig. 5.3.b it corresponds to the deepest antiresonance of the system as a whole. The resulting time domain response is graphed in fig. 5.18 and it is very interesting. Response level of every dof is different. Orange colour corresponds to the 2nd dof and it responds violently to the force, while the 7th dof represented by red is resistant to movement. Dofs 4 and 5 are even more stationary and they are not even seen under the 7th dof's response. This behaviour can be explained clearly with a quick glance at fig. 5.3.a. Every dof has a different response magnitude at the frequency of $40Hz$.

Considering every dof, steady state behaviour establishes itself in the system after 32 second. This means that the first 16384 samples have to be neglected in the FRF estimation.

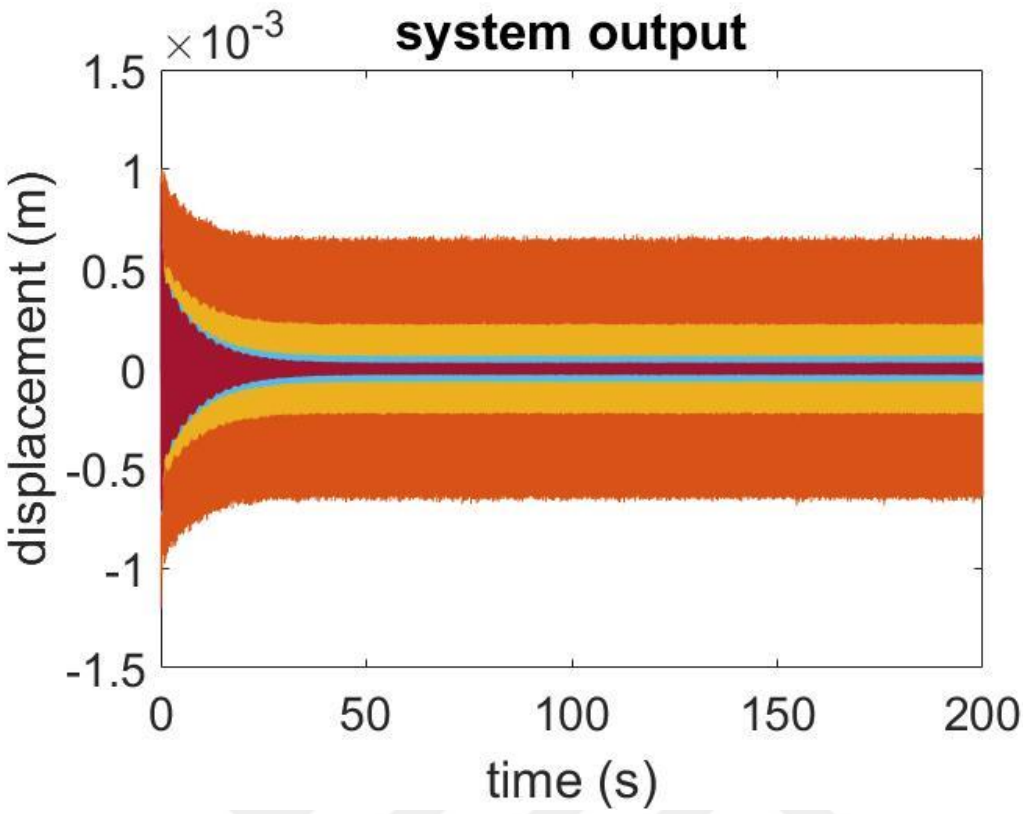

Figure 5.18: Response of each degree of freedom to a harmonic excitation with a frequency of 40Hz, with 3% noise in output.

The FRF estimation of this time history can be seen in fig. 5.19. There is the expected virtual mode at $40Hz$.

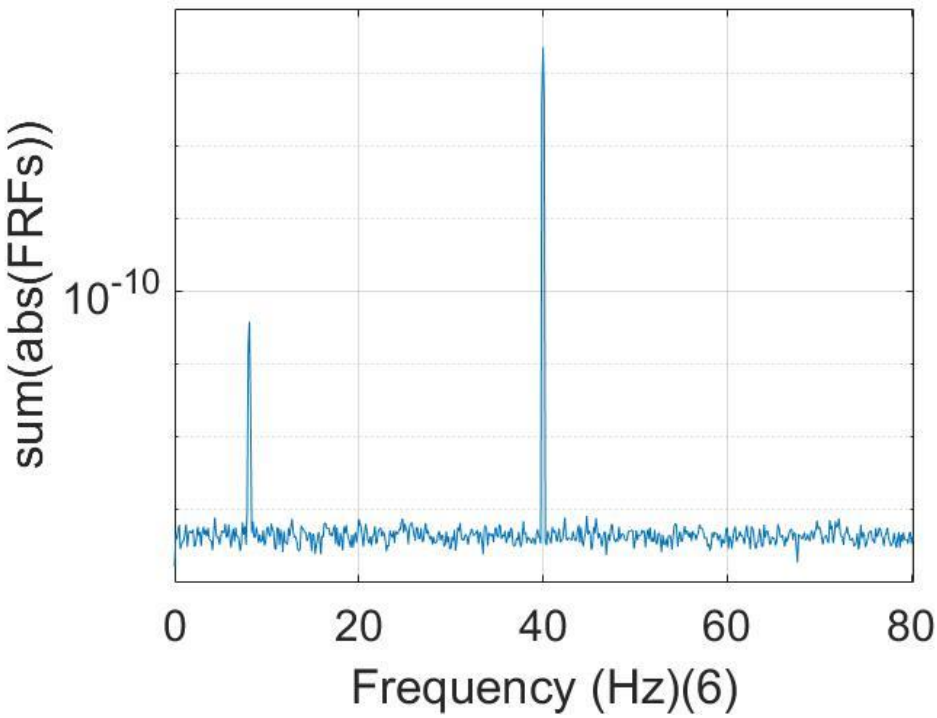

Figure 5.19: Sum of the FRF estimation of each dof with an excitation frequency of 40Hz.

Another intriguing thing to analyse is what happens if the excitation frequency is high enough that it does not correspond to a natural frequency or their strong harmonics. When an excitation with a frequency of $90Hz$ and $200Hz$ is applied to the 3rd dof, the responses shown in fig. 5.20 is obtained. Passage to steady state of every dof's response takes 60 seconds and 50 seconds respectively for 90Hz and 200Hz. Expectedly the response levels fell harshly. Only the 3rd dof shows significant motion because that is the point where the force is applied. The FRF is reported in fig. 5.21. Even though the damping ratio is far from being accurate and the FRF magnitude is very low, the first mode is visually detectable in both cases.

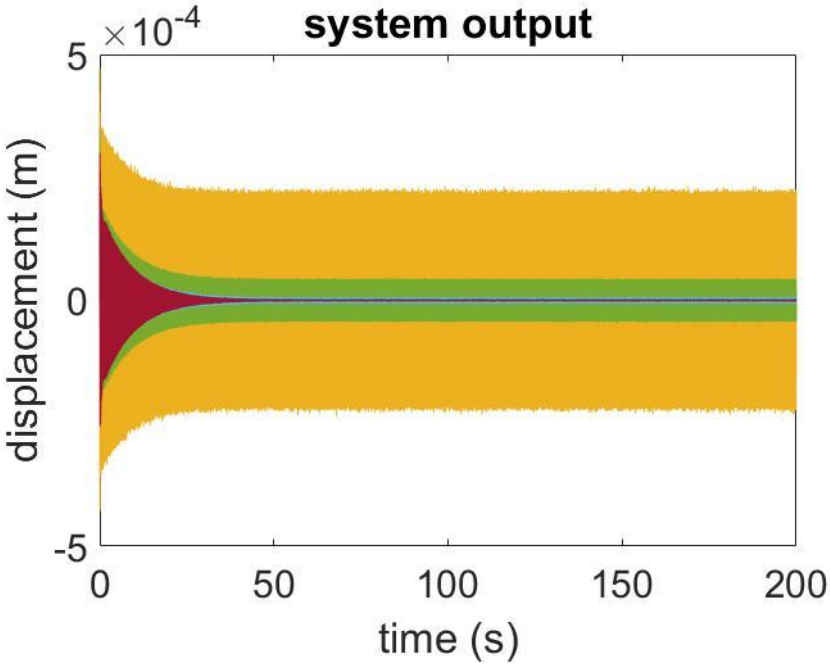

(a)

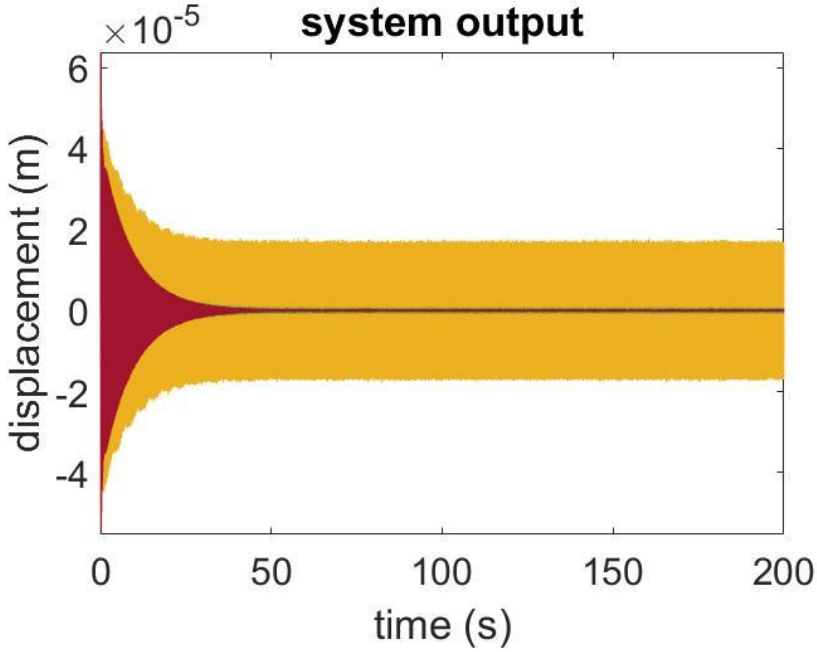

(b)

Figure 5.20: Response of each degree of freedom to a harmonic excitation with a frequency of (a) 90 Hz and (b) 200Hz, with 3% noise in output.

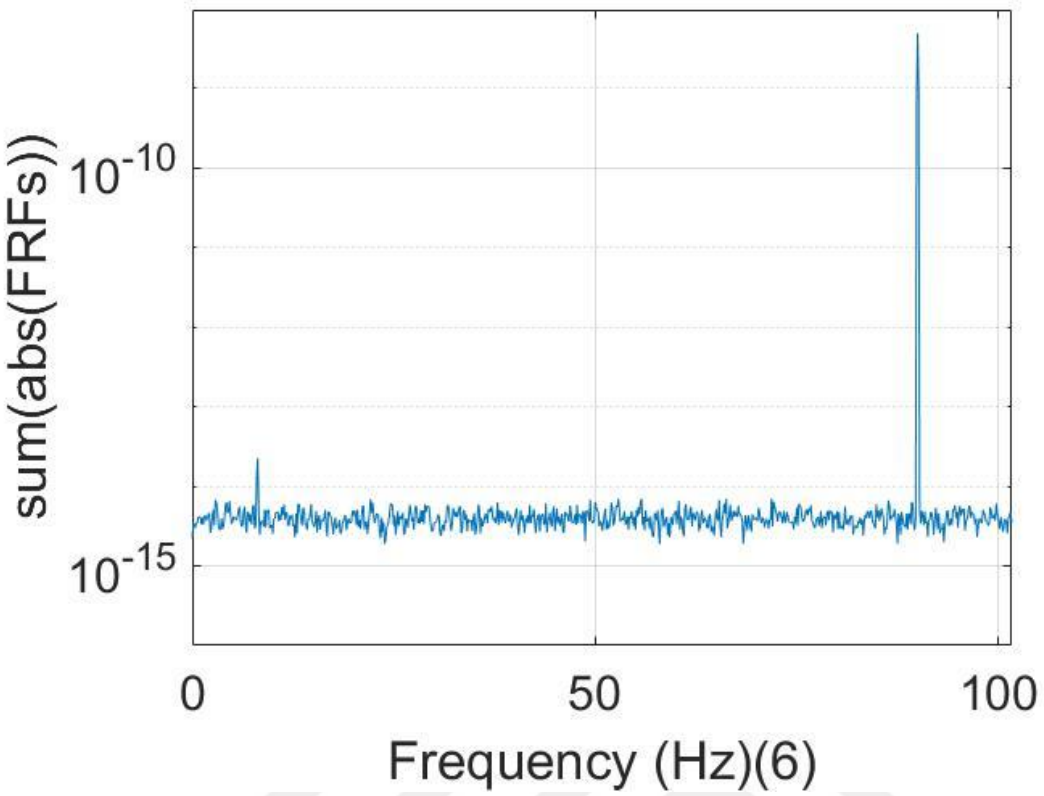

(a)

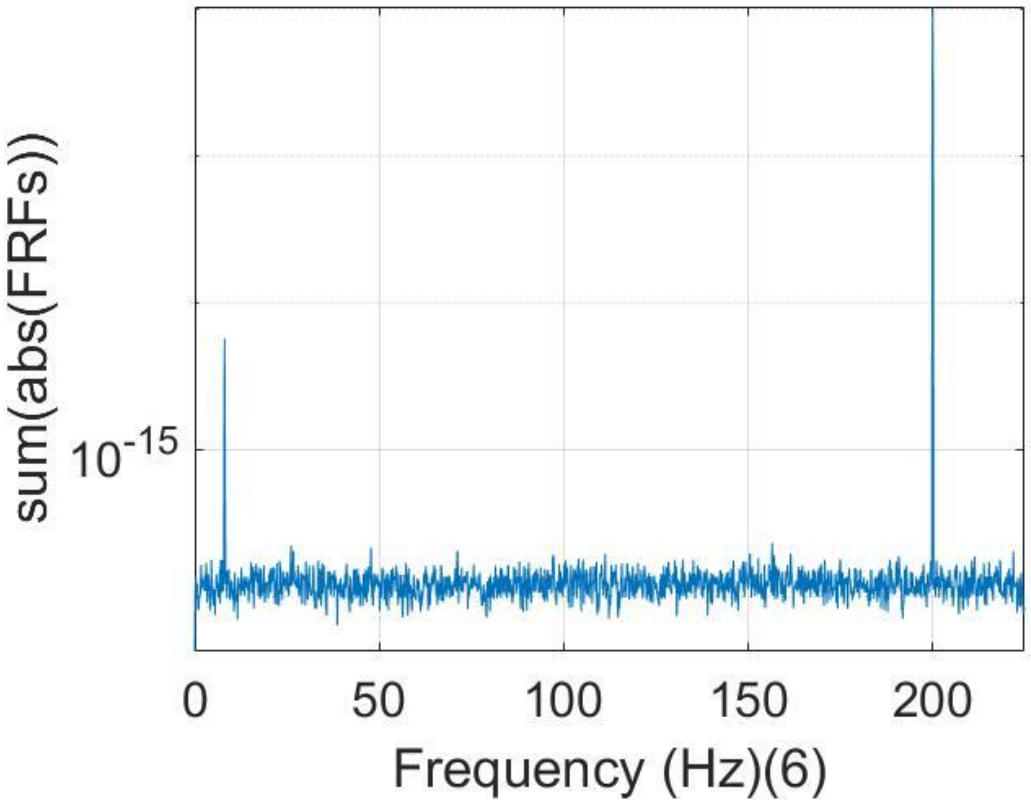

(b)

Figure 5.21: Sum of the FRF estimation of each dof with an excitation frequency of (a) 90Hz. (b) 200Hz.

An interesting observation can be made when the signals' transient part is not chopped out; analytical modes present themselves visually in the case of 200 Hz excitation frequency. The FRF estimation in this case is incredibly sensitive to the selection of the reference dof, and 1st dof is by far the most accurate one.

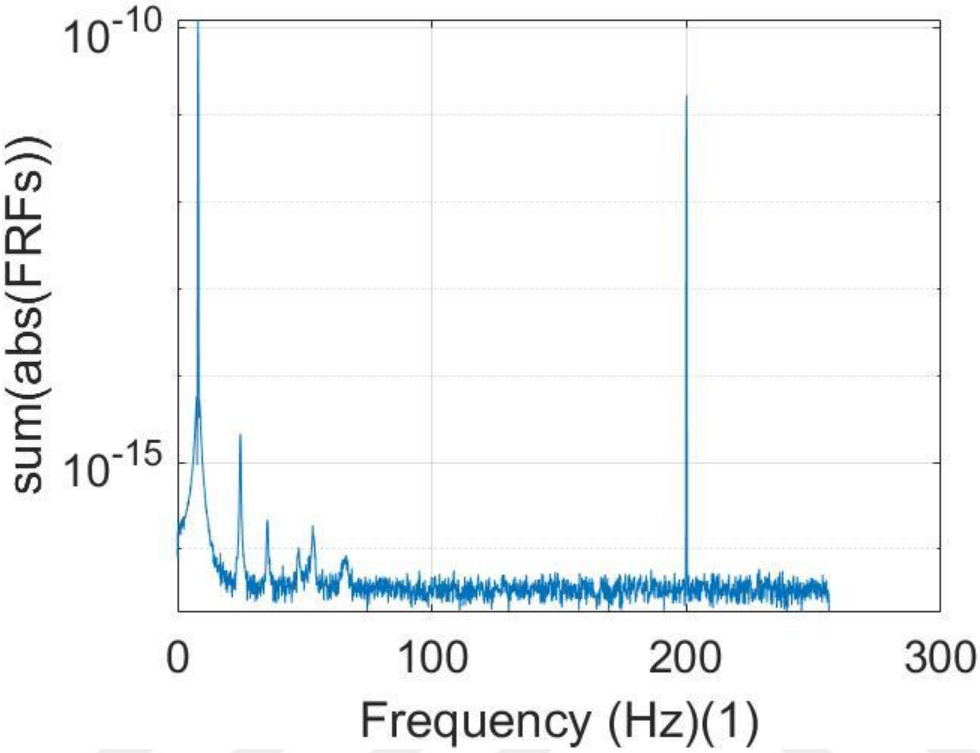

(c)

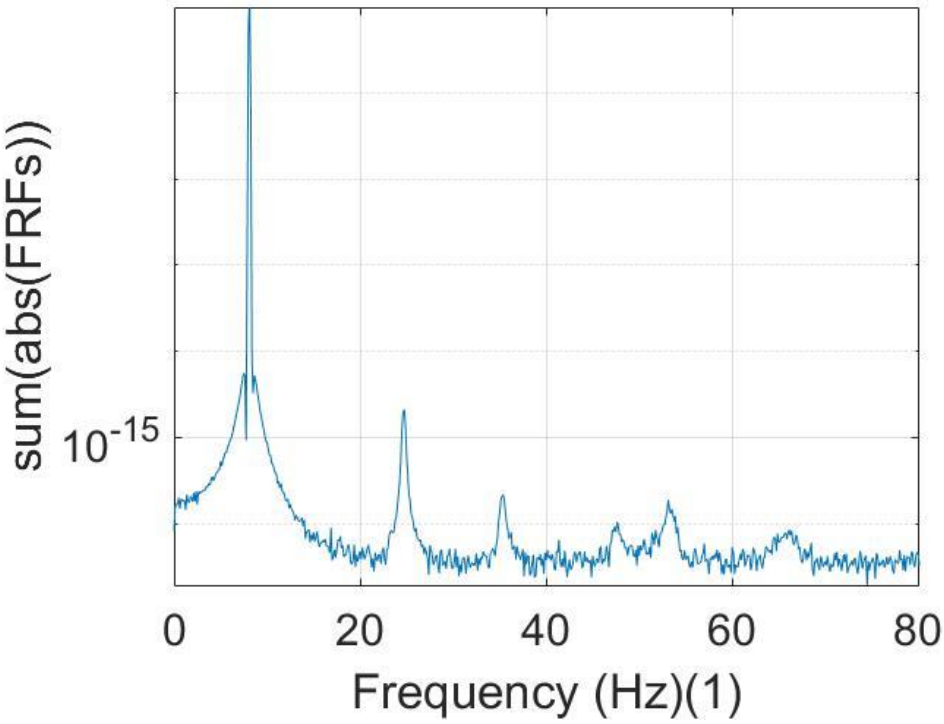

(d)

Figure 5.22: (c) Sum of the FRF estimation of each dof with an excitation frequency of 200Hz, transient signal included (d) zoomed in version to place emphasis on the frequency range up to 80Hz.

Unfortunately, the fact that the modes are visually present does not mean that they are detectable by the RFP-Z algorithm. Only the 1st and the 2nd analytical modes are extracted. With only 2 modes identified there is no point in evaluating the extracted modal parameters so that part is skipped.

Some conclusions can be made from this subchapter. The most obvious one is that OMA method does not work well when there is a harmonic input present. This is actually an expected conclusion because one of the required assumptions to use the OMA method is that the excitation signal must be a stochastic realization (white noise)[17][18]. As a consequence, RFP-Z algorithm cannot extract the modal parameters from the poor FRF estimations and thus when there is no possibility to perform EMA, usage of RFP-Z algorithm should be avoided for harmonic excitations.

Since this conclusion is reached, there is no point in continuing this subchapter with different noise levels and thus the next force typology will be observed.

5.3 Harmonic Excitation with Random Contribution

5.3.1 Excitation close to an eigenfrequency

The aim of this subchapter is to see if having a random force contribution may evade the inaccuracy problem seen in the case with only harmonic excitation. The typology of the force is mainly harmonic and there is a modest contribution of a stochastic random force. Precisely the amplitude of the harmonic force is $500N$ with a frequency of $10Hz$, whilst the random part utilizes a mean of $0N$ and a 99.7% probability to be within $\pm 15N$. It is worth noting that this random force contribution is not considered as noise because it is not directly manipulating the signal but rather is the force itself.

Just as the previous chapters the first case to be put under trial is applying a 3% noise in the output. The acquired response reported in fig. 5.23 shows a very high level of similarity to the response reported in fig. 5.13. 34th second can be taken as the beginning of the steady-state response.

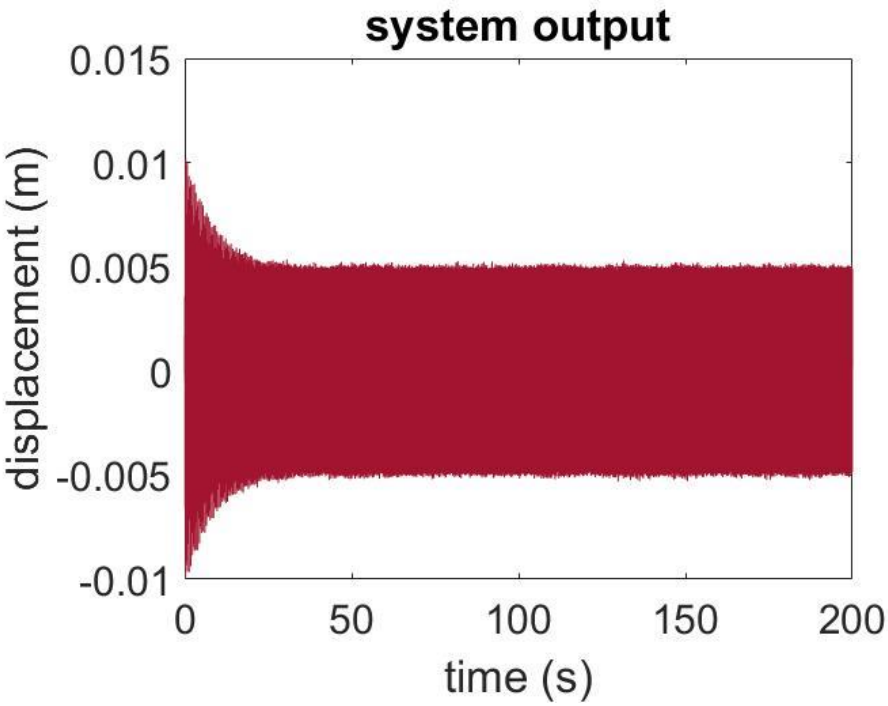

Figure 5.23: Response of each degree of freedom to a harmonic excitation with a frequency of 10Hz, with 3% noise in output.

Visually speaking, the FRF estimations of this response are very inaccurate. By setting the reference dof as 7, 2 analytical and 1 virtual mode can be seen(fig. 5.24) but the FRF does not resemble the analytical FRF.

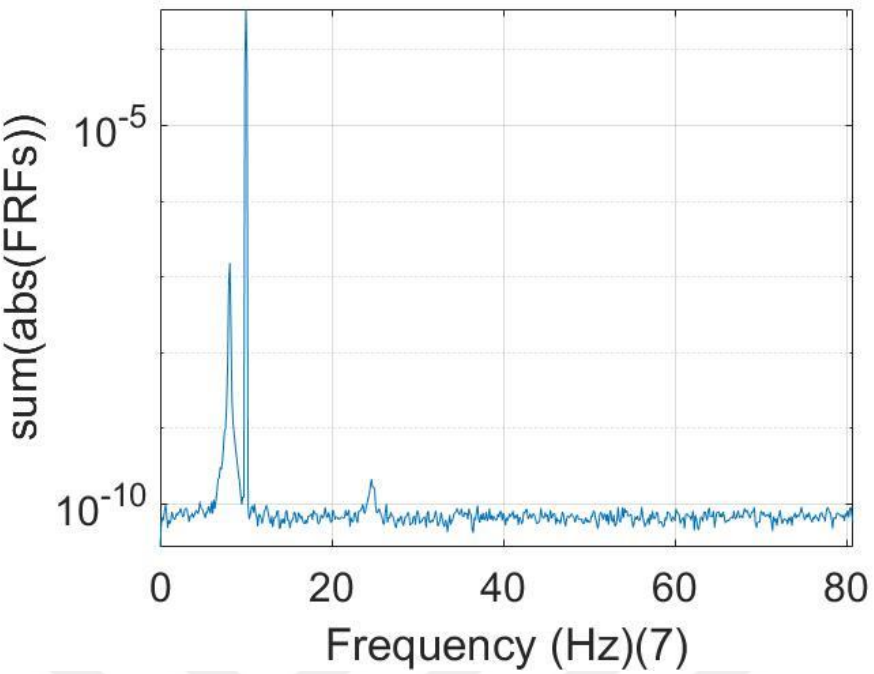

Figure 5.24: Sum of the FRF estimation of each dof with an excitation frequency of 10Hz.

The random force is then increased tenfold to check if it would enhance the FRF estimation. Resulting response (fig. 5.25), while still giving hints of a steady-state behaviour after a transient decay, is clearly more random in nature. 40th second marks the end of the initial decay.

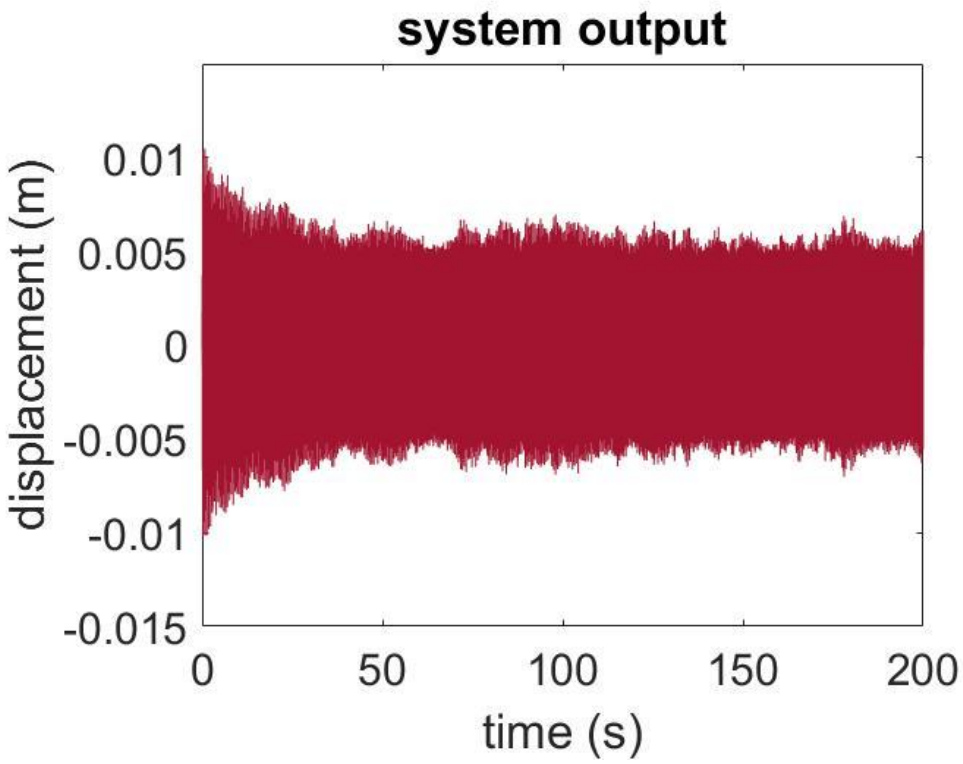

Figure 5.25: Response of each degree of freedom to a harmonic excitation with a frequency of 10Hz, with 3% noise in output.

There is a noticeable improvement in the FRF estimation when the 1st dof is selected as the reference one (fig. 5.26). Apart from the fact that one of the twin modes is lost, all the other analytical modes are estimated correctly. Also, the virtual mode is not extracted between the model orders 43-70.

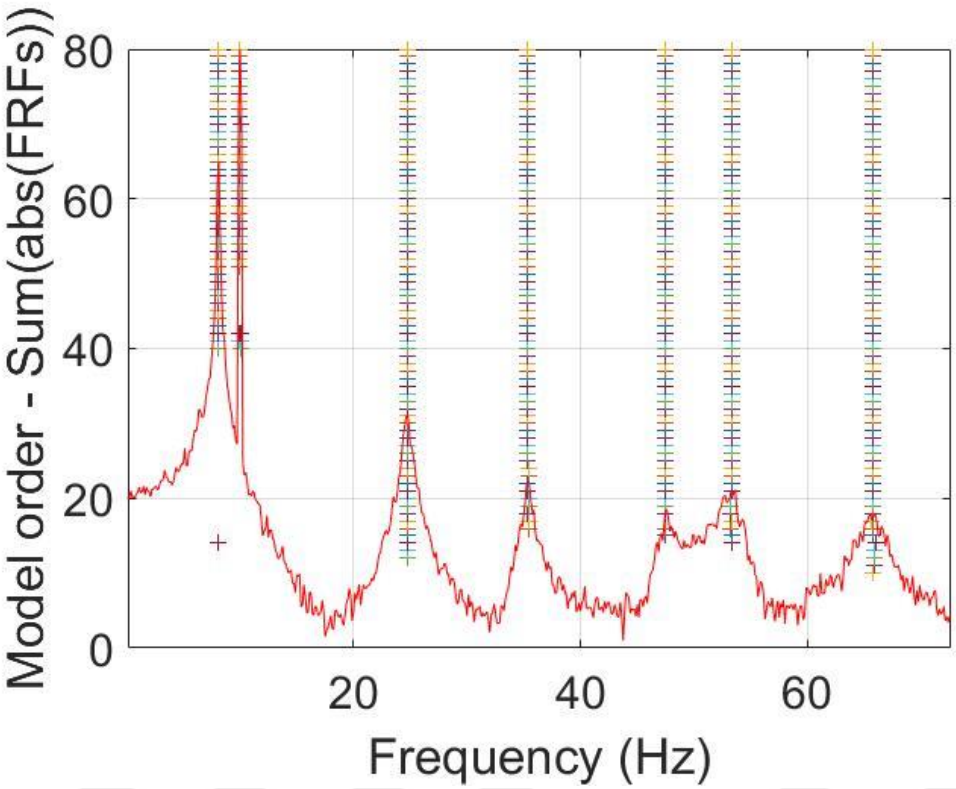

Figure 5.26: Response of each degree of freedom to a harmonic excitation with a frequency of 10Hz, with 3% noise in output. Crosses represent the detected mode for a certain model order.

The FRF built by the identified parameters will be far from reality because of the missing modes, but the identified modes' parameters (table 5.8) are not completely inaccurate. Not surprisingly the natural frequencies all exhibit a good accuracy. The damping ratios of modes 2, 3, 6 and 7 are all underestimated, but the level of the underestimation is milder with respect to the previous instance. 5th and especially 1st modes have their damping ratios underestimated greatly.

MODE	1	VIRTUAL	2	3	5	6	7
f_n $[Hz]$	8.11	10.00	24.72	35.34	47.41	53.40	65.70
ζ	0.07%	0.0014%	1.41%	1.14%	0.76%	1.28%	1.36%

Table 5.8: Extracted modal parameters (reference dof:1 model order:58).

The MAC matrix can be observed in table 5.9. The detected separate modes' shapes are identified with an accuracy similar to that of chapter 5.1 and they are all within acceptable ranges. The virtual mode stands out due to its extremely low damping ratio. The identified mode shape of the twin mode shows only 48% of congruency with the analytical one, and this result highlights again that this combination of methods cannot detect modes which are close to each

other with a good accuracy. Another interesting finding is that: the extracted mode shape of the virtual mode shows 91% similarity to that of the 1st analytical mode, due to both having not distant natural frequencies while possessing low damping (hence a good separation).

	1	2	3	4	5	6	7
1	0.9991	0.0018	0.0030	6.1716e-04	9.8427e-04	0.0082	2.1252e-04
2	0.9130	0.0232	0.0300	0.0342	0.0161	0.0170	0.0099
3	0.0075	0.9920	0.0024	0.0015	0.0016	0.0017	0.0011
4	0.0277	0.0300	0.9086	0.0079	0.0042	0.0150	0.0152
5	0.0076	0.0042	0.0131	0.0134	0.4916	0.3295	0.0865
6	0.0058	0.0045	0.0031	1.5333e-04	0.0085	0.9631	0.0321
7	0.0014	0.0026	0.0030	7.4049e-04	5.4579e-04	0.0327	0.9716

Table 5.9: MAC Matrix related to the table 5.8.

5.3.2 Excitation far from an eigenfrequency

Considering the accuracy level of the previous test, it would be interesting to analyse the preceding situation where the excitation frequency is far away from any natural frequency (200 Hz to be exact) so that the virtual mode can not affect the extraction of analytical modes. Keeping all the other parameters of the force same, the resulting time domain response is reported in figure 5.27. Expectedly the response is 2 orders of magnitude weaker, and the steady-state behaviour cannot be observed.

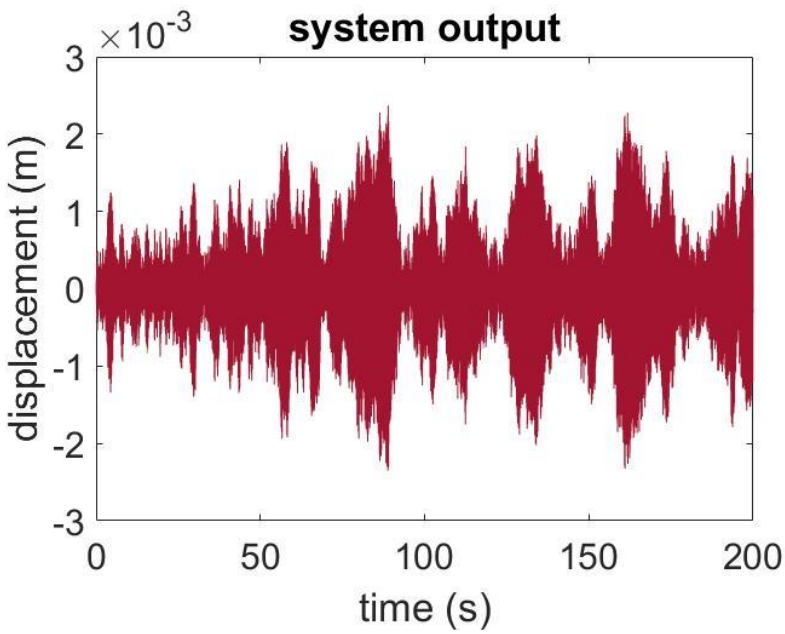

Figure 5.27: Response of each degree of freedom to a harmonic excitation with a frequency of 200Hz, with 3% noise in output.

The FRF estimation from the response and the consequent stabilization diagram can be seen is fig. 5.28 (with dof #4 as the reference). Unlike the previous situation the first mode is detected from a lesser model order. Table 5.10 reports the extracted parameters. Same degree of underestimation in 1st and 4th modes damping ratio as the previous instances is observed. The MAC matrix (table 5.11) highlights very high similarity in separate modes' shapes and poor relevancy between the twin mode shapes. These findings are nearly identical to the results in chapter 5.1.1.

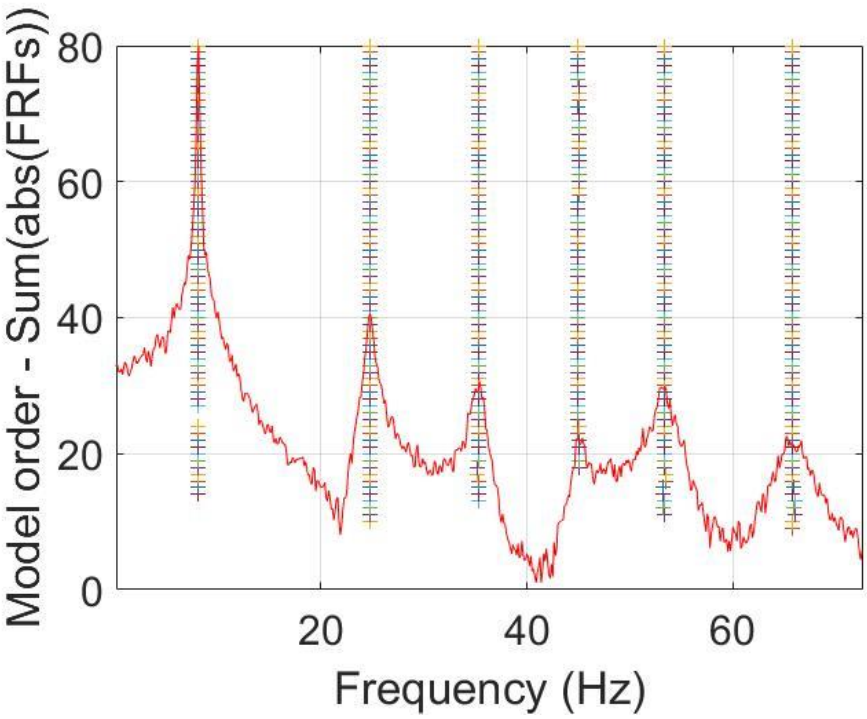

Figure 5.28: Response of each degree of freedom to a harmonic excitation with a frequency of 200Hz, with 3% noise in output.

MODE	1	2	3	4	6	7
f_n $[Hz]$	8.11	24.74	35.31	44.98	53.34	65.71
ζ	0.056%	1.38%	1.44%	0.87%	1.42%	1.74%

Table 5.10: Extracted modal parameters (reference dof:4 model order:77).

	1	2	3	4	5	6	7
1	0.9990	0.0034	0.0028	1.0024e-04	0.0010	0.0054	2.8148e-04
2	0.0072	0.9924	0.0022	0.0022	0.0019	0.0013	0.0015
3	0.0153	0.0382	0.9171	0.0062	0.0078	0.0151	0.0129
4	0.0130	0.0213	0.0414	0.3602	0.0841	0.2943	0.0890
5	0.0077	0.0018	0.0015	1.9311e-04	0.0056	0.9569	0.0447
6	0.0014	0.0025	3.9793e-04	0.0016	1.5172e-04	0.0300	0.9772
7	NaN	NaN	NaN	NaN	NaN	NaN	NaN

Table 5.11: MAC Matrix related to the table 5.10.

5.3.3 High excitation frequency with high output noise

Further increasing the noise level in the output signals yield the response see in the fig. 5.29.

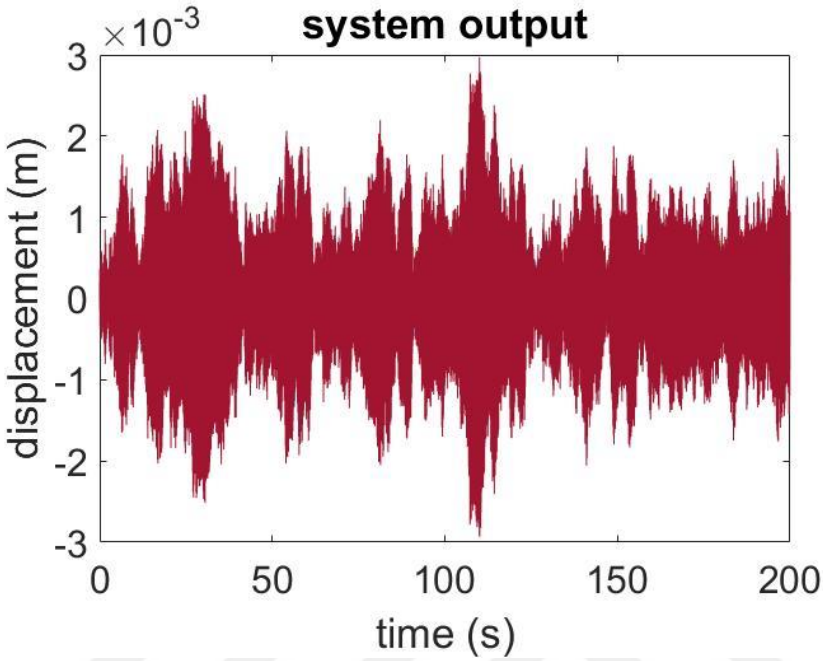

Figure 5.29: Response of each degree of freedom to a harmonic excitation with a frequency of 200Hz, with 10% noise in input and output.

Again, the best FRF estimation belongs to the situation where the 4th dof is the reference. One obvious observation is that there is only 5 detected analytical modes (fig. 5.30). The levels of estimated damping ratios are not considerably different than those of the previous cases. This can be examined in fig. 5.31. Although it can be examined that the damping estimation of 7th analytical mode is severely affected by the noise and is underestimated.

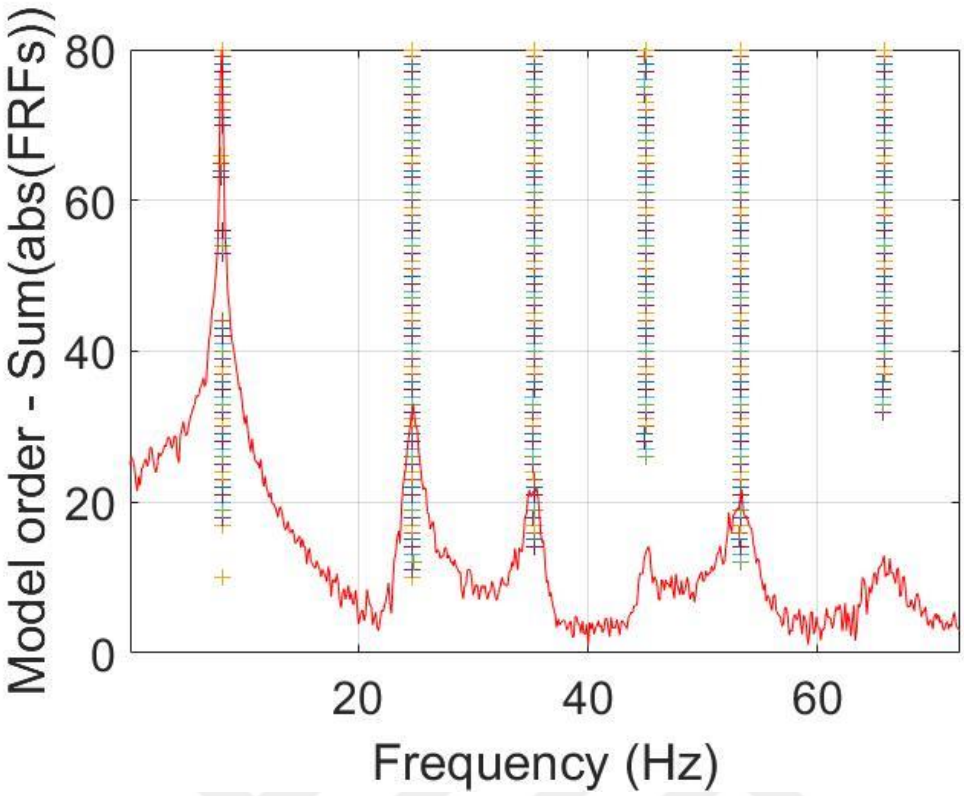

Figure 5.30: Stabilization chart over the response of the system to a harmonic excitation with a frequency of 200Hz, with 10% noise in input and output (reference dof #4).

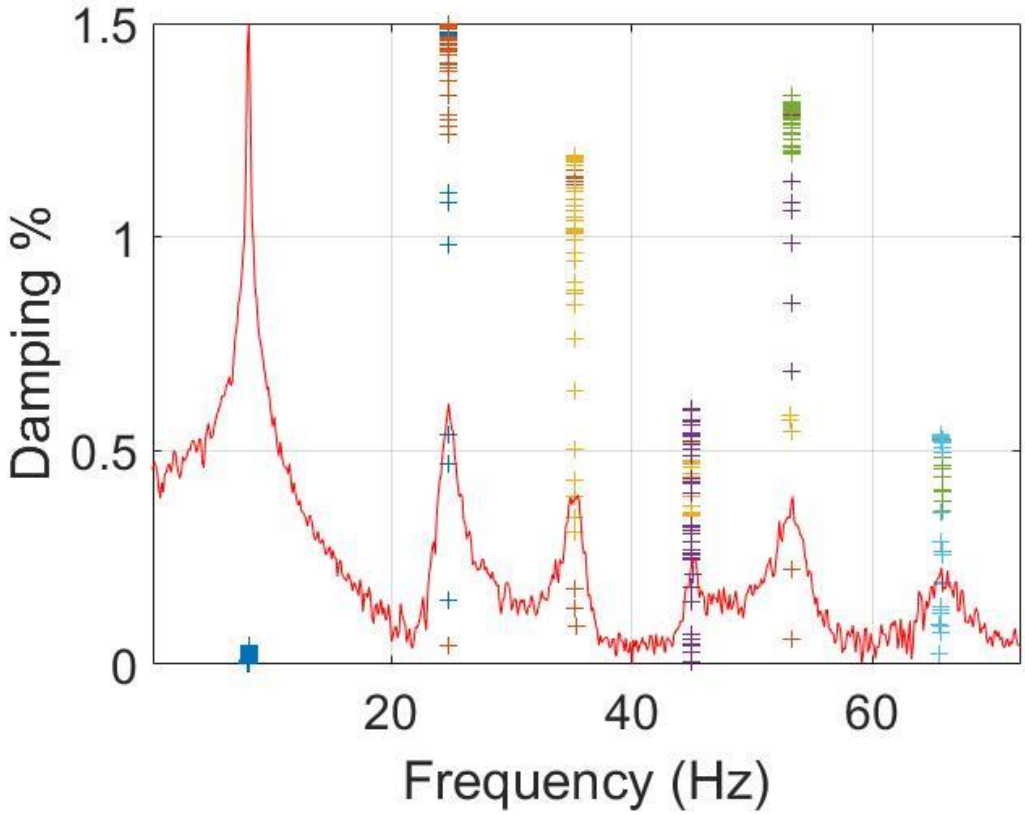

Figure 5.31: Extracted damping ratios over the response of the system to a harmonic excitation with a frequency of 200Hz, with 10% noise in input and output (reference dof #4).

5.4 Inaccuracies Related to Spectral Line Density

Until this point, the analysis of the combination of cross power spectral density FRF estimation and RFP-Z modal parameter extraction has yielded some unexpected results . In the case of purely random excitation, the extracted damping ratio of the first mode is severely underestimated, causing it to dominate any constructed FRF. This phenomenon resulted in the observation that this combination of methods is way more inaccurate than they really are. Also, it hindered the visual analysis of the constructed FRF since the only significant peak is the first one.

We have encountered another similar abnormality in this case of harmonic input; the extracted damping ratio of the virtual mode, which basically a tall and very localized spike in the estimated FRF, is expected to be extemely low, but we have obtained a result in the range of 1-2%.

The former abnormality is a severe underestimation of the expected value while the second one is a harsh overestimation. This may seem like they originate from different roots due to having opposite trends, but taking a step back hints their common property; both abnormalities occur in peaks which are relatively tall and steep, as if there are not enough spectral lines in the estimated FRF to model those peaks with a good resolution.

The number of generated spectral lines was set to 2^{12} throughout this chapter and this value was not altered at any point to keep the results consistent. Very often technicians say that it is good to have a small spectral line amount for low computational burden and a smooth FRF, but in the particular cases mentioned above it might be necessary to boost the spectral line amount as it will improve the fitting. This value is set to 2^{15} as it is a nice compromise between the resolution and computational efficiency.

Another important consideration is that the lower limit of the frequency band to analyse f_{min} should not be too near to the peak itself, otherwise there can be a loss of data. The peaks in question are close to 8 Hz and 10 Hz, so a low f_{min} value is necessary. This parameter is set to 2 Hz, as it is suitable and realistic; most of the accelerometers cannot sense frequencies lower than that value.

With the aim of recreating the random excitation case, fig. 5.32 underlines why it is generally considered better to not exaggerate the spectral line count. Due to a higher resolution the resulting graph is verry rugged. Moving this estimation to the RFP-Z algorithm and setting the upper frequency analysis band to 20 Hz yields the damping ratio extractions seen in fig. 33. The improvement with respect to the previous cases is obvious. As the model order reaches 43, the identified damping ratio is 0.20 which is really close to the analytical value of 0.22.

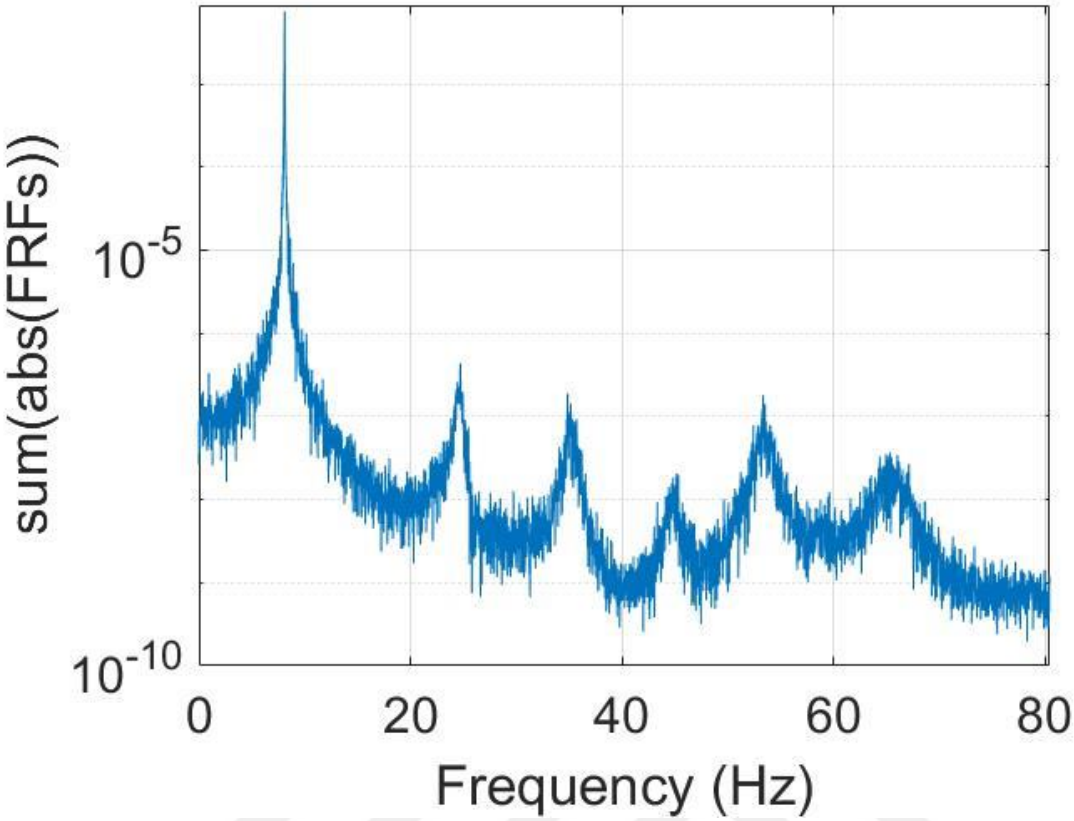

Figure 5.32: FRF Estimation of a purely random excitation with 2^{15} spectral lines.

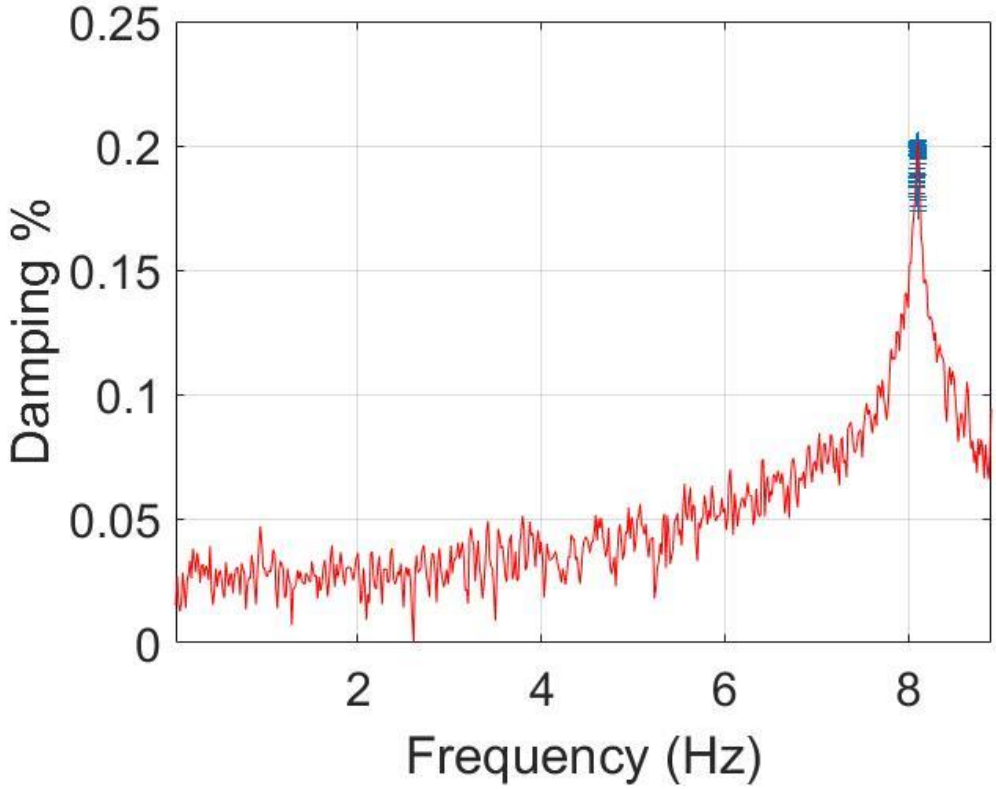

Figure 5.33: 1st damping ratio extraction of fig. 5.32.

Although this represents a very significant increase in the accuracy of the 1st mode's parameter extraction, other peaks are affected in an opposite manner. Increased jaggedness of the FRF estimation hinders the extraction performance of the remaining damping ratios, causing them to be underestimated. The twin mode is not even detected. This observation is backed by the data reported in table 5.12. Since the natural frequencies are always accurate in the same level only the damping ratios of the high sld (spectral line density) case is reported. It is worth noting that the 1st damping ratio is now extracted as 0.17%, this is a result of changing the upper frequency band limit.

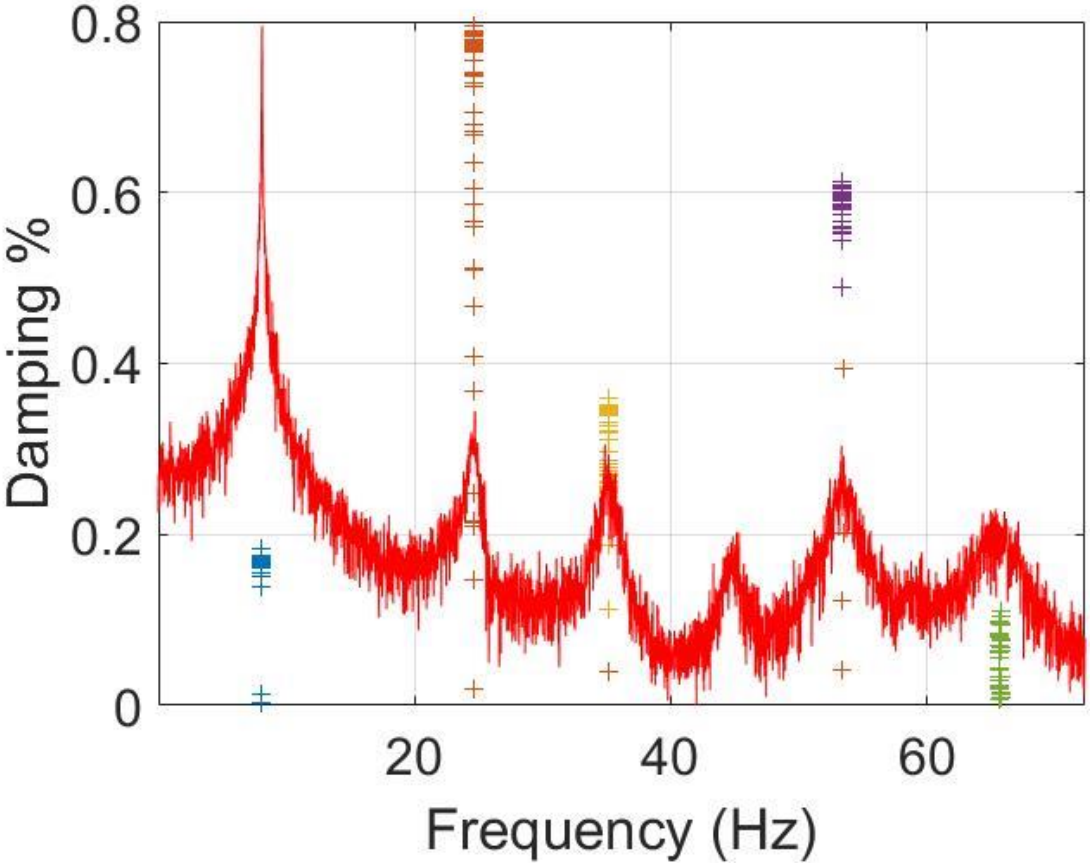

Figure 5.34: Damping ratio extractions of all detected modes in fig. 5.32.

MODE	1	2	3	4	6	7
f_n $[Hz]$	8.12	24.71	35.29	45.02	53.46	65.88
$\zeta_{low\ sld}$	0.016%	1.21%	1.44%	0.42%	1.64%	1.96%
$\zeta_{high\ sld}$	0.17%	0.72%	0.34%	-	0.58%	.01-.12%

Table 5.12: Extracted modal parameters (reference dof:6).

Observations related to the MAC matrix are not reported because there are not any significant changes.

Repeating the same procedure for the case with a harmonic excitation at 10 Hz gives the damping ratio extractions depicted in fig. 5.35. The values are extremely low, but this is exactly what is expected in this case.

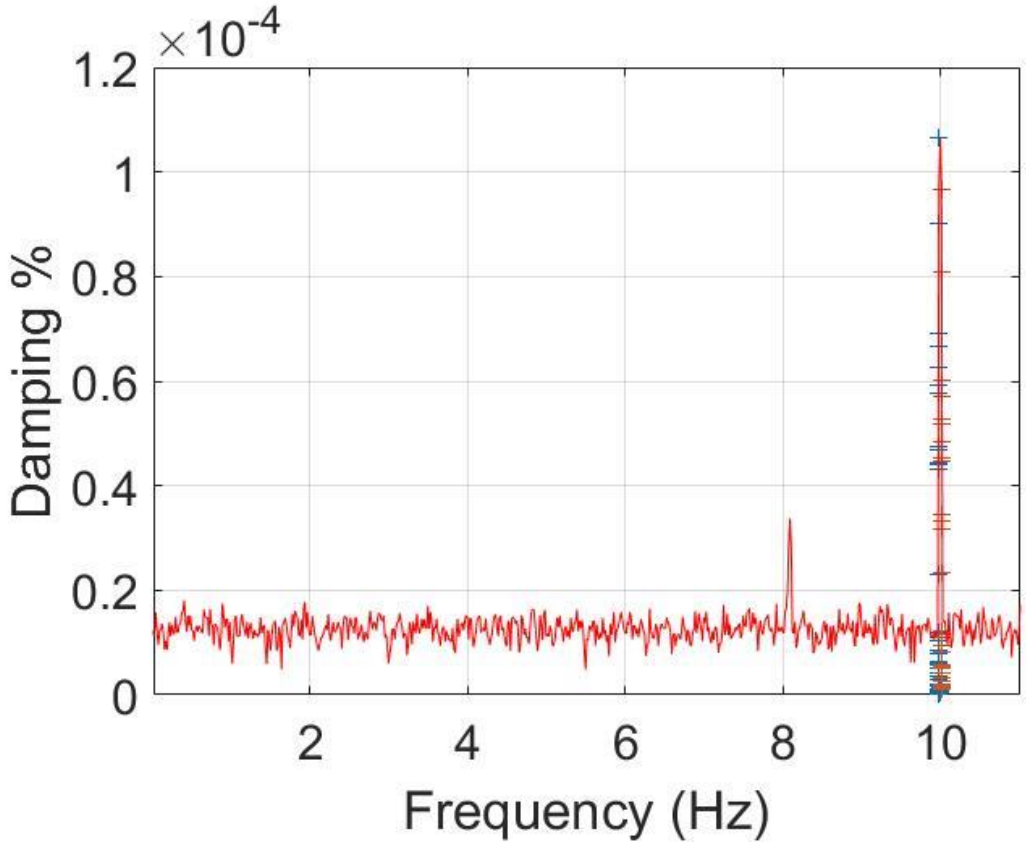

Figure 5.35: Extracted damping ratios of the harmonic excitation virtual mode.

According to these findings, we can conclude that increasing the spectral line density is necessary when the parameters of localized steep peaks are to be extracted.

5.5 Final Remarks

Chapter 5 yields several conclusions about the compatibility of RFP-Z method with OMA method under various circumstances. The most obvious result is that the natural frequencies and mode shapes of well separated modes are extracted very accurately. In the case of twin modes one of them is lost: the detected natural frequency is reasonably accurate while the mode shape is very poorly correlated. A limited amount of noise such as 3% output does not affect the accuracy considerably but elevating the noise to the higher level damages the parameter extraction process. Noise in the input signal is completely irrelevant.

The damping ratio remains the main problem in modal parameter identification. All the analytical modes in our system are underdamped. This poor result is not related to the model order. In the first subchapter, about the purely random excitation, raising the maximum model order is not mentioned to avoid repetition, but in fig. 5.36 it can be seen that increasing model order beyond 30 only slightly increases the accuracy of the 1st mode's damping estimation initially and then it decays by increasing the model order further. This inaccuracy should be considered as an exception and its cause and remedy is thoroughly discussed in chapter 5.4. Conversely the 4th mode's extraction seems to improve with the increasing model order. It approaches to 1%, but even elevating the model order up to 80 does not bring it to an acceptable range.

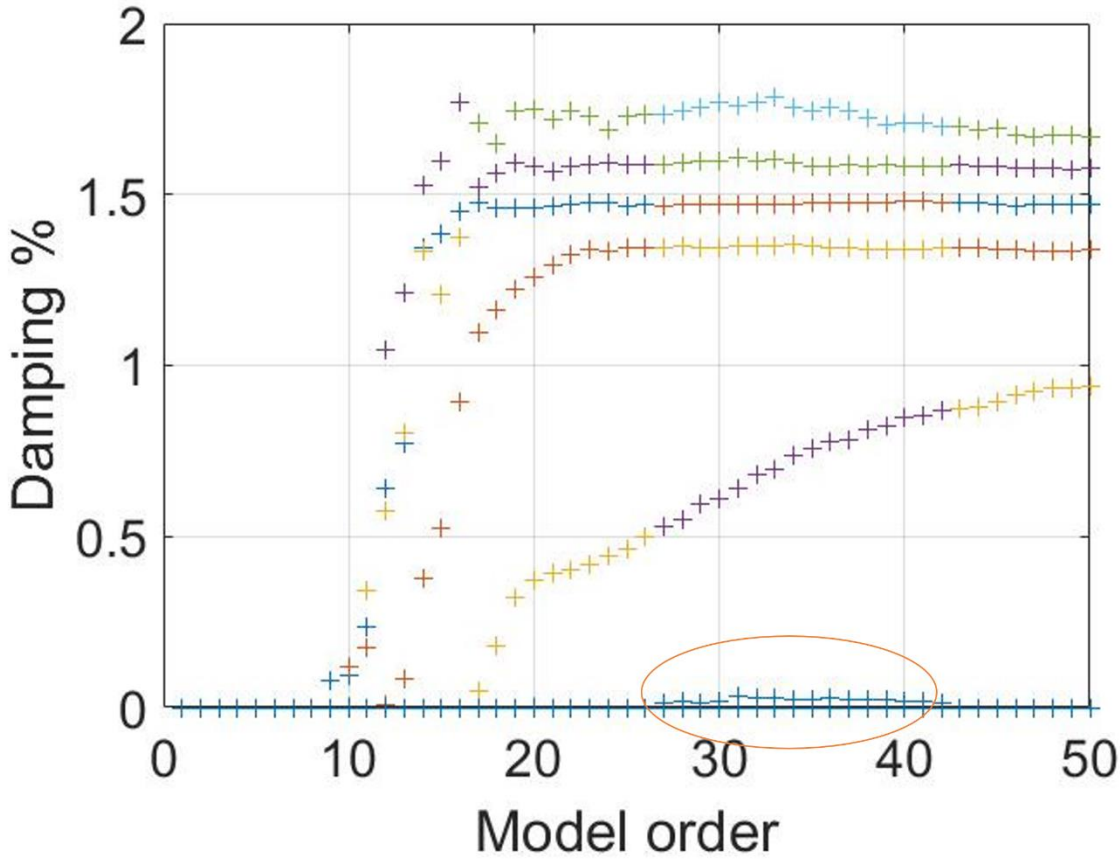

Figure 5.36: Effect of model order on the extracted damping ratios.

Another result underlined in this chapter is that the OMA method is not suitable when only a harmonic excitation is present. This not surprising result is already a fundamental knowledge in the scientific literature.

Combining the harmonic excitation with a random one might improve the quality of RFP-Z method. The random force contribution needs to be big enough to render the force signal stochastic. Another requirement is about the excitation frequency; if it is close to an analytical mode's resonance frequency it makes the mode undetectable by the algorithm. Additionally, an excitation frequency close to the first few harmonics of any mode should be evaded if possible. In any case having a harmonic force contribution will create a virtual mode at the excitation frequency.

In the case of a combination of a random and a harmonic force, noise sustains its effect. At low noise levels OMA and RFP-Z method generate result with the same accuracy of the case with only a random force factor. Increasing the noise decreases the accuracy in the same way.

6. Verification of RFP-Z in the Input-Output Case

In contrast to the previous one, this chapter will analyse the accuracy of the RFP-Z method with an EMA approach. All the mentioned characteristics above such as the force typology, magnitude and the noise level are maintained. An exception is the reference dof, because in EMA the input signal is also present ergo the use of Welch's Periodogram does not require an output signal to be selected as a reference.

An initial parameter that will be certainly interesting to tweak will be the noise level in the input signal. Alongside analyses similar to those in the previous chapter, whether the effect of the input noise is greater, equal or lesser than the output signal will be explored.

Executing a proper EMA in real life is a hard task as there are different complications. Besides the need of a proper test set up which may be expensive depending on the shape and size of the specimen, there is also the fact that sensors and shakers may influence the dynamic behaviour of the structure. This problem is even greater when there are not enough sensors/shakers to give excitation and receive output signals simultaneously. Using different batches of sensors/shakers may result in incoherent FRF in each experiment. Even with all these problems, it is very likely that especially a big structure is not eligible for experimental testing.

All the requirements and hardships mentioned in the paragraph above are shadowed by one thing; EMA is much more accurate than OMA since it uses more information. The results obtained in this chapter are expected to be more precise with respect to those of the previous one. A comparison between EMA and OMA in accuracy can be done once the results are reached.

6.1 Random Excitation

6.1.1 %3 Noise in Output

Just as in the previous case the first force typology to analyse is a purely random excitation. The noise level in the output is set to 3% and no noise is added in the input signal. The resulting response is seen in fig. 6.1.

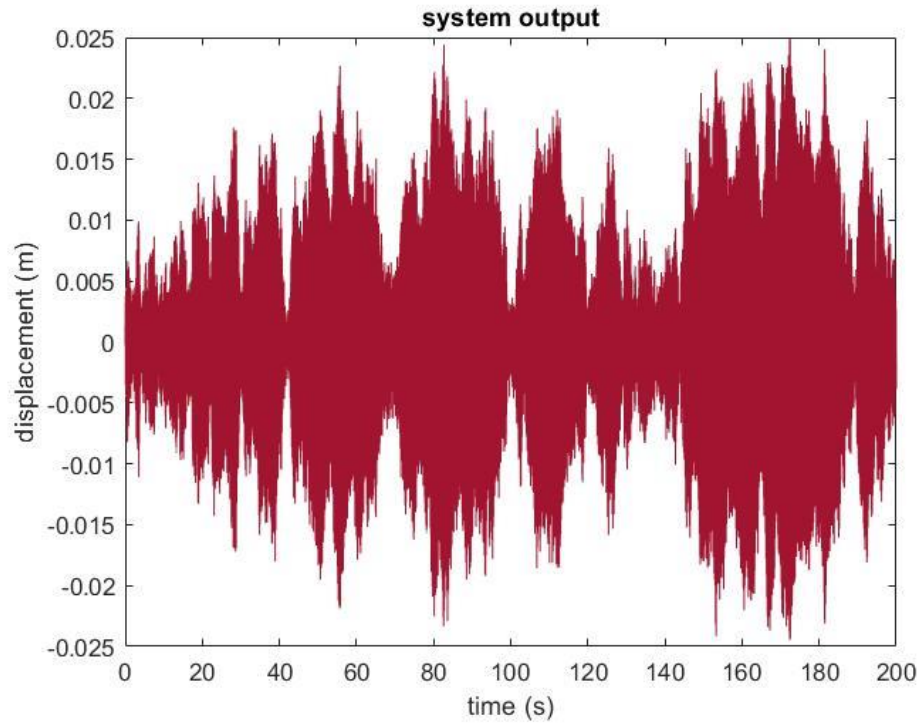

Figure 6.1: Response of each dof to a purely random signal with 3% noise in the output.

The accuracy enhancement due to passing to EMA method clearly shows itself in the estimated FRFs. In Figure 6.2 the stabilization chart obtained after running the RFP-z algorithm on the estimated FRF can be seen. The FRF itself visually shows a clear difference. It is precisely estimated and all of the analytical modes are detected, even the twin modes. Additionally, the morphology of the mode peaks is almost identical to the analytical FRF. The only obvious difference is the noise, especially when the response magnitude gets lower.

Besides from the ability to detect all the modes, combining RFP-z with EMA approach also excels in extracting the damping ratios. In fig. 6.3 the black circles represent the true location of the analytical damping ratios. Well separated modes are detected with an excellent precision. The twin modes' damping ratios are underestimated but the error is within acceptable levels, considering the orders of magnitude worth of errors in the previous cases. 1st modes' ratio draws attention because by utilizing OMA it could only be detected accurately with a high spectral density ratio, which in turn decreases the accuracy of the other modes.

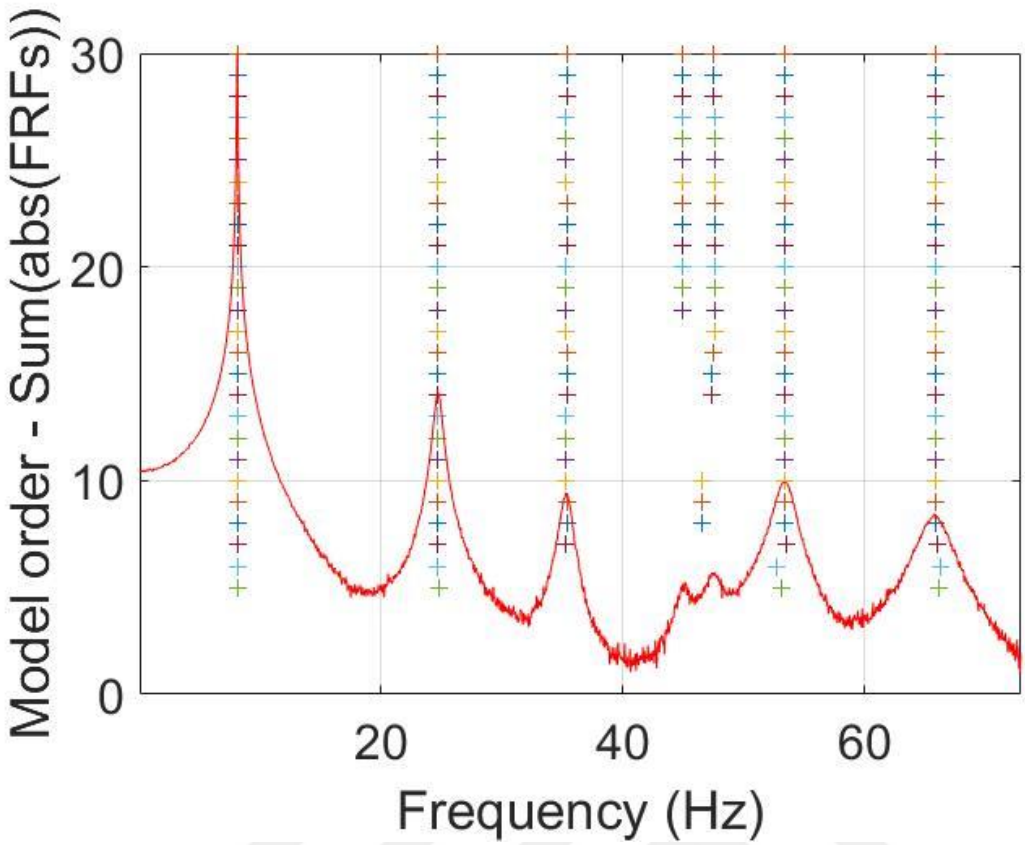

Figure 6.2: FRF estimation of fig. 6.1 overlaid with the detected modes (stabilization chart).

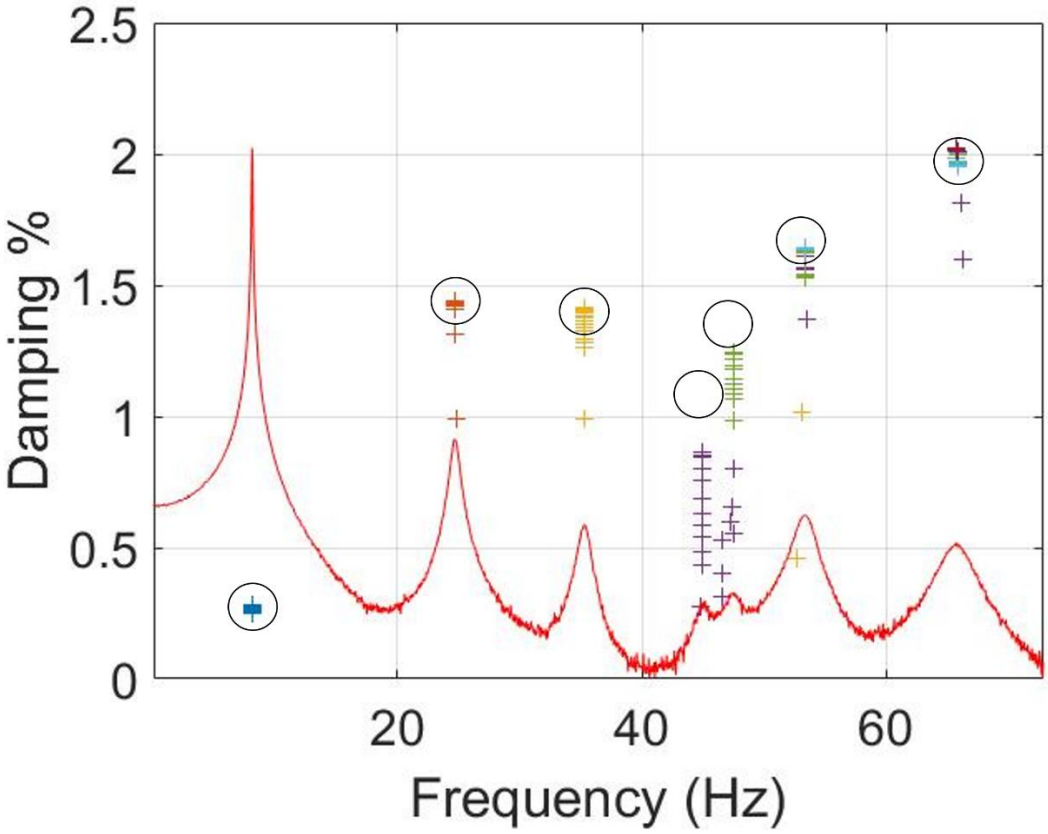

Figure 6.3: FRF estimation of fig. 6.1 overlaid with the detected damping ratios.

Among all the model orders the 30th one yields the best result in both having the minimum error in a least squares sense and the damping ratio accuracy. It should be noted that the difference in model orders is not as steep as in the OMA case, apart from the twin modes all the frequencies and the damping ratios are detected within a narrow range in each model order, save few exceptional cases.

The acquired modal parameters can be seen in table 6.1. The last row indicates the difference between the damping ratios in this table and table 5.1. The analytical modes 2, 3, 6 and 7 show an excellent accuracy. Modes 4 and 5 suffer from a nonnegligible error, due to being so close together. Mode 1 also shows a considerable amount of error. The frequency values in the other hand show superb similarity to the analytical values.

MODE	1	2	3	4	5	6	7
f_n $[Hz]$	8.09	24.71	35.32	44.97	47.52	53.40	65.81
ζ	0.25%	1.44%	1.42%	0.86%	1.24%	1.65%	2.02%
DAMPING ERROR	12%	0%	0.7%	25.2%	10.1%	2.5%	2.5%

Table 6.1: Extracted modal parameters (model order:30).

The effects of increasing the model order can be seen in fig. 6.4. There is an improvement in the accuracy as the model order is increased until model order 40. A least square approximation announces that model order 38 is the most accurate one. Its associated extracted modal parameters are reported in table 6.2.

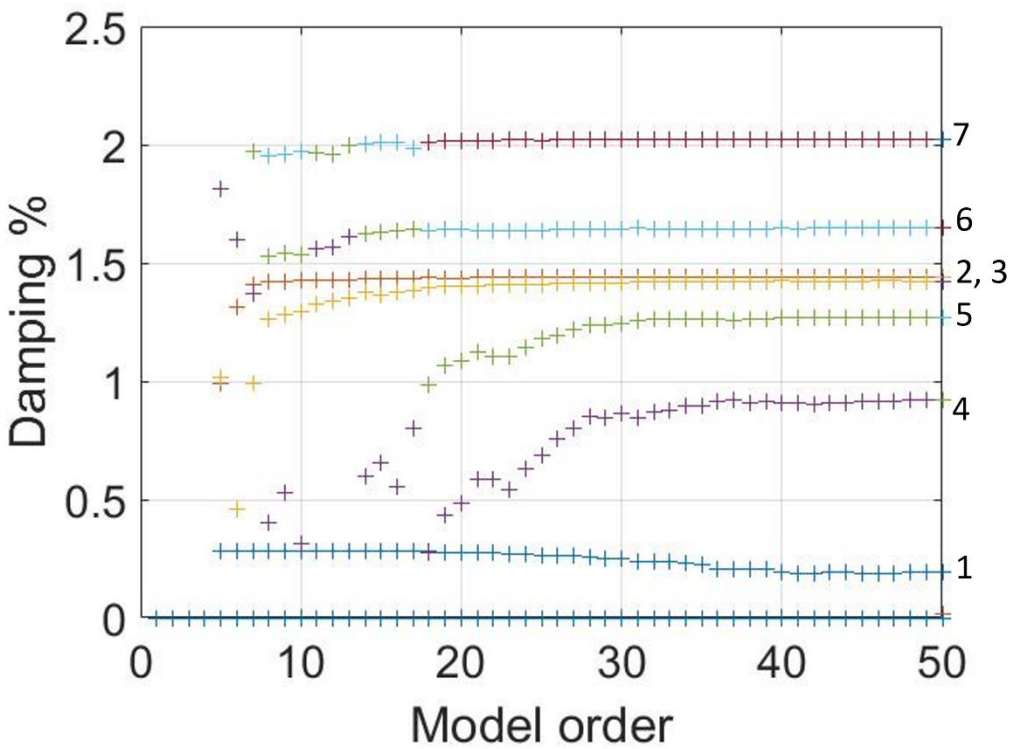

Figure 6.4: Effect of model order on the extracted damping ratios.

MODE	1	2	3	4	5	6	7
f_n $[Hz]$	8.09	24.71	35.31	44.99	47.52	53.40	65.81
ζ	0.21%	1.43%	1.40%	0.92%	1.27%	1.64%	2.01%
DAMPING ERROR	4.5%	0.7%	2%	20%	8 %	1.9%	2 %

Table 6.2: Extracted modal parameters (model order:38).

Using the 38th model order decisively improves the results. Error of the 1st mode is pulled down to acceptable levels. While the twin modes' ratios still have an undeniable level of error, the accuracy is improved with the change in the model order.

To analyse the truthfulness of the extracted residues the MAC matrix seen in table 6.3 is to be evaluated. Mode shapes demonstrate a remarkable accuracy. The extracted shapes of the well separated modes are nearly identical while the twin modes' shapes show a similarity of 98.5%. These findings clearly represent the viability of RFP-z algorithm with EMA with low noise on output.

	1	2	3	4	5	6	7
1	0.9972	0.0024	0.0022	3.5258e-05	0.0011	0.0045	0.0022
2	0.0019	0.9998	0.0016	0.0017	0.0018	0.0012	1.8804e-04
3	0.0026	0.0018	0.9984	2.0659e-04	0.0043	6.3579e-04	1.4840e-04
4	5.7004e-04	0.0055	5.7077e-04	0.9849	9.8034e-04	0.0026	0.0011
5	9.0549e-04	0.0015	0.0037	0.0011	0.9901	0.0032	0.0030
6	0.0056	0.0012	1.9591e-04	2.1205e-04	0.0015	0.9983	2.8693e-04
7	8.6399e-05	9.8663e-05	3.1020e-04	0.0012	1.6698e-04	2.7211e-04	0.9977

Table 6.3: MAC Matrix related to the table 6.2.

The constructed FRF using aforementioned modal parameters is visually identical to that of the analytical FRF as it can be seen below.

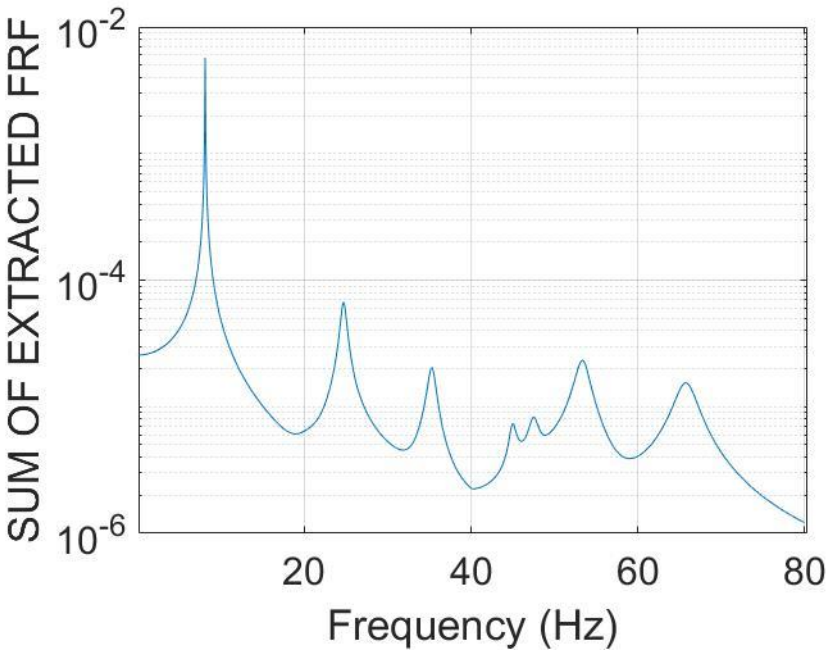

Figure 6.5: Constructed FRF in the case of 3% noise in the output (model order 38).

6.1.2 3% Noise in input and output

To test if noise in the input affects the accuracy while the input signal it is involved in the FRF estimation process, a 3% noise is included in it. The resulting time domain response can be seen in fig. 6.6.

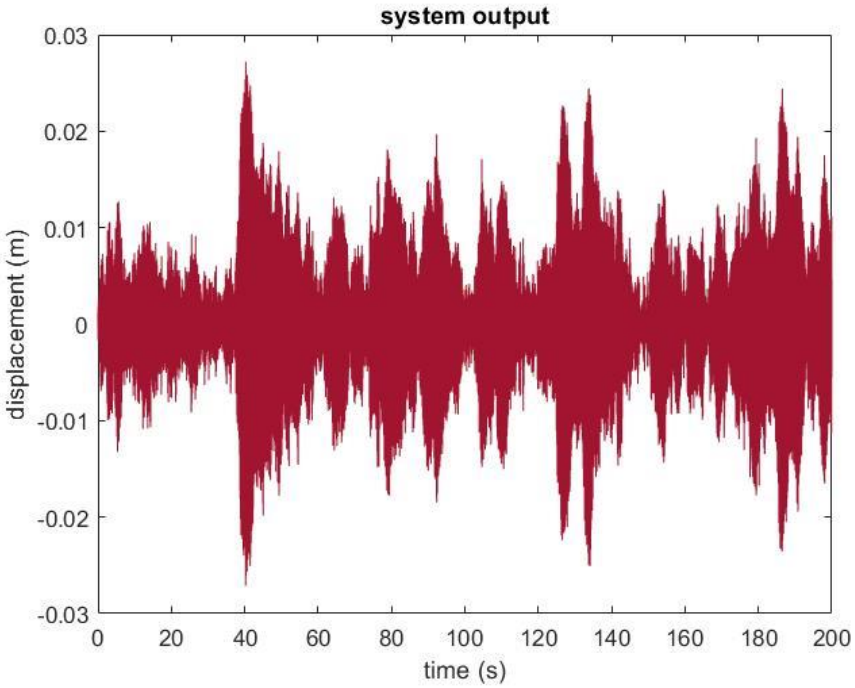

Figure 6.6: Response of each dof to a purely random signal with 3% noise in the input and the output.

To observe the effects of the model order, an iterative simulation is done until the 60th model order. In fig. 6.7 the trend of the damping ratios with an increasing model order can be seen. The most impactful effect after a certain order level is seen on the first damping ratio, and it is closest to reality in the 49th model order. In fact, that is also the most accurate modal order least-squares wise. Same figure also highlights that the 7 analytical dofs are successfully extracted in most of the model orders.

The estimated modal parameters are reported in table 6.4.

MODE	1	2	3	4	5	6	7
f_n $[Hz]$	8.09	24.70	35.31	45.02	47.51	53.40	65.80
ζ	0.22%	1.44%	1.43%	1.00%	1.32%	1.65%	2.04%
DAMPING ERROR	0%	0%	0%	13%	4.3%	2.5%	3.6 %

Table 6.4: Extracted modal parameters (model order:49).

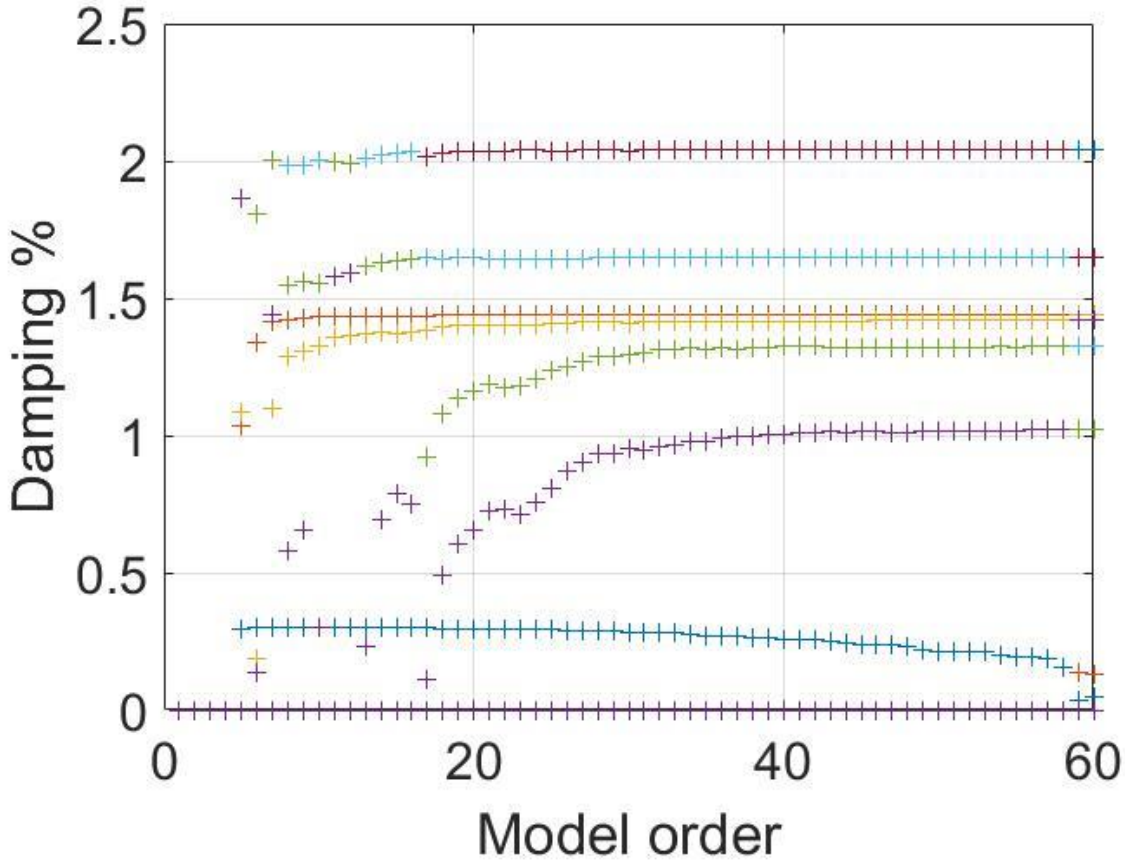

Figure 6.7: Effect of model order on the extracted damping ratios.

The results in the table above shows excellent extraction accuracy. However, it must be kept in mind that the increase in accuracy with respect to the case without the input noise is due to higher model order. To compare the results of two cases, the extracted parameters of the 38th model order is reported in table 6.5.

MODE	1	2	3	4	5	6	7
f_n $[Hz]$	8.09	24.70	35.31	45.01	47.52	53.40	65.80
ζ	0.27%	1.43%	1.42%	1.00%	1.31%	1.65%	2.04%
DAMPING ERROR	22.7%	0.7%	0%	13%	5.1 %	2,5%	3,6 %

Table 6.5: Extracted modal parameters (model order:38).

The fall in the accuracy is clearly seen in the first mode's damping ratio. In mode 2, 3, 6 and 7 there is no significant difference between 2 distinct cases. The damping ratio extractions of the twin modes are paradoxically more accurate in the case with the additional input noise.

The MAC matrix of the most accurate model order (#49) can be analysed below. The diagonal values show some variance with respect to those of table 6.3 but there is not any significant difference between accuracy levels.

	1	2	3	4	5	6	7
1	0.9982	0.0025	0.0031	6.0911e-05	0.0012	0.0065	9.9377e-04
2	0.0018	0.9998	0.0015	0.0017	0.0018	0.0013	2.2104e-04
3	0.0023	0.0019	0.9985	1.2700e-04	0.0046	4.8636e-04	8.7674e-05
4	2.0314e-05	0.0054	6.2429e-04	0.9865	4.7648e-04	0.0012	1.8795e-04
5	6.5227e-04	0.0016	0.0035	8.9195e-04	0.9899	0.0041	0.0022
6	0.0057	0.0011	2.1597e-04	1.8038e-04	0.0015	0.9980	2.2848e-04
7	9.9828e-05	1.2007e-04	3.3636e-04	0.0013	1.5684e-04	2.6893e-04	0.9975

Table 6.6: MAC Matrix related to the table 6.4.

Similar to the previous case without input noise, the constructed FRF is visually indifferentiable form the analytical one.

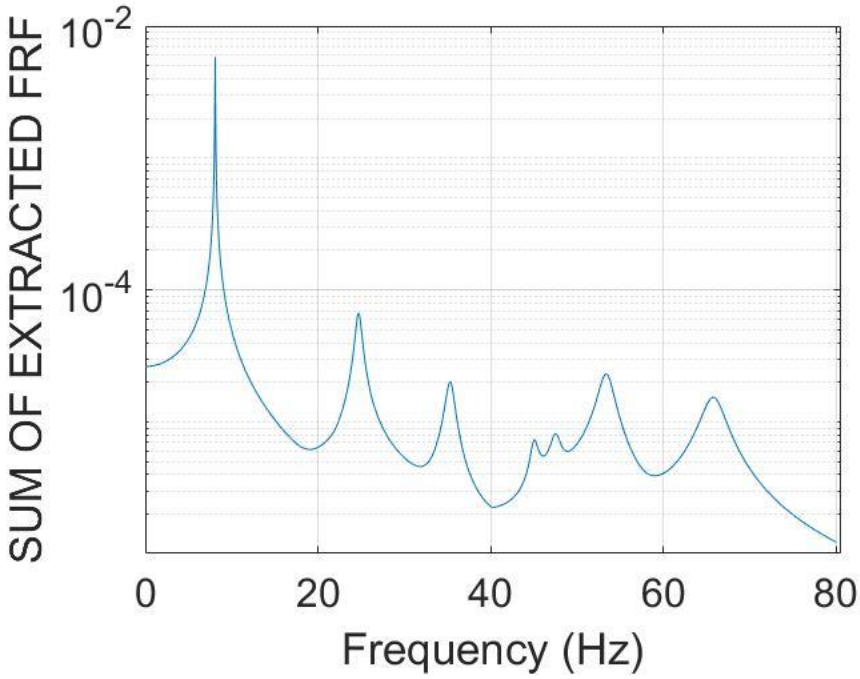

Figure 6.8: Constructed FRF in the case of 3% noise in the output (model order 49).

From these results a simple conclusion can be drawn; including a small noise, in a similar level to that of the output noise, does not hinder the RFP-z algorithm's accuracy given that higher model orders can be employed. Additional noise does not affect the accuracy but rather the time required for the modal parameters extraction.

6.1.3 %10 Noise in input and output

To test the viability of the modal parameter extraction under severe noise conditions the noise levels are boosted up to 10% in both input and output. The response to a random force can be seen in fig 6.9.

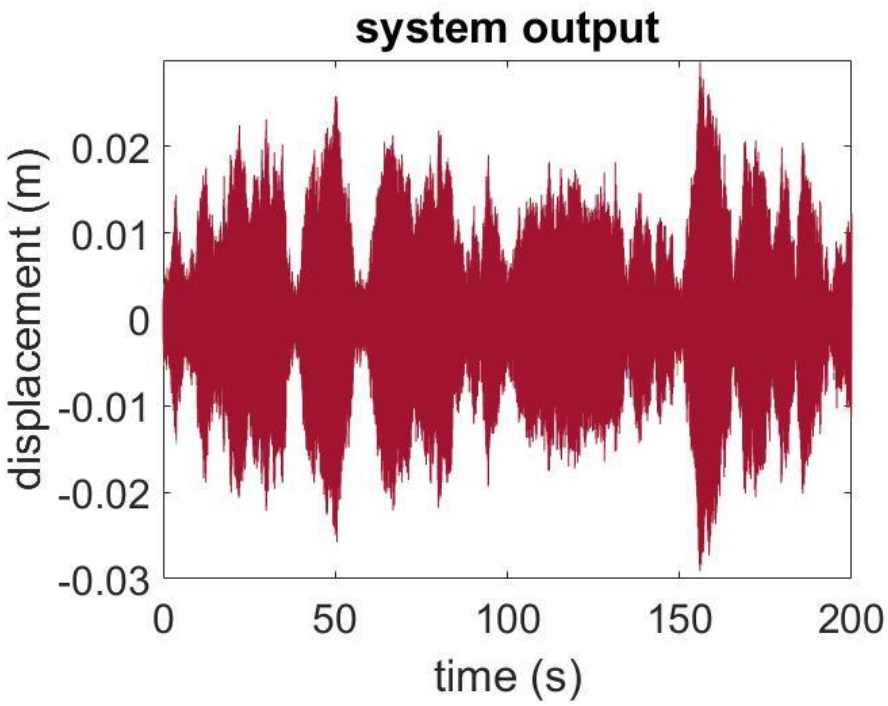

Figure 6.9: Response of each dof to a purely random signal with 10% noise in the input and the output.

The FRF estimation of this case is expectedly rougher. This ruggedness makes it difficult for the RFP-z algorithm to detect all the modes. In fact, this expectation can be confirmed via the stabilization chart in fig. 6.10. Even with increasing the model order up to 60 does not prove useful in detecting more than 6 modes. The twin modes become indistinguishable with noise; they cannot be detected as 2 different modes. Aside from the detected mode number, extracted damping ratios seen in fig. 6.11 also put the effect of noise under the spotlight.

Increasing the model order partially mitigates these problems, but with the cost of time inefficiency. As seen in the stabilization chart in fig. 6.12 all 7 modes are extracted after the 80th model order. Fig. 6.13 highlights the trend of damping ratios with increasing model order, up to 120. The first mode's damping ratio, which is normally overestimated, restores accuracy when the model order nears to 120. In the other hand the twin modes only slightly improve their accuracy, especially the 4th mode which is detected only at higher model orders. It should also be noted that running the iterative process up to the 120th model order takes circa 35 times longer than running it up to 30th model order.

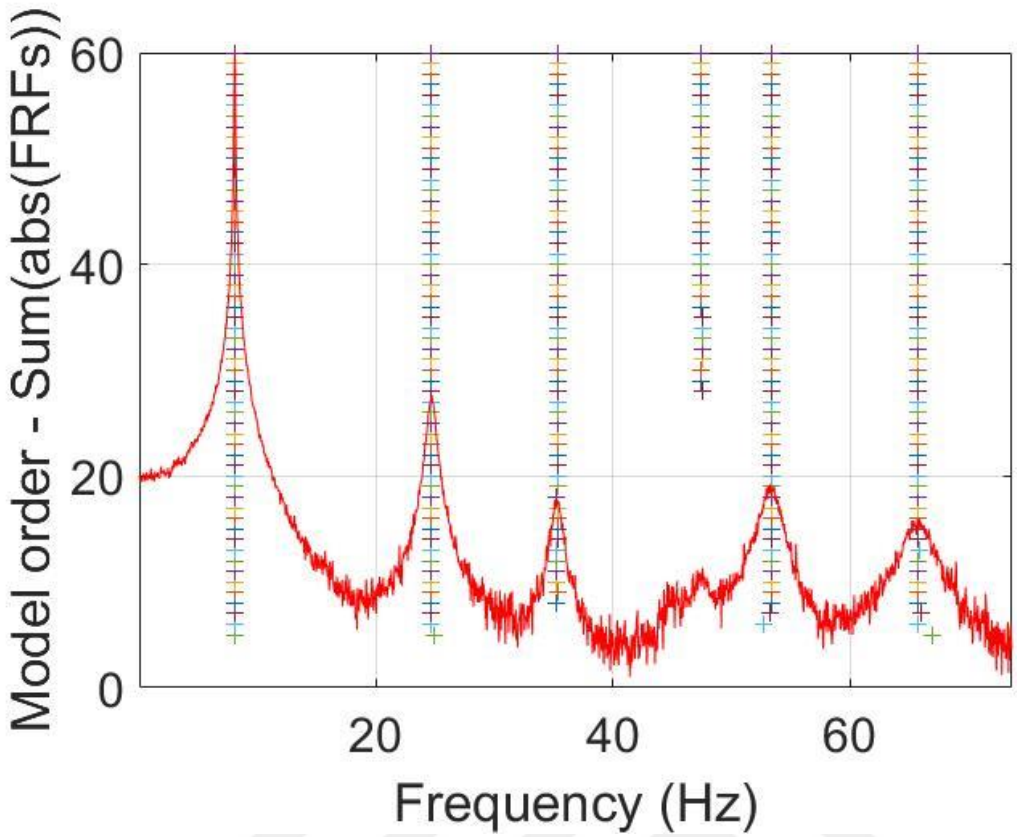

Figure 6.10: FRF estimation of fig. 6.9 overlaid with the detected modes up to model order 60 (stabilization chart).

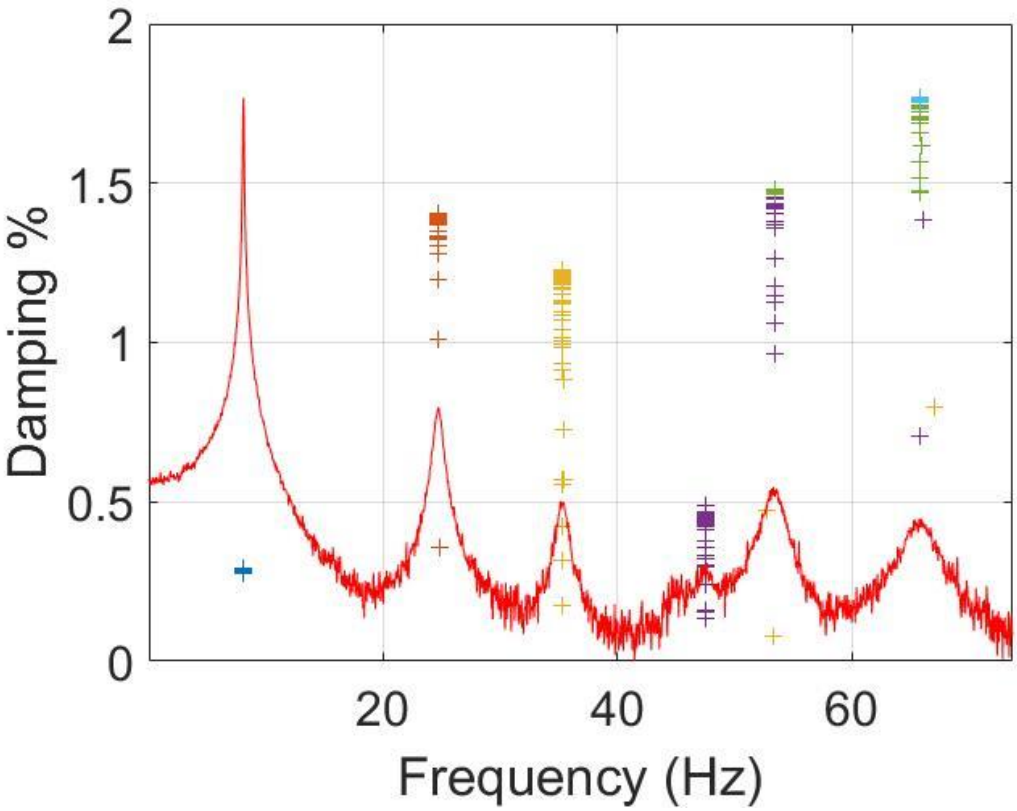

Figure 6.11: FRF estimation of fig. 6.9 overlaid with the detected damping ratios.

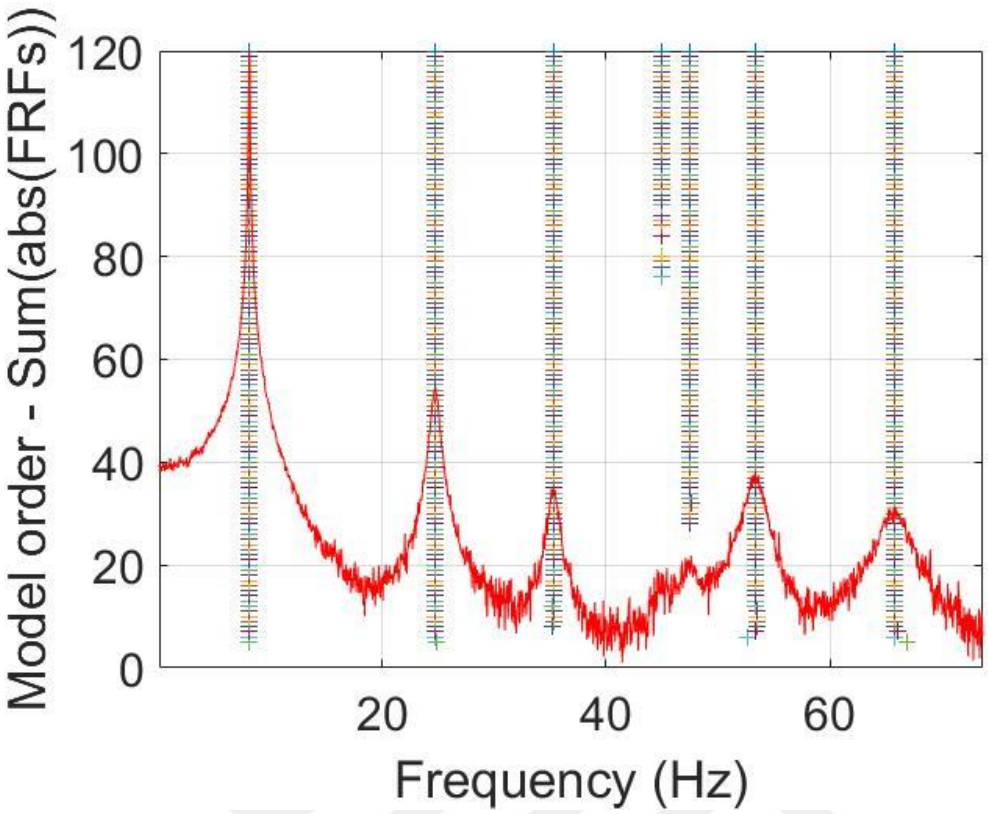

Figure 6.10: FRF estimation of fig. 6.9 overlaid with the detected modes up to model order 120 (stabilization chart).

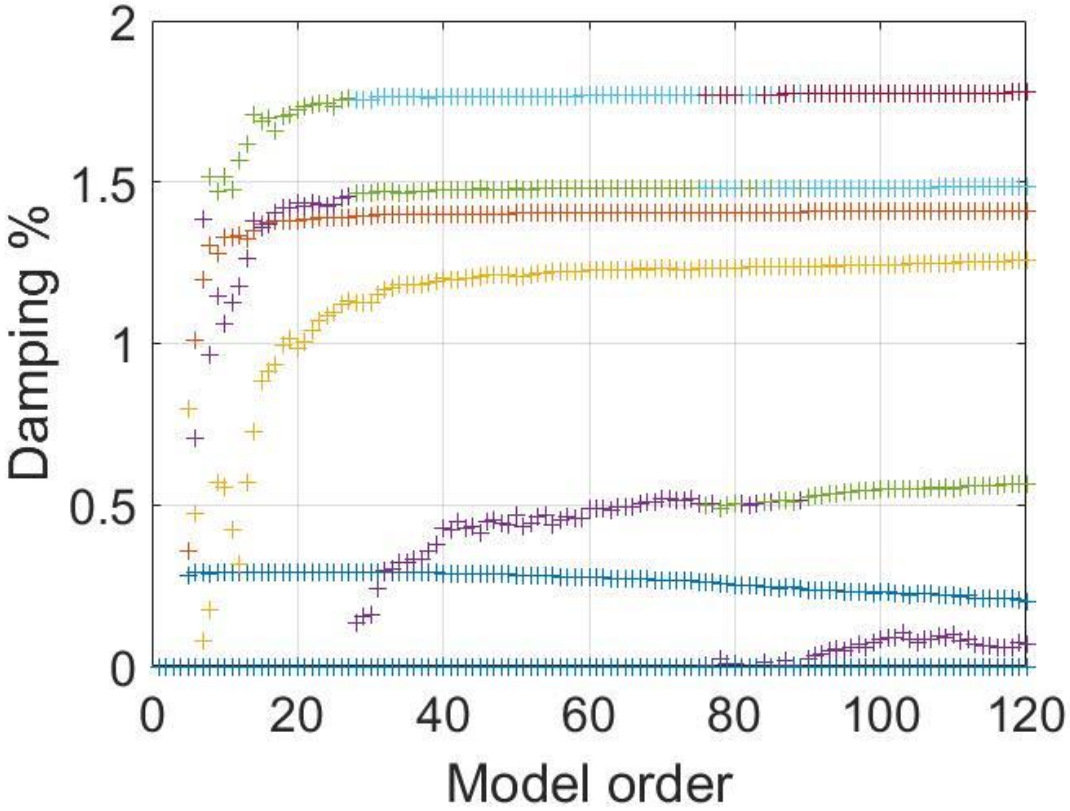

Figure 6.11: Effect of model order on the extracted damping ratios when high noise is present.

Approximating the constructed FRF to the analytical one for each model order indicates that 109th order is the most accurate one. In table 6.7 its extracted modal parameters are reported. Additionally in table 6.8 the extracted modal parameters of model order 38 is reported in order to compare the accuracy with the previous cases.

MODE	1	2	3	4	5	6	7
f_n $[Hz]$	8.09	24.70	35.32	45.01	47.50	53.40	65.81
ζ	0.22%	1.41%	1.25%	0.08%	0.55%	1.48%	1.78%
DAMPING ERROR	0%	2.1%	12.6%	93.0%	60.1 %	8.1%	9.6 %

Table 6.7: Extracted modal parameters (model order:109).

MODE	1	2	3	5	6	7
f_n $[Hz]$	8.09	24.70	35.32	47.49	53.40	65.81
ζ	0.29%	1.40%	1.19%	0.35%	1.47%	1.76%
DAMPING ERROR	31.8%	2.8%	16.8%	74.6 %	8.7%	10.7 %

Table 6.8: Extracted modal parameters (model order:38).

The latter table shows that high noise affects the accuracy of the modal parameter identification severely. For cases with a significant noise floor a high number of iterations is the only way to achieve partially viable information. This is only for well-separated modes, as already hard twin modes do not yield any meaningful damping ratio estimation.

The model order is not increased above 120 in this thesis due to computational difficulties but in a professional/academic scenario higher model orders may provide better estimations. Still, the fact that the 1st mode's damping ratio has reached to its real value hints that slightly improving the other mode's damping ratio estimations will result in underestimating the 1st one.

Analysing the MAC matrix of the 109th model order (table 6.9) indicates that the residues are extracted in an accurate manner. Like the natural frequencies, mode shapes are extracted successfully even with high noise present in both signals.

	1	2	3	4	5	6	7
1	0.9997	0.0023	0.0038	4.9937e-05	0.0013	0.0061	4.2311e-05
2	0.0016	0.9997	0.0017	0.0016	0.0017	0.0010	2.6626e-04
3	0.0012	0.0015	0.9944	0.0015	0.0048	9.4529e-04	8.7342e-05
4	0.0017	0.0043	0.0035	0.9605	0.0491	0.0058	0.0018
5	7.5467e-05	0.0054	0.0040	0.0168	0.9938	0.0042	0.0015
6	0.0053	0.0016	3.8655e-04	1.6516e-04	0.0018	0.9973	2.9916e-04
7	1.8269e-04	9.8420e-05	3.2479e-04	0.0018	1.3880e-04	5.2417e-04	0.9966

Table 6.9: MAC Matrix related to the table 6.6.

The FRF constructed using the extracted parameters of the 109th model order is graphed in fig. 6.12 and it show significant differences with respects to the analytical FRF. The magnitude and the damping ratio (steepness) of the well-separated modes are still quite accurate taking into account the high noise corrupting the signal, but the underestimation of the twin mode's damping is clearly visible as a disproportionate spike.

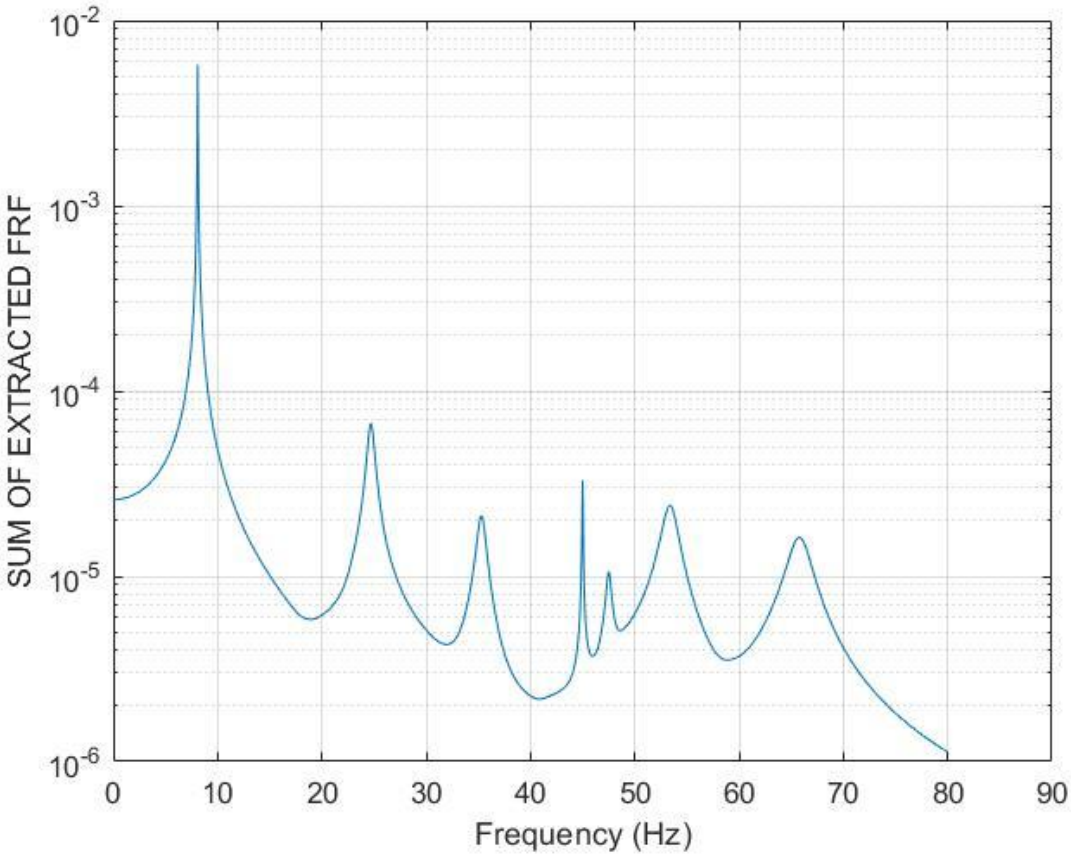

Figure 6.12: Constructed FRF in the case of 10% noise in the output (model order 109).

6.2 Harmonic Excitation

In EMA the input and the output signals are cross correlated in the frequency domain in order to derive the transfer function, which we call the response. When a random excitation is present the frequency spectrum of the excitation is similar to that of the white noise, but in case of a purely harmonic excitation its frequency spectrum is merely a spike at the excitation frequency This situation renders the calculation of cross power spectral density for the FRF estimation useless.

The excitation reported as Eq. 6.1 is applied to the 3rd dof. No noise is included in neither input nor output signals for reasons to be discussed in the next paragraph. The frequency spectrum of the excitation and the responses can be seen in fig. 6.13. Output spectrum contains the information of all 7 dofs but they overlap. Visually it seems like the magnitude is 0 in frequencies other than the specific excitation frequency, but in reality the spectrum shows an asymptotic behaviour around 0. The absence of noise shows its effect on the time domain-response (fig. 6.14). 60th second marks the end of the transient decay. The non-nullity of the output spectrum results in the FRF estimation seen in fig. 6.15, using the Eq. 3.6. The only useful information in such an estimation is the detection of the first mode and its natural frequency.

$$F(t) = 500 * \sin(2\pi * 8t) \tag{6.1}$$

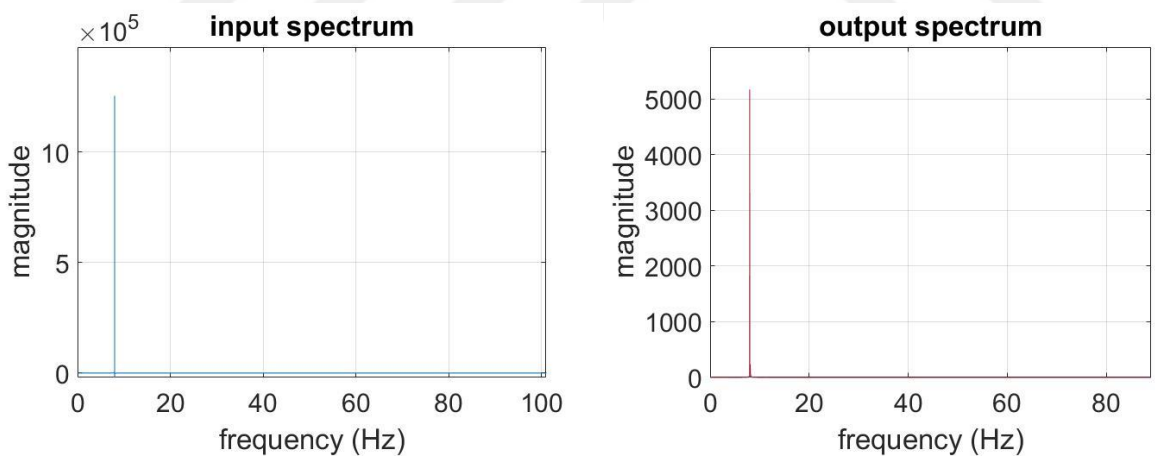

(a) (b)

Figure 6.13: Input and output spectrum of the harmonic excitation with the frequency of 8 Hz.

Including a 1% noise floor in the output signal slightly corrupts the signal spectrum. When zoomed out it is visually indistinguishable from fig. 6.13(b). However, when zoomed in the effect of noise is clearly seen. In fig 6.16 the same signals spectrum is seen when the output noise is null and 1% respectively.

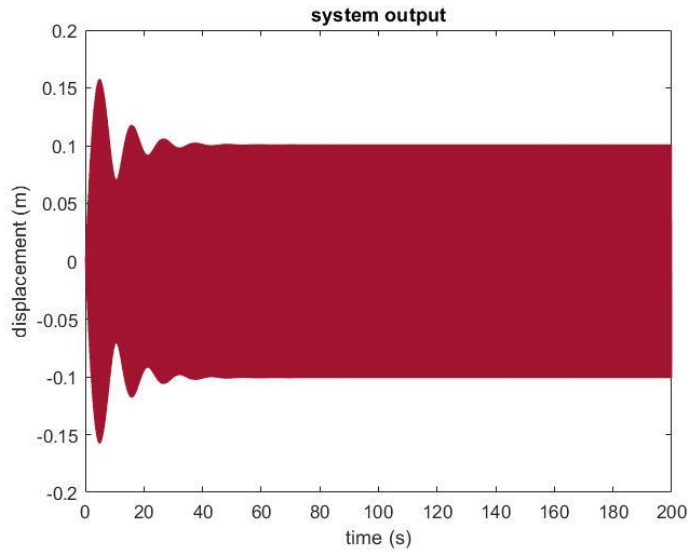

Figure 6.14: Time domain response to the force in eq. 6.1, in the absence of noise.

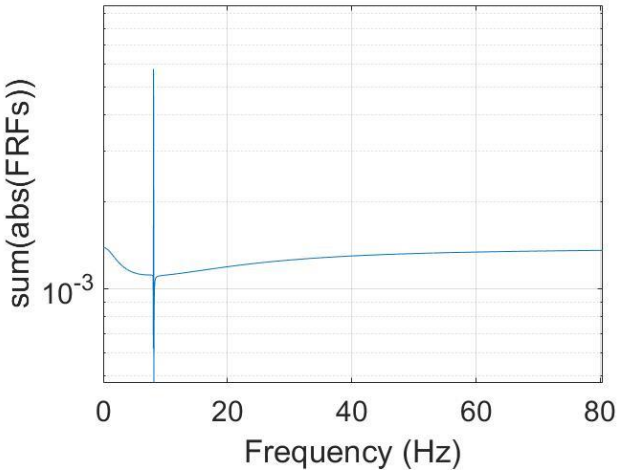

Figure 6.15: FRF estimation using the signals in fig. 6.13.

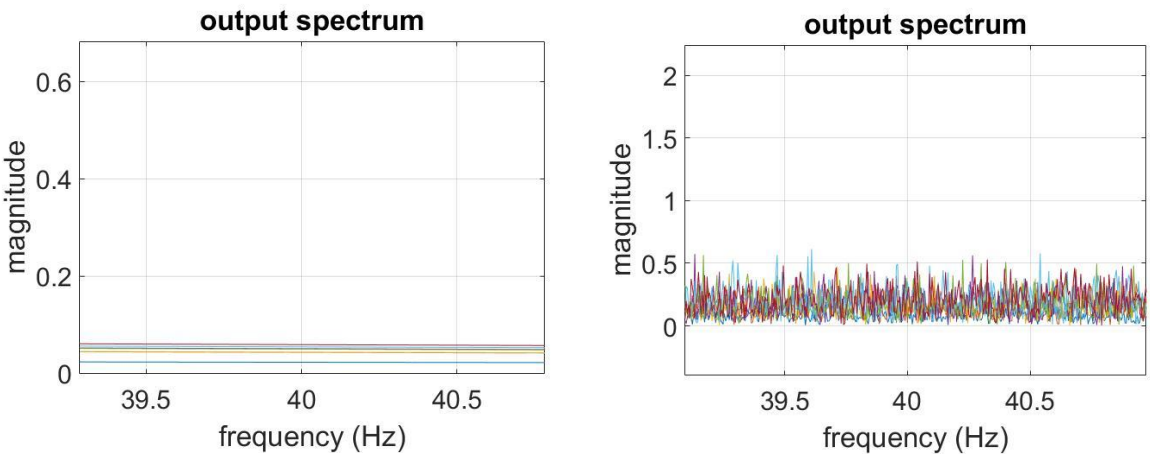

(a) (b)

Figure 6.16: Output spectrum zoomed around 40 Hz with (a) null noise and (b) 1% noise.

The ruggedness of fig. 6.16(b) resembles a white noise. In fact, as it can be seen in fig. 6.17, the FRF estimation resembles a slanted white noise with an antiresonance at the excitation frequency. This result is due to numerical reasons. When the input spectrum is close to null at a certain frequency, the noise in the output suggests that the response magnitude to that frequency is high and vice versa. So further away the frequency goes from the excitation frequency, this larger the response estimation gets.

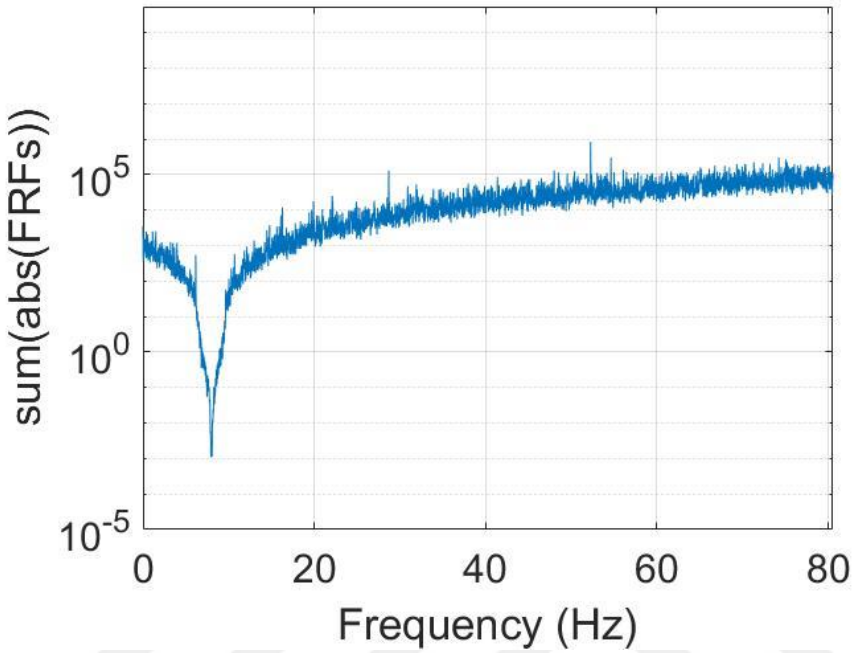

Figure 6.17: FRF estimation of a harmonic signal with 1% noise in the output.

Increasing noise further uplifts the magnitude of the response and affects the steepness of the antiresonance (figure 6.18).

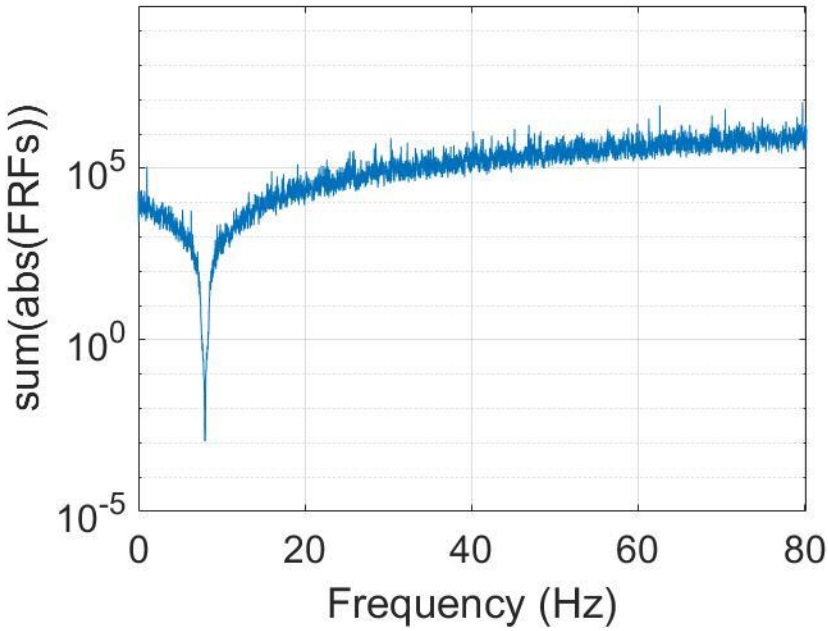

Figure 6.18: FRF estimation of a harmonic signal with 10% noise in the output.

It can thus be derived that a harmonic excitation is not suitable for the combination of cross power spectral density and RFP-z methods which is the focus of this thesis. This is due to the fact that noise is omnipresent and even the slightest noise will corrupt the signals to the point of uselessness.

In a purely exploratory point of view, it is interesting to see the behaviour of high excitation frequency in the ideal case of the absence of noise. Setting the excitation frequency at 200 Hz, as reported in Eq. 6.2, yields the FRF estimation in fig. 6.19. All the analytical modes are roughly present as spectral spike, but some are more prevalent than others. Apart from the 1st and the 7th mode, the modes are quite dispersed as if spectral leakage is present. This is not due to the transient part of the signal which has been cropped. Also, it should be mentioned that the spiked highlighted in grey are just numerical errors. Since the excitation frequency is 200 Hz no mode can be excited in particular. Of course, this FRF estimation is not suitable to proceed with RFP-Z method.

$$F(t) = 500 * \sin(2\pi * 200t) \tag{6.2}$$

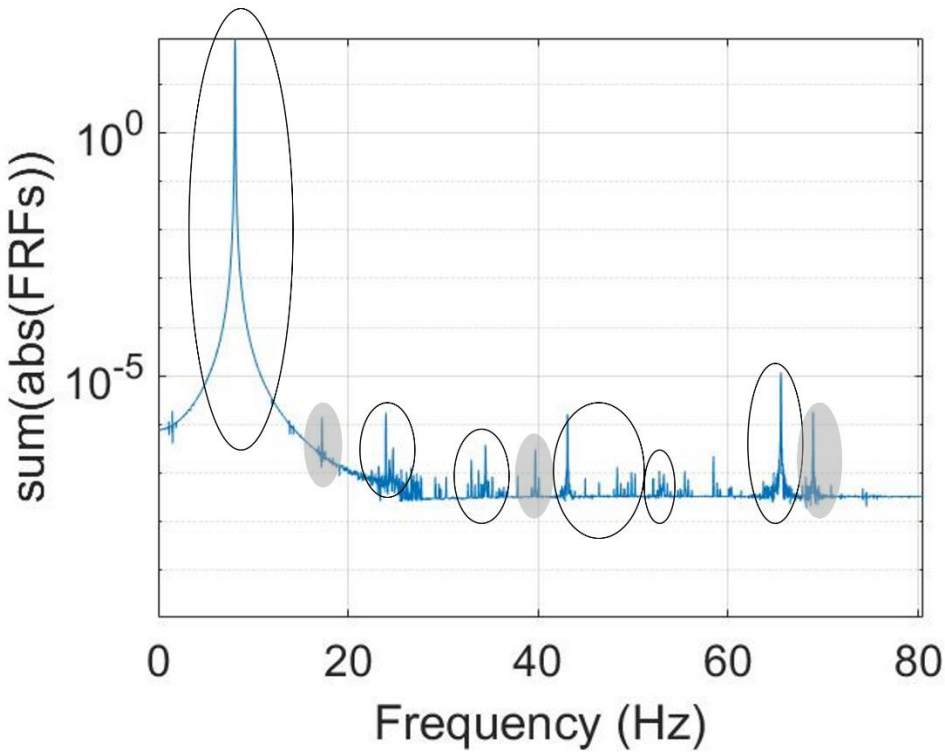

Figure 6.19: FRF estimation of a harmonic signal with high excitation frequency and no noise.

Comparing the FRF with fig. 5.3 indicates that the magnitude is not coherent. Running the RFP-z algorithm up to the 80th model order produces unstable results. The stabilization chart below shows the abundance of the spurious modes. Fig. 6.21 show the cumulative number of detected modes for each frequency. Extracted damping ratios in fig. 6.22 show the same level of chaotic distribution. These poor results are due to the matrix in Eq. 2.11 being close singular or badly scaled.

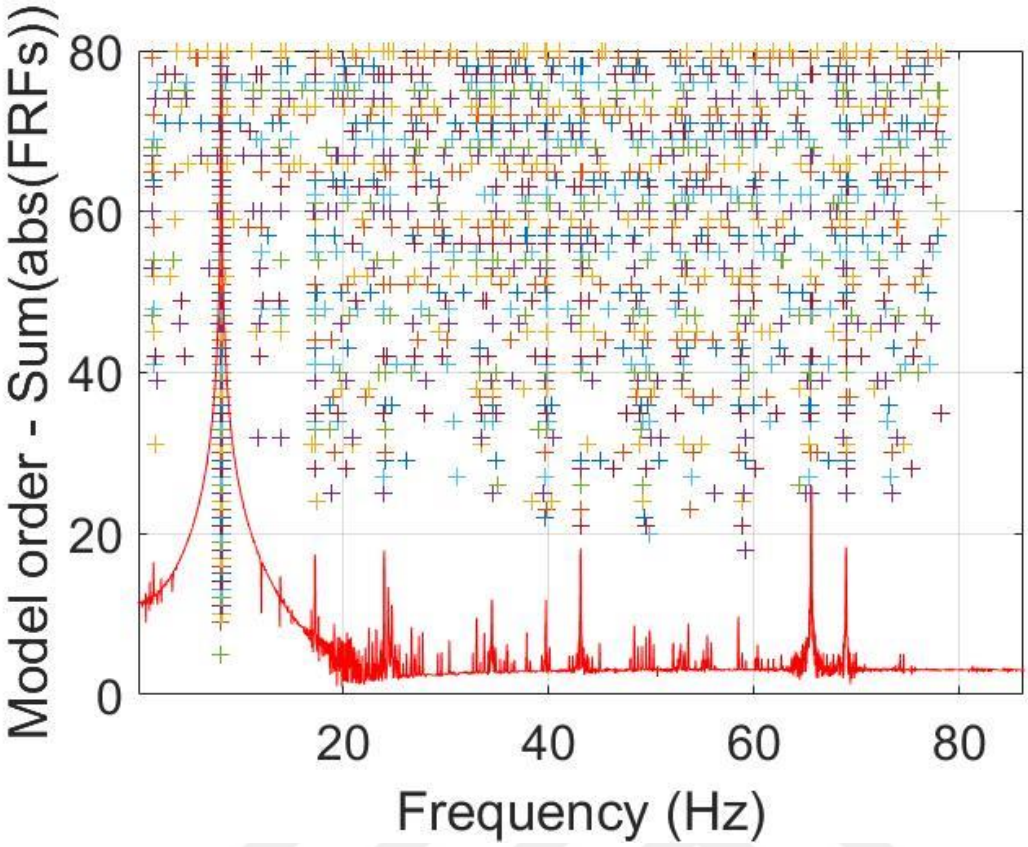

Figure 6.20: Stabilization chart of fig 6.17.

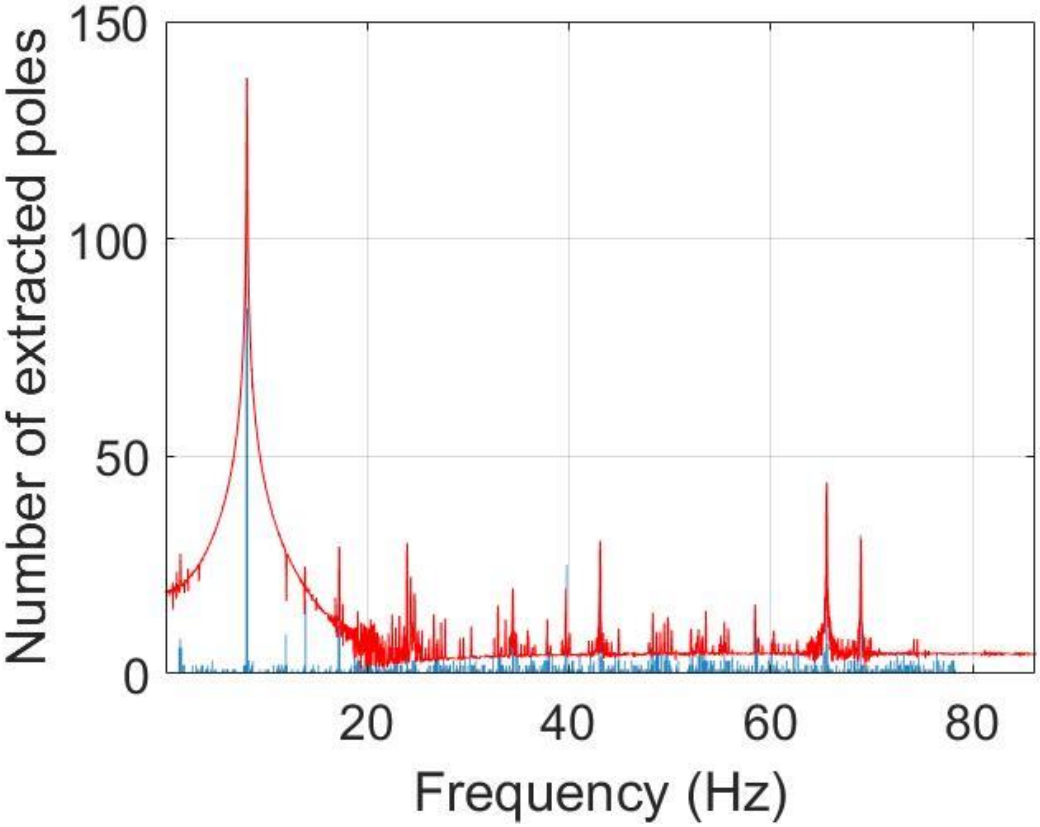

Figure 6.21: Detected modes of fig 6.17.

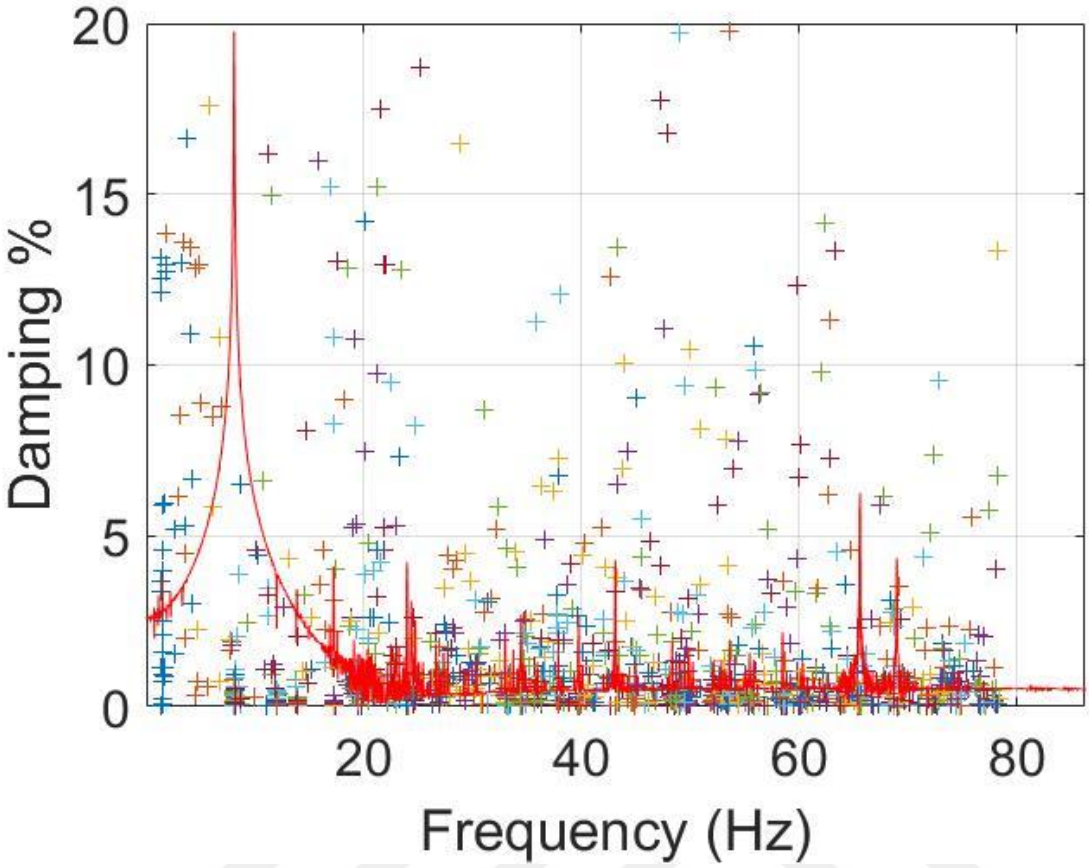

Figure 6.22: Extracted damping ratios of fig 6.17.

There is not any model order in which all the analytical modes are detected with accurate natural frequencies and damping ratios, so further analysis is redundant.

6.3. Harmonic Excitation with Random Contribution

6.3.1 3% Noise in Output

Just as the OMA case, by including a stochastic random contribution to a harmonic excitation it is expected to improve the accuracy of modal parameter identification. To test this force typology, initially a harmonic excitation with 10 Hz frequency and 500N amplitude which is accompanied by a random contribution with a mean of $0N$ and a 99.7% probability to be within $\pm 15N$ is applied to 3rd dof. A noise floor of 3% is included in the output signal. Fig. 6.23 shows that the random contribution of this magnitude is not strong enough to give a random response. The FRF estimation will not be any better than the previous cases. In fact, RFP-Z algorithm can only extract the 1st mode with poor accuracy from the estimated FRF.

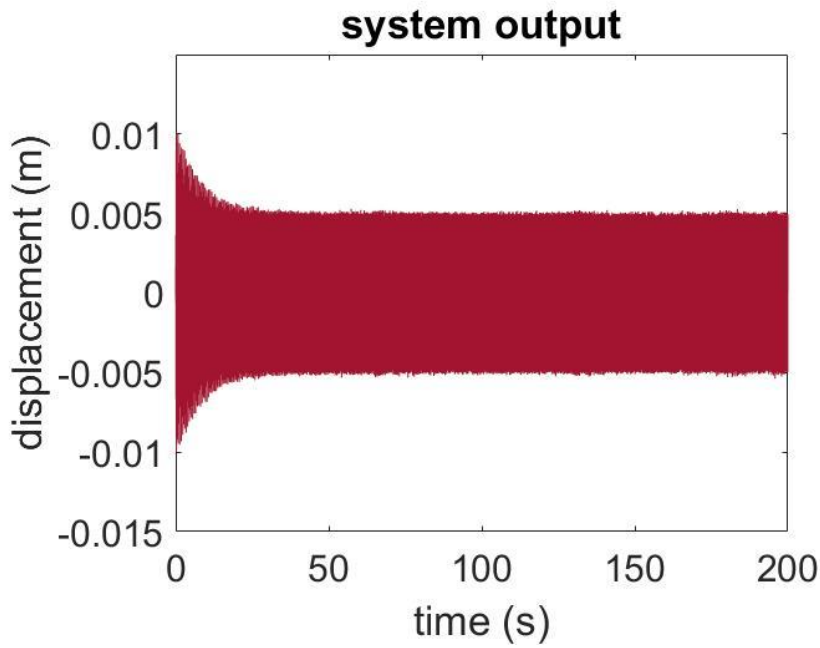

Figure 6.23: Time domain response of a harmonic excitation with mild random contribution.

By multiplying the random force contribution tenfold, the time domain response starts to resemble a random signal. Still a transient decay is present until the 25th second. RFP-z algorithm is run up to 80 model order iterations and its associated stabilization diagram and extracted damping ratios are given in fig. 6.25 & 6.26. There certainly is an improvement, boosting the random contribution of the force facilitates the FRF estimation greatly and thus improving the accuracy of RFP-z method. The extracted parameters are:

MODE	1	2	3	5	6	7
f_n $[Hz]$	8.09	24.71	35.30	47.56	53.40	65.82
ζ	0.22%	1.42%	1.13%	0.19%	1.42%	1.61%
DAMPING ERROR	0%	1.4%	21%	86.2 %	11.8%	18.3 %

Table 6.10: Extracted modal parameters (model order:78).

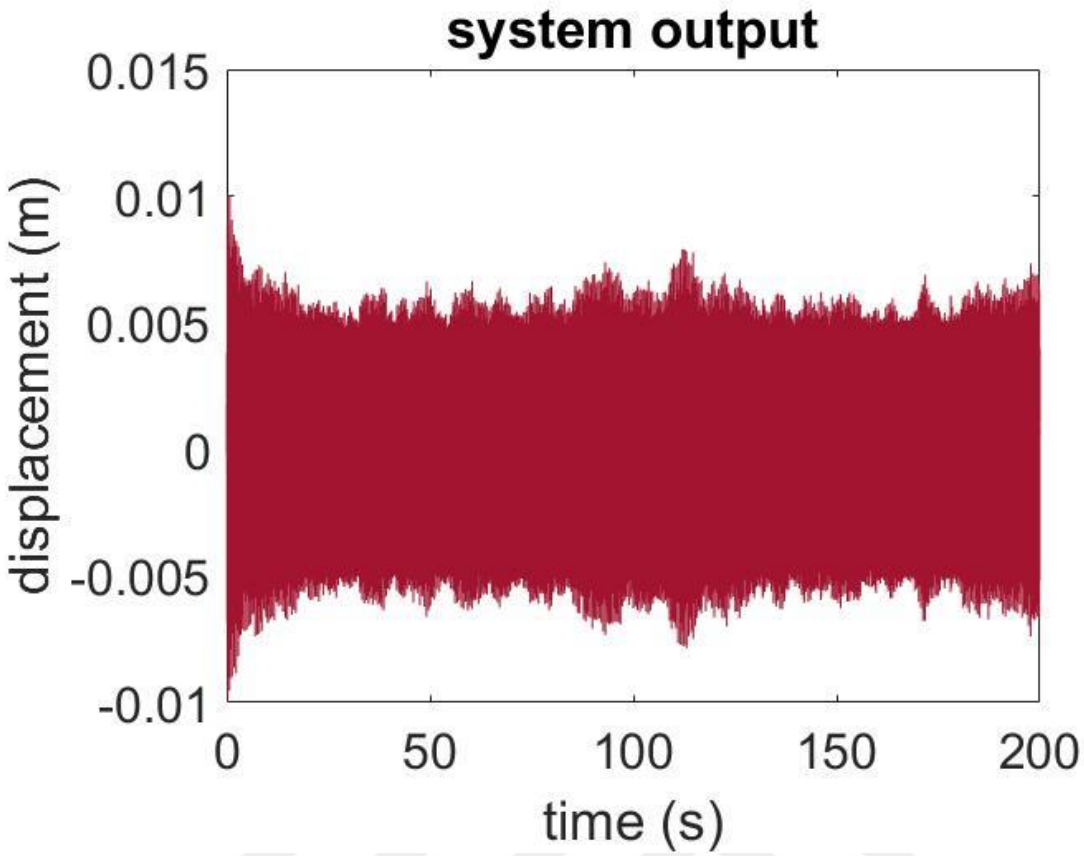

Figure 6.24: Time domain response of a harmonic excitation with moderate random contribution.

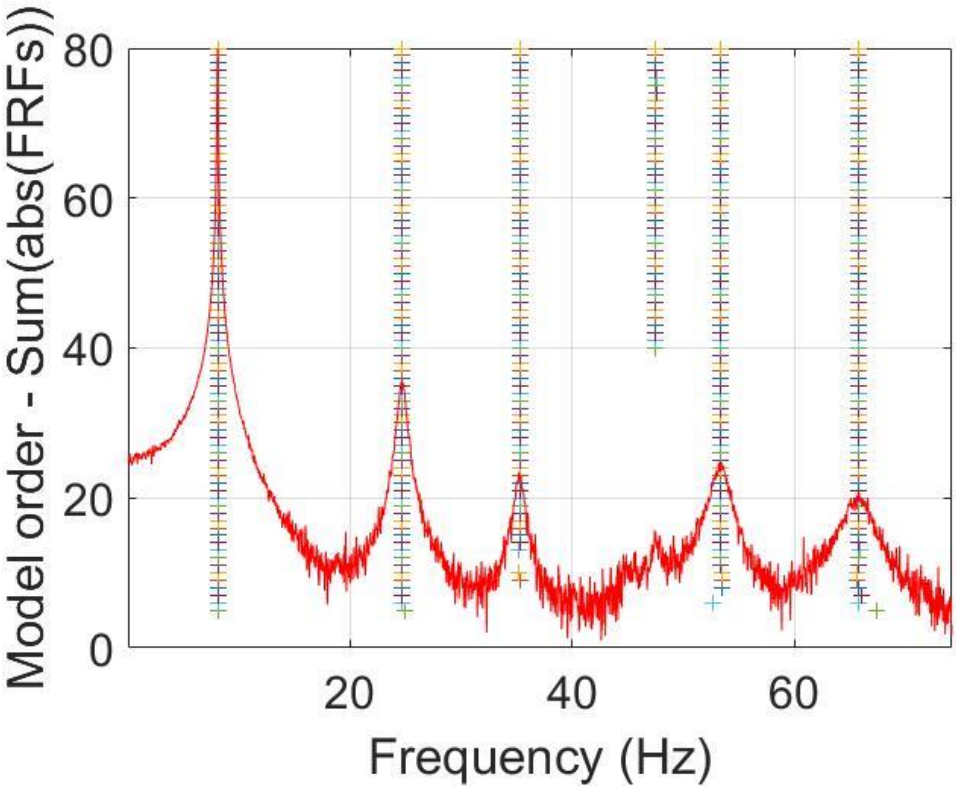

Figure 6.25: stabilization diagram associated with fig. 6.24.

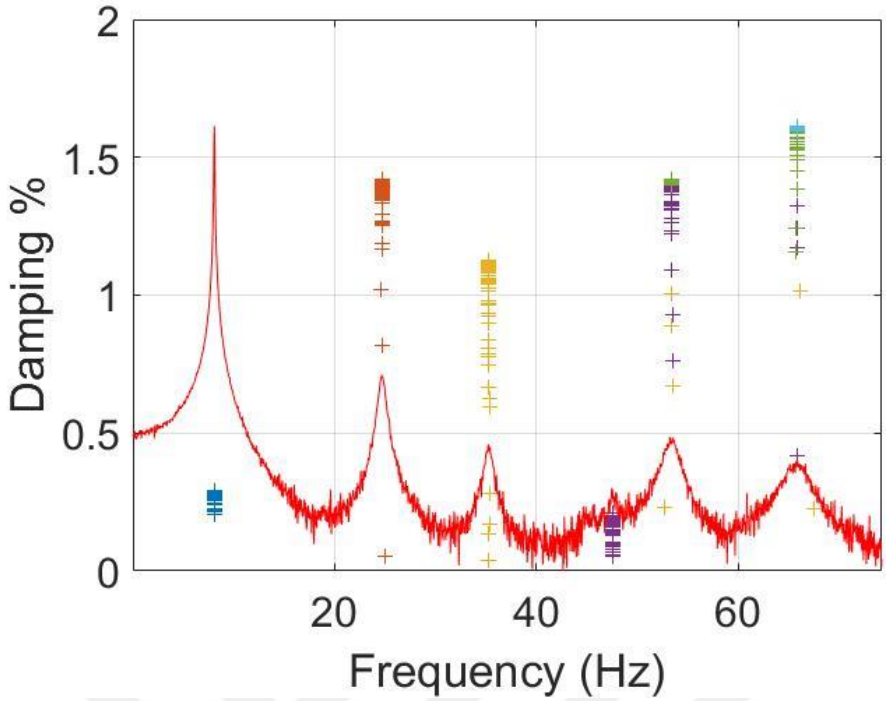

Figure 6.26: extracted damping ratios associated with fig. 6.24.

Among the 6 detected modes, 1st and 2nd ones exhibit good accuracy in both damping and natural frequency. The rest of the modes show quite inaccurate damping ratios, especially the twin mode's damping is heavily underestimated.

Moving on to MAC analysis (table 6.11), one can say that the extracted mode shapes manifest excellent accuracy.

	1	2	3	4	5	6	7
1	0.9996	0.0023	0.0044	7.3031e-05	0.0011	0.0067	3.6556e-05
2	0.0019	0.9998	0.0015	0.0016	0.0018	0.0014	2.3364e-04
3	0.0028	0.0035	0.9958	1.5236e-04	0.0057	0.0012	5.2714e-04
4	2.3599e-04	3.2517e-04	0.0042	0.0330	0.9805	0.0078	0.0025
5	0.0065	8.6095e-04	2.2597e-04	1.1022e-04	0.0023	0.9959	6.7790e-04
6	4.4110e-04	0.0011	3.3890e-04	0.0012	1.1145e-04	5.6742e-04	0.9963
7	NaN	NaN	NaN	NaN	NaN	NaN	NaN

Table 6.11: MAC Matrix related to the table 6.10.

Increasing the random force contribution by another order of magnitude will render the input signal more similar to excitation seen in subchapter 6.1. As seen in fig. 6.27, the input signal still retains a strong harmonic spike but also a spectra of input elements dispersed like white noise. The resulting time domain response is reported in fig. 6.28. It seems significantly more arbitrary.

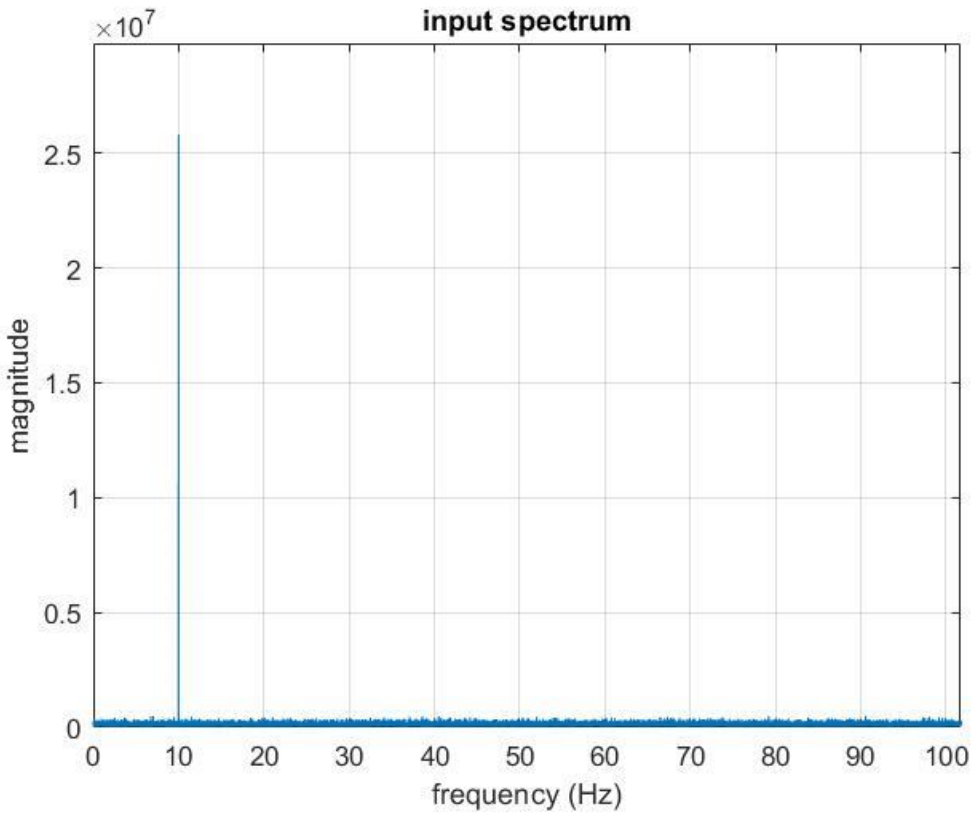

Figure 6.27: Input spectrum of a force with high random contribution.

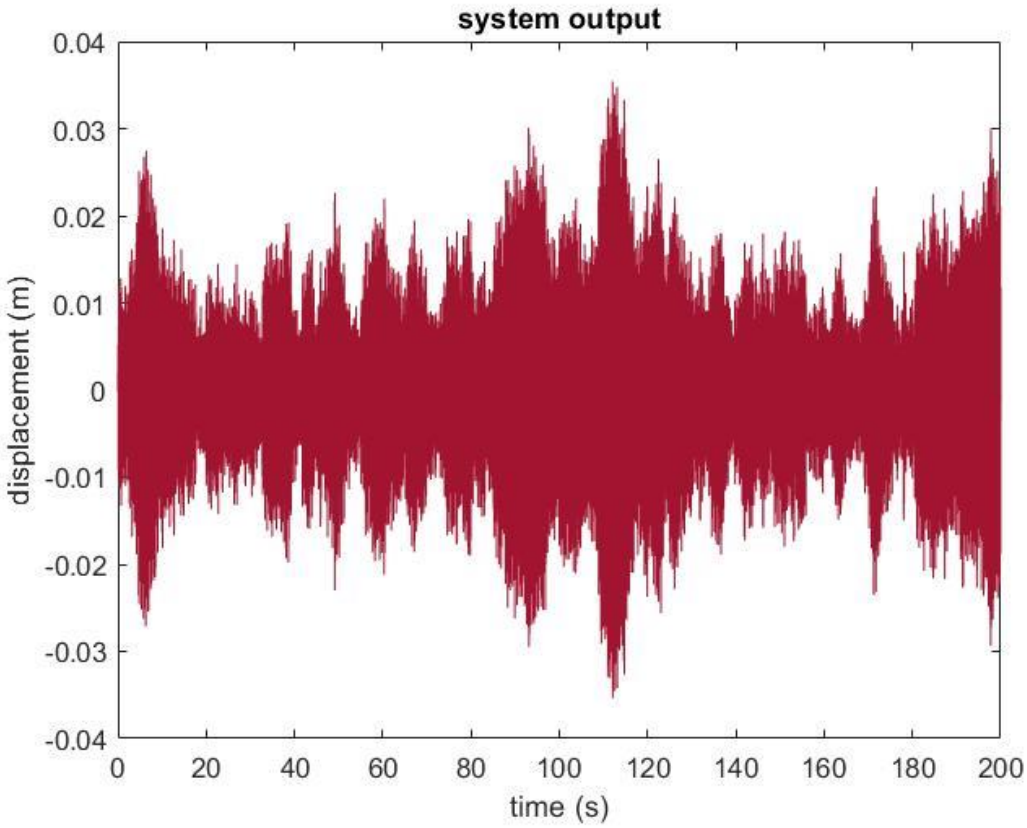

Figure 6.28: Time domain response of a harmonic excitation with high random contribution.

A moderate amount of consistent randomness in the input spectrum greatly improves the FRF estimation accuracy as seen in fig. 6.29. This results in RFP-z method detecting every analytical mode. Table 6.12 reports the extracted modal parameters and figure 6.30 underlines the excellence of the constructed FRF.

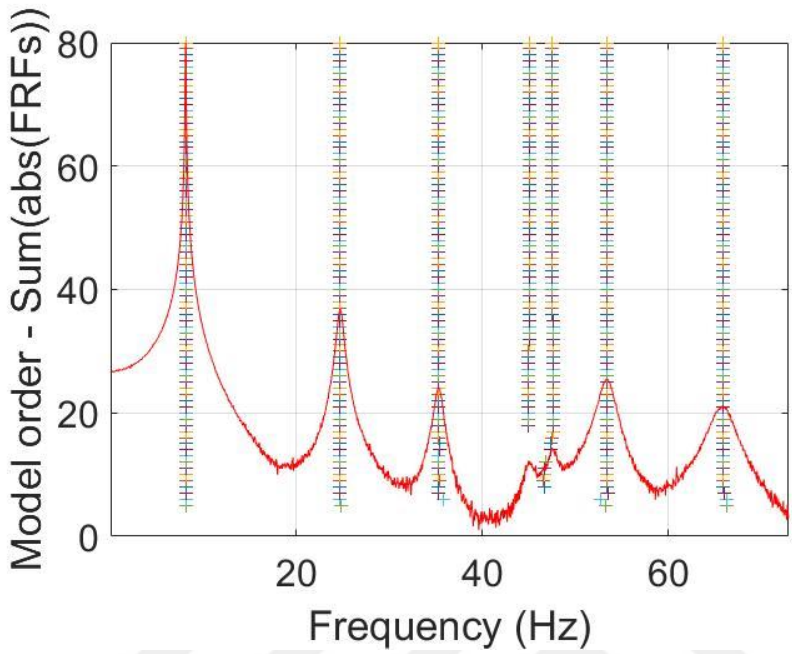

Figure 6.29: stabilization diagram associated to fig. 6.28.

MODE	1	2	3	4	5	6	7
f_n $[Hz]$	8.09	24.71	35.31	45.01	47.52	53.40	65.81
ζ	0.22%	1.44%	1.41%	0.89%	1.24%	1.64%	2.02%
DAMPING ERROR	0%	0%	1.4%	22.6%	10.1 %	1.9%	4.4 %

Table 6.12: Extracted modal parameters (model order:42).

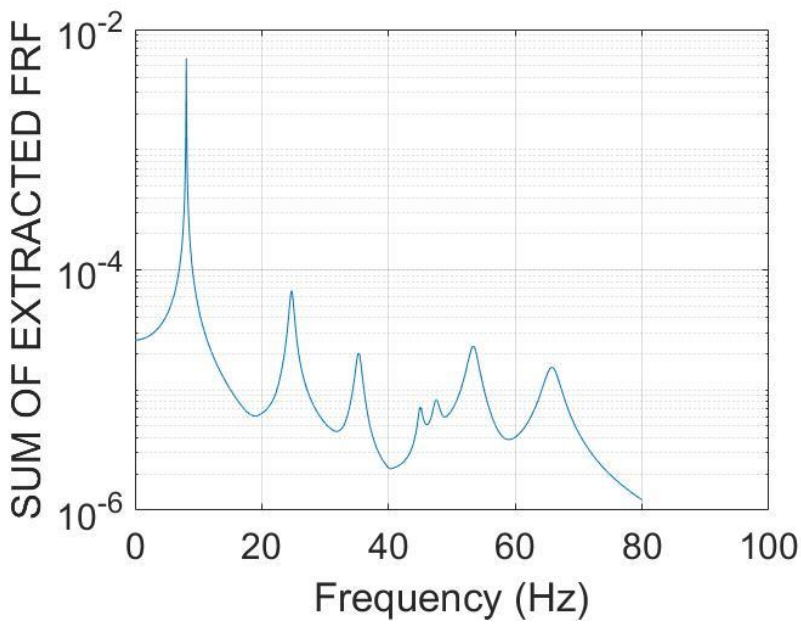

Figure 6.30: Constructed FRF using extracted parameters reported in table 6.12.

Related MAC matrix manifest exceeding accuracy.

	1	2	3	4	5	6	7
1	0.9990	0.0024	0.0028	7.8089e-05	0.0011	0.0053	7.5500e-04
2	0.0018	0.9998	0.0015	0.0017	0.0018	0.0012	2.0099e-04
3	0.0024	0.0020	0.9983	1.0719e-04	0.0047	5.7859e-04	9.2787e-05
4	1.4268e-04	0.0029	4.4266e-04	0.9863	0.0025	0.0031	0.0012
5	2.9294e-04	3.0380e-04	0.0047	0.0012	0.9886	0.0049	0.0026
6	0.0059	0.0010	2.0828e-04	1.1527e-04	0.0015	0.9981	3.0262e-04
7	1.3697e-04	2.2521e-04	3.2430e-04	0.0012	1.4302e-04	3.3347e-04	0.9975

Table 6.13: MAC Matrix related to the table 6.12.

These results are very similar to those in subchapter 6.1.1. Increasing the random force contribution in this case expectedly produced the same results with a pure random excitation. To emphasize on a mixture of harmonic and random input signal, excitations with moderate random contribution will be analysed for the remainder of this chapter.

Before altering the noise level to analyse its effect, the consequences of shifting the excitation frequency will be analysed. An excitation with a frequency of 24.7 Hz, which corresponds to the 2nd natural frequency of the system, is applied. A zoomed in section of the time-domain response is reported below in order to make it easy to see the initial growth. It can be said that there is a transient behaviour until the 4th second.

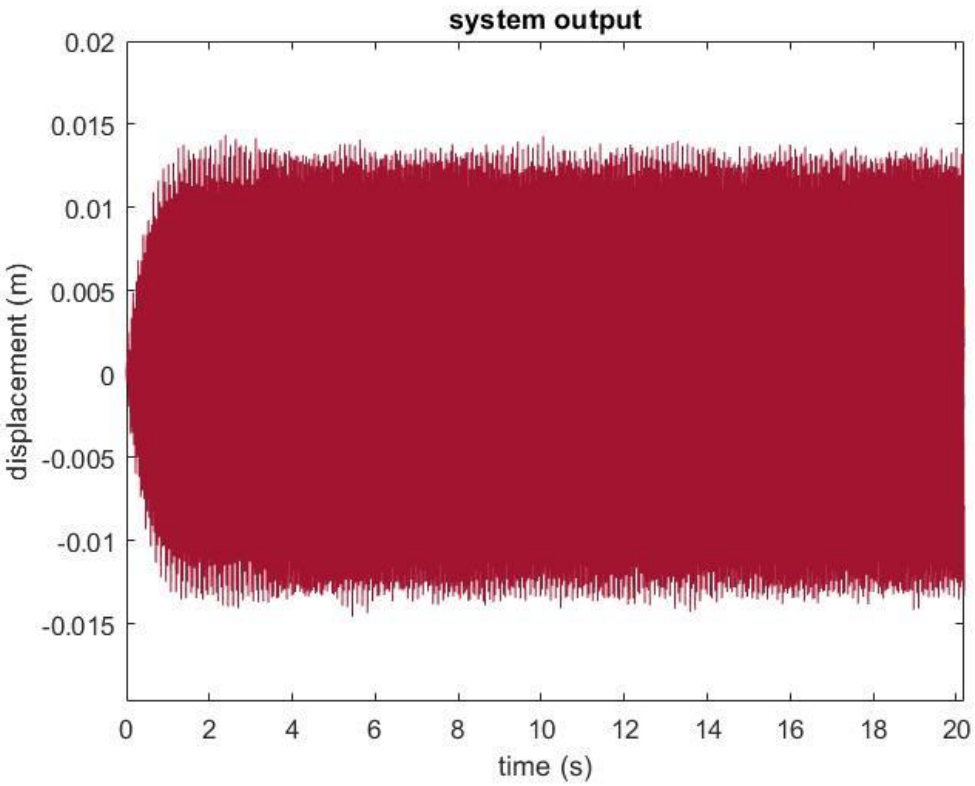

Figure 6.31: Time domain response of a harmonic excitation with moderate random contribution.

The effects of such an excitation frequency are immediately observed. The response is naturally larger and more importantly it is more consistent. In contrast to fig. 6.24. it is less arbitrary and steadier. In other words, it can be argued that the harmonic contribution of the force dominates the response. This can be seen like the opposite case of we just analysed in fig. 6.28 where the random contribution of the force dominated the response. As a result, the FRF estimation got more rugged and hence only 5 analytical modes are detected by the RFP-z algorithm.

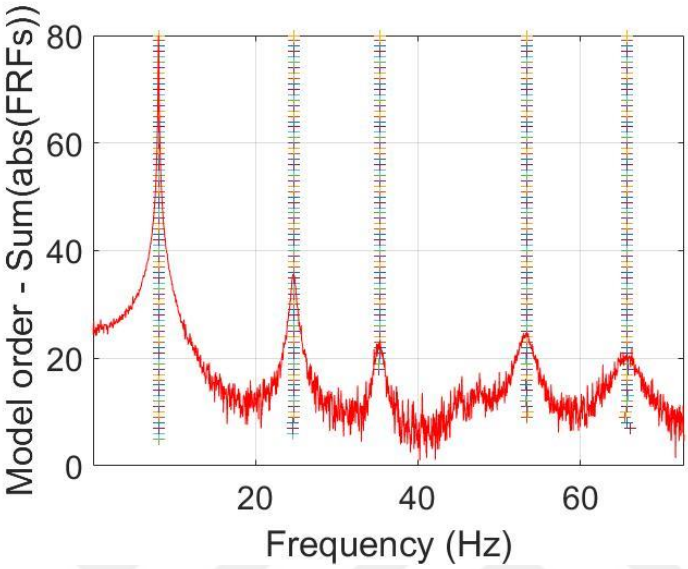

Figure 6.32: stabilization diagram associated to fig. 6.31.

And the extracted modal parameters are:

MODE	1	2	3	6	7
f_n $[Hz]$	8.09	24.71	35.30	53.39	65.79
ζ	0.28%	1.44%	0.87%	1.17%	1.18%
DAMPING ERROR	27.3%	0%	46.2%	27.3%	40.1 %

Table 6.14: Extracted modal parameters (model order:80).

The MAC matrix shows excellent accuracy, which always has been the case for the well separated modes when the noise is small.

	1	2	3	4	5	6	7
1	0.9999	0.0015	0.0027	3.2645e-05	0.0015	0.0066	1.9189e-05
2	0.0019	0.9991	0.0014	0.0016	0.0020	0.0014	3.4960e-04
3	0.0067	0.0096	0.9897	0.0016	0.0065	3.2453e-04	2.5733e-04
4	0.0045	0.0015	3.9434e-04	4.8625e-04	0.0041	0.9942	7.4225e-04
5	2.3532e-04	8.7923e-04	4.8084e-04	0.0019	1.5597e-04	0.0018	0.9931
6	NaN	NaN	NaN	NaN	NaN	NaN	NaN
7	NaN	NaN	NaN	NaN	NaN	NaN	NaN

Table 6.15: MAC Matrix related to table 6.14.

The steep fall in accuracy of extracted damping ratios is clear to see, with the exception of the 2nd mode. It would be interesting to find if the accuracy of the extracted damping ratio of a given mode is related to whether the excitation frequency is close to its natural frequency. Keeping all the parameters same, with the exception of excitation frequency, which is set subsequently to the other natural frequencies, the extracted parameters are as follows:

MODE	1
f_n $[Hz]$	8.09
ζ	0.066%
DAMPING ERROR	70%

Table 6.16: Extracted modal parameters when excitation frequency is 8.1 Hz (model order:80).

MODE	1	2	3	4	5	6	7
f_n $[Hz]$	8.10	24.71	35.33	44.99	47.51	53.40	65.83
ζ	0.22%	1.44%	1.38%	0.55%	1.01%	1.61%	1.92%
DAMPING ERROR	0%	0%	3.5%	52.2%	26.8%	0%	2.5 %

Table 6.17: Extracted modal parameters when excitation frequency is 35.32 Hz (model order:49).

MODE	1	2	3	4	5	6	7
f_n $[Hz]$	8.09	24.71	35.31	45.01	47.51	53.40	65.81
ζ	0.21%	1.44%	1.41%	0.92%	1.25%	1.64%	2.01%
DAMPING ERROR	4.5%	0%	1.4%	19.1%	9.4%	1.9%	2 %

Table 6.18: Extracted modal parameters when excitation frequency is 45.03 Hz (model order:43).

MODE	1	2	3	4	5	6	7
f_n $[Hz]$	8.10	24.71	35.32	45.01	47.51	53.40	65.80
ζ	0.22%	1.44%	1.42%	0.92%	1.26%	1.65%	2.01%
DAMPING ERROR	0%	0%	0.7%	19.1%	8.7%	2.5%	2 %

Table 6.19: Extracted modal parameters when excitation frequency is 47.55 Hz (model order:45).

MODE	1	2	3	4	5	6	7
f_n $[Hz]$	8.09	24.71	35.31	44.95	47.52	53.40	65.83
ζ	0.22%	1.43%	1.35%	0.43%	0.85%	1.58%	1.92%
DAMPING ERROR	0%	0.7%	5.6%	62.6%	38.4%	1.9%	2.5 %

Table 6.20: Extracted modal parameters when excitation frequency is 53.46 Hz (model order:65).

MODE	1	2	3	4	5	6	7
f_n $[Hz]$	8.09	24.71	35.31	44.99	47.52	53.39	65.83
ζ	0.22%	1.44%	1.37%	0.62%	1.04%	1.60%	1.95%
DAMPING ERROR	0%	0%	4.2%	54.8%	24.6%	0.6%	1.0 %

Table 6.21: Extracted modal parameters when excitation frequency is 65.99 Hz (model order:60).

These interesting results make it possible to develop some arguments. First of all, there is a general trend that the accuracy improves as the excitation frequency increases. Secondly, When the excitation frequency is near a mode's natural frequency, its modal parameters are extracted with a better accuracy. Also, there are several modes which are more easily extractable in any case. For example, the 2nd mode, except case in table 6.16, is always identified with an excellent accuracy whilst the 4th mode shows quite poor accuracy even when the excitation frequency is nearby. Of course, this is due to the separation level of the mode.

A final analysis is done at the anti-resonant frequency of 40.5 Hz. Extracted modal parameters are as follows:

MODE	1	2	3	4	5	6	7
f_n $[Hz]$	8.09	24.71	35.31	45.00	47.51	53.39	65.80
ζ	0.22%	1.44%	1.42%	0.95%	1.32%	1.65%	2.02%
DAMPING ERROR	0%	0%	0.7%	17.4%	4.3%	2.5%	2.5 %

Table 6.22: Extracted modal parameters when excitation frequency is 40.5 Hz (model order:50).

Not surprisingly these are the most accurate results so far (for harmonic & random force with moderate random contribution). The opposite effect of what happened in resonant frequencies is observed here; anti-resonance hinders the impact of the harmonic excitation, so random contribution dominates the response. This results in a "more arbitrary" response and thus a better estimated FRF, and finally a better working RFP-z case.

6.3.2 3% Noise in both Input and Output

In the previous subchapter effects of 2 important parameters are analysed: random force contribution magnitude and excitation frequency. Therefore, comprehensive analysis of those two parameters will be bypassed in this subchapter. To see if the inclusion of noise in the input signals reduces the accuracy in the same rate, tests will be performed with excitations having moderate random contribution and the following frequencies:

- 35.32 Hz (natural frequency of a well-separated mode)
- 40.50 Hz (frequency of the anti-resonance)
- 47.55 Hz (natural frequency of a twin mode)

The former case yields the following extracted parameters:

MODE	1	2	3	4	5	6	7
$f_n\ [Hz]$	8.10	24.70	35.31	45.00	47.50	53.40	65.84
ζ	0.29%	1.38%	1.35%	0.50%	0.97%	1.58%	1.87%
DAMPING ERROR	31.8%	4.2%	5.6%	56.5%	29.7%	1.9%	5.1 %

Table 6.23: Extracted modal parameters when excitation frequency is 35.32 Hz (model order:80) with %3 noise in input and output.

An initial observation can be done on the number of model orders in which all the analytical modes are detected. In the case with only output noise, the 7 modes were detected starting from the 18th model order whereas in this case the starting point is 27th model order. Also, the fact that damping ratio extraction error is increased in every single mode highlights the effect of newly introduced noise. Table 6.24 indicates that the accuracy of extracted mode shapes are not affected significantly.

	1	2	3	4	5	6	7
1	0.9998	0.0018	0.0026	1.9622e-05	0.0011	0.0064	1.4052e-04
2	0.0019	0.9997	0.0014	0.0017	0.0019	0.0013	2.5362e-04
3	0.0022	0.0017	0.9976	2.8800e-04	0.0053	2.6205e-04	5.0844e-05
4	1.4568e-04	0.0028	9.2221e-04	0.9848	0.0139	0.0017	9.5506e-04
5	0.0017	0.0031	0.0032	0.0081	0.9915	0.0059	0.0033
6	0.0060	9.9448e-04	5.8543e-04	2.1285e-04	0.0022	0.9973	4.1384e-04
7	4.2676e-05	1.1529e-04	4.1146e-04	0.0019	2.7209e-04	4.2643e-04	0.9969

Table 6.24: MAC Matrix related to table 6.23.

Moving onwards to the second case (40.50 Hz) yields the following extracted parameters:

MODE	1	2	3	4	5	6	7
$f_n\ [Hz]$	8.09	24.70	35.31	45.00	47.52	53.41	65.84
ζ	0.28%	1.42%	1.39%	0.94%	1.28%	1.60%	1.97%
DAMPING ERROR	27.3%	1.4%	2.8%	18.3%	7.2%	0.6%	0 %

Table 6.25: Extracted modal parameters when excitation frequency is 40.5 Hz (model order:79).

From model order #19 the algorithm could detect all the modes. The 6th and 7th modes' damping extractions actually improved. The first 5 modes' extractions show greater inaccuracies since the addition of the noise, but still the growth of inaccuracy is relatively smaller with respect to the case in which the excitation frequency corresponds to a natural frequency. As clearly seen in the related MAC matrix, accuracy of the extracted mode shapes is not affected by the additional noise significantly.

	1	2	3	4	5	6	7
1	0.9998	0.0018	0.0030	6.0118e-05	0.0012	0.0065	2.0480e-04
2	0.0019	0.9997	0.0015	0.0019	0.0018	0.0013	2.7510e-04
3	0.0023	0.0022	0.9982	7.4982e-05	0.0050	4.8799e-04	1.3666e-04
4	5.7826e-05	0.0029	2.3029e-04	0.9881	7.2546e-04	7.9803e-04	2.8914e-04
5	8.8565e-04	5.4505e-04	0.0043	0.0010	0.9883	0.0055	0.0034
6	0.0053	0.0011	2.5413e-04	1.6323e-04	0.0016	0.9981	5.2866e-04
7	1.0751e-04	7.7475e-05	2.8837e-04	0.0014	1.5622e-04	4.7810e-04	0.9967

Table 6.26: MAC Matrix related to table 6.25.

In the last case (47.55 Hz) the following modal parameters are extracted:

MODE	1	2	3	4	5	6	7
$f_n\ [Hz]$	8.09	24.70	35.32	45.01	47.51	53.40	65.80
ζ	0.22%	1.44%	1.42%	0.92%	1.26%	1.65%	2.01%
DAMPING ERROR	0%	0%	0.7%	19.1%	8.7%	2.5%	2 %

Table 6.27: Extracted modal parameters when excitation frequency is 47.55 Hz (model order:44).

All the modes are detected from the 21st model order.

6.3.3 10% Noise in both Input and Output

The effect of severe noise conditions will be analysed in this subchapter in a similar fashion to the preceding one. Same three excitation frequency values will be used in tests.

The stabilization diagram of the first case (35.32 Hz) is reported in fig. 6.33 and its extracted parameter are reported int able 6.27. Distortion of the estimated FRF due to noise is clearly visible.

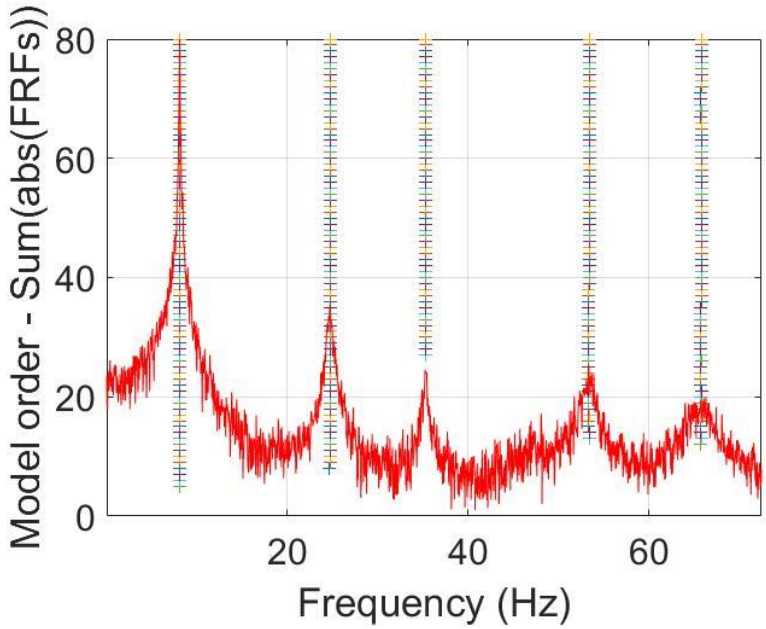

Figure 6.32: Resulting stabilization diagram of the case with an excitation frequency of 35.32 Hz and 10% noise in both input and output.

MODE	1	2	3	6	7
f_n $[Hz]$	8.09	24.70	35.28	53.36	65.75
ζ	0.25%	1.25%	0.62%	0.85%	0.66%
DAMPING ERROR	13,6%	13.2%	56.6%	47.2%	66.5 %

Table 6.27: Extracted modal parameters when excitation frequency is 35.32 Hz (model order:78) with %10 noise in input and output.

At this point we can only deduce the expected decrease in the number of detected modes and damping extraction accuracy. Every single mode's damping ratio is extracted lesser than the case with lower noise. This reduction leads to unacceptable levels of inaccuracies. Only the first mode's damping is closer to the truth because it was already overestimated in the previous case.

The parasitic nature of the estimated FRF also hints that increasing the model order further would not render the detection of the twin modes possible.

Another intriguing result is that every diagonal element in the MAC matrix, for the detected modes, is bigger than ~%99. This finding outlines that mode shapes, like natural frequencies, are extracted in an accurate way regardless of the noise content.

	1	2	3	4	5	6	7
1	0.9998	0.0015	0.0023	6.6634e-05	0.0014	0.0056	9.7284e-06
2	0.0032	0.9989	0.0018	0.0020	0.0021	0.0018	2.8491e-04
3	0.0030	0.0018	0.9970	2.1697e-04	0.0066	1.7396e-04	0.0013
4	0.0036	9.4390e-04	6.7769e-05	0.0013	0.0030	0.9897	0.0028
5	1.3465e-04	1.2846e-04	0.0010	4.2693e-04	7.2447e-04	0.0017	0.9933
6	NaN	NaN	NaN	NaN	NaN	NaN	NaN
7	NaN	NaN	NaN	NaN	NaN	NaN	NaN

Table 6.28: MAC Matrix related to table 6.27.

To verify the hypotheses suggested in the previous paragraph we move on to the second case (40.5 Hz) which corresponds to the anti-resonance. Fig. 6.33 depicts a similar stabilization chart to the previous case, but the fact that there are more model orders with 5 detected modes betrays that having the excitation frequency shifted towards anti-resonant values improves the extraction accuracy. The extracted parameters are listed in table 6.29.

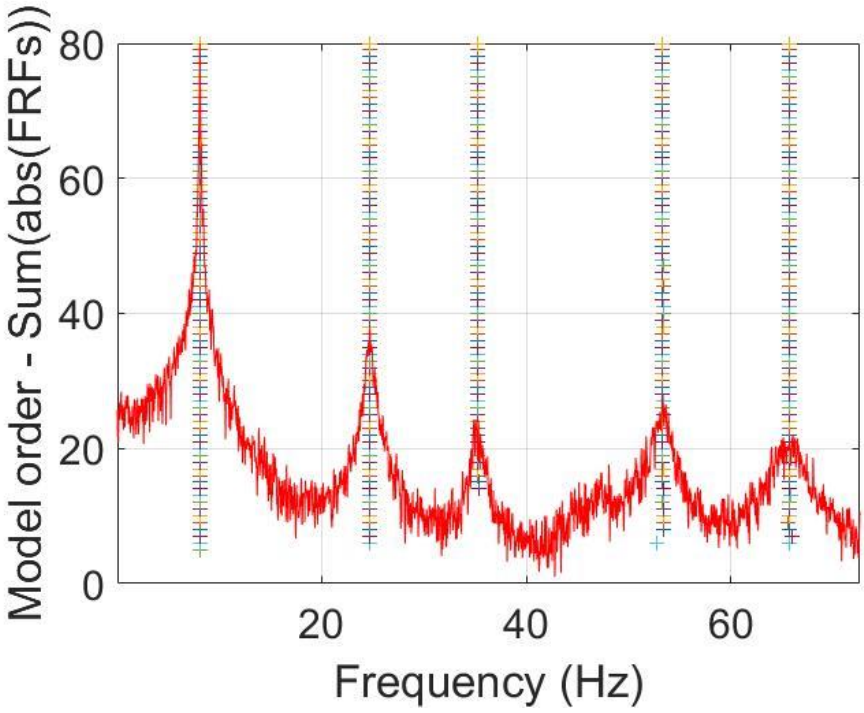

Figure 6.33: Resulting stabilization diagram of the case with an excitation frequency of 40.50 Hz and 10% noise in both input and output.

MODE	1	2	3	6	7
f_n $[Hz]$	8.0910	24.7016	35.2501	53.3558	65.7607
ζ	0.25%	1.30%	0.95%	1.17%	1.30%
DAMPING ERROR	13,6%	9.7%	33.6%	27.3%	34.0 %

Table 6.29: Extracted modal parameters when excitation frequency is 40.50 Hz (model order:78) with %10 noise in input and output.

These findings empower two notions: High noise effects the accuracy severely and harmonic excitations with frequencies corresponding to anti-resonant frequencies are more suitable for modal parameter extraction. A MAC matrix with utmost accuracy once again shows that mode shapes are easy to extract also under high noise.

	1	2	3	4	5	6	7
1	0.9998	0.0017	0.0024	5.0079e-05	0.0012	0.0056	4.9424e-05
2	0.0028	0.9992	0.0017	0.0018	0.0018	0.0014	2.5449e-04
3	0.0022	0.0021	0.9964	1.9629e-04	0.0052	3.4487e-04	9.2020e-04
4	0.0044	0.0010	2.0751e-04	7.2388e-04	0.0028	0.9945	8.1459e-04
5	2.0984e-04	1.2970e-04	4.0143e-04	0.0011	2.9711e-04	9.0994e-04	0.9958
6	NaN	NaN	NaN	NaN	NaN	NaN	NaN
7	NaN	NaN	NaN	NaN	NaN	NaN	NaN

Table 6.30: MAC Matrix related to table 6.29.

Finally, the excitation is raised to 47.55 Hz to see if it will help in detecting the twin modes. Fig. 6.34 shows that moving the excitation frequency to the resonant frequency of hard-to-detect modes renders those modes easier to extract.

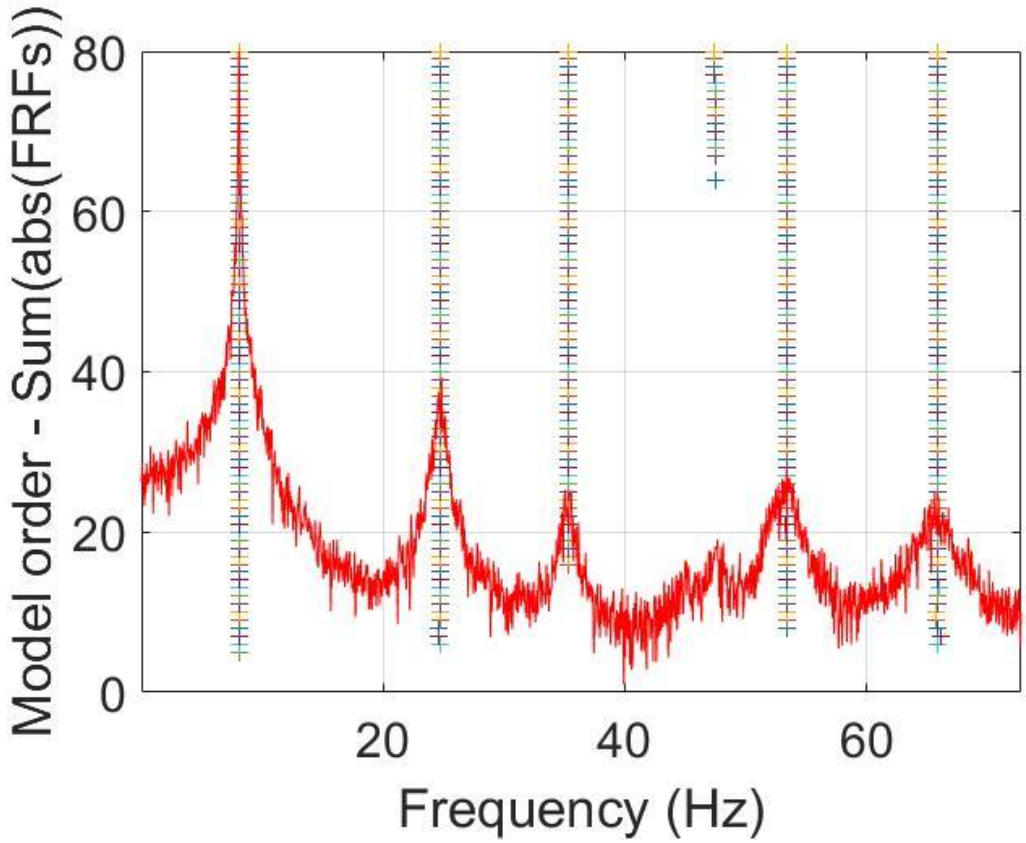

Figure 6.34: Resulting stabilization diagram of the case with an excitation frequency of 47.55 Hz and 10% noise in both input and output.

Related extracted parameters are reported below:

MODE	1	2	3	5	6	7
f_n $[Hz]$	8.09	24.71	35.31	47.47	53.40	65.86
ζ	0.31%	1.30%	0.75%	0.02%	1.09%	1.21%
DAMPING ERROR	40,9%	9.7%	47.6%	98.6%	32.3%	38.6 %

Table 6.31: Extracted modal parameters when excitation frequency is 47.55 Hz (model order:78) with %10 noise in input and output.

With respect to the previous case a fall in accuracy is observed. This is an expected result since we moved towards a harmonic frequency. Even though the damping ratio is extremely inaccurate, natural frequency and the mode shape extraction is quite accurate.

	1	2	3	4	5	6	7
1	0.9998	0.0016	0.0023	1.5191e-05	0.0011	0.0060	1.5537e-05
2	0.0013	0.9990	0.0013	0.0022	0.0025	0.0013	1.1732e-04
3	0.0023	0.0033	0.9943	8.6981e-04	0.0040	1.1631e-04	3.8820e-04
4	0.0015	5.8688e-05	0.0136	0.0469	0.9207	0.0278	0.0203
5	0.0068	8.5132e-04	2.6007e-04	7.8910e-04	0.0025	0.9923	0.0015
6	7.7723e-06	4.4084e-05	3.6981e-04	0.0015	0.0010	0.0012	0.9954
7	NaN	NaN	NaN	NaN	NaN	NaN	NaN

Table 6.32: MAC Matrix related to table 6.31.

7. Conclusion

The preceding two chapters include many observations of the RFP-z viability under varying circumstances. The result will be compared in this chapter in order to draw more general conclusions. Since there are more than one important parameter which affects the accuracy of the method, each of them will be compared separately in different subchapters. These parameters include:

- FRF estimation method (EMA vs. OMA) and the reference dof in OMA case
- Noise level
- Force typology
- Excitation frequency in presence of a harmonic force contribution
- Spectral line density
- Model order (of RFP-z)

It should be noted that in all the simulations in this chapter the RFP-z method will analyse the frequency band between 2 Hz and 80 Hz. This is relevant information because changing the analysis band might affect the accuracy of the results. 2 Hz is selected as the lower boundary because it is low enough to not crop the first peak while being realistic (most commercial accelerometers cannot sense responses lower than 2 Hz).

7.1 FRF Estimation Method

In the area of modal analysis, it is a well-known fact that there is not really a competition between EMA and OMA methods. The former is more accurate by a great margin since it has more information while the latter is relatively less expensive and easier to conduct. For critical systems such as aircraft parts EMA should be conducted regardless of the costs, if possible. In most of the other cases OMA is more feasible and new methods of increasing its accuracy are developed every year.

A primary conclusion we can draw relates to the reference dof selected when utilizing the OMA method. There is not a simple way to deduce a priori which dof will yield better results when chosen as the reference. The ideal case may not only change from structure to structure, but also depending on the circumstances such as force typology and SNR. This is clearly seen from the fact that there was not any single dof to persist as the optimal reference throughout chapter 5. There are various papers in the literature to tackle this problem and develop ways to pick an optimal reference dof [12].

EMA and OMA methods can be contrasted numerically under the generic circumstance with following parameters: A purely random excitation with 3% noise in the output signal, running the RFP-z algorithm for up to 80 model orders and having 2^{14} spectral lines for both EMA and OMA. The results of the best model orders are reported in table 7.1. Since the natural frequencies are very accurate in every case they are not repeatedly reported. For the same reason MAC matrix values are also kept outside of the comparison.

mode		1	2	3	4	5	6	7
fn (analytical) [Hz]	-	8.09	24.7	35.3	45.0	47.5	53.4	65.9
ζ (analytical)	-	0.22%	1.44%	1.43%	1.15%	1.38%	1.61%	1.97%
ζ (OMA RDOF 2) model order 44	-	0.16%	1.20%	0.95%	-	0.21%	1.04%	0.42%
damping error	-	27.3%	16.7%	33.6%	-	84.8%	35.4%	78.7%
ζ (OMA RDOF 4) model order 43	-	0.16%	1.13%	0.86%	0.39%	-	1.03%	0.50%
damping error	-	27.3%	21.5%	39.9%	66.1%	-	36.0%	74.6%
ζ (OMA RDOF 6) model order 47	-	0.16%	1.11%	0.81%	0.31%	-	1.08%	1.08%
damping error	-	27.3%	22.9%	43.4%	73.0%	-	32.9%	45.2%
fn (EMA) [Hz]	8.08	8.11	24.7	35.3	45.0	47.5	53.4	65.8
ζ (EMA) model order 78	0.16%	0.25%	1.57%	1.51%	1%	1.33%	1.71%	2.09%
damping error	27.3%	13.6%	9.0%	5.6%	13.0%	3.6%	6.2%	6.1%

Table 7.1: Comparison between EMA and OMA.

The table above can be examined for some interesting observations. First of all, RDOF 6 seems to be the optimal case for OMA, but there is no significant difference between reference DOFs other than the 7th modes damping ratio. This is not an important conclusion since the results in this regard is very situational.

As it can be seen, while OMA method could never detect all the modes (although the missing mode changes with RDOF), EMA did detect all of the modes. In fact, it detected eight modes because the algorithm misinterpreted the first mode as two separate modes. According to all the simulations in this thesis so far, this is not a common result but it is reported nonetheless to highlight the possibility. This is due utilizing a high model order of 78. The comparison of damping ratio's error values demonstrates the superiority of the EMA in case of accuracy.

Another factor contributing to inaccuracy of the 1st mode is the fact that its natural frequency is nearby to lower limit of the analysed frequency band. This results in partial cropping of the peak and hence some information loss about the mode.

Another trend that persisted throughout this thesis is that the best model order in OMA is usually a moderate value in the range of 20-50, and increasing it further decreases the accuracy. In the other hand the accuracy of EMA increases continuously with the model order, at least until 80.

Also, it can be safely deduced that OMA expectedly shows its worst performance in estimating ergo extracting the twin modes. In EMA twin modes are comparatively problematic as well, but not in the same scope of OMA.

For the rest of this chapter, EMA will be utilized as the FRF estimation technique, since a comparison between not so low accuracies would yield healthier conclusions.

7.2 Noise Level

Perhaps the most obvious parameter that would affect the modal parameter extraction accuracy is the noise level. SNR is a value with utmost importance in any field involved with signal processing and it should always be kept within acceptable levels.

In this subchapter the following cases will be compared:

-No noise (unrealistic optimal case)

-3% Noise in the output signal

-3% Noise in both input & output

-10% Noise in the output signal

-10% Noise in both input & output

This way it is expected to see the consequences of having noise present in every signal as well as examining the impact level of increasing the noise.

EMA method is utilized with a spectral line density of 2^{14}. Excitation is purely random with a standard deviation of $500N$. The results are reported in table 7.2.

mode	1	2	3	4	5	6	7
fn (analytical) [Hz]	8.09	24.7	35.3	45.0	47.5	53.4	65.9
ζ (analytical)	0.22%	1.44%	1.43%	1.15%	1.38%	1.61%	1.97%
ζ (No Noise) model order 14	0.22%	1.57%	1.53%	1.23%	1.48%	1.75%	2.25%
damping error	0.0%	9.0%	7.0%	7.0%	7.2%	8.7%	14.2%
ζ (3% Output Noise) model order 32	0.39%	1.56%	1.49%	1.01%	1.35%	1.71%	2.08%
damping error	77.3%	8.3%	4.2%	12.2%	2.2%	6.2%	5.6%
ζ (3% I/O Noise) model order 78	0.33%	1.57%	1.51%	1.08%	1.38%	1.71%	2.10%
damping error	50.0%	9.0%	5.6%	6.1%	0.0%	6.2%	6.6%
ζ (10% Output Noise) model order 79	0.28%	1.55%	1.38%	0.30%	0.80%	1.61%	1.93%
damping error	27.3%	7.6%	3.5%	73.9%	42.0%	0.0%	2.0%
ζ (10% I/O Noise) model order 78	0.32%	1.55%	1.34%	0.09%	0.60%	1.56%	1.84%
damping error	45.5%	7.6%	6.3%	92.2%	56.5%	3.1%	6.6%

Table 7.2: Comparison between varying noise presence.

By reading the table above we can immediately see that the scenario with the absence of noise is the best one accuracy wise. With the presence of noise, the accuracies start to fall and some modes are seemingly affected more than others. The first mode directly catches attention due to its abrupt fall in accuracy, but it should be noted that its fall in accuracy is due to several reasons independent from the noise content. First, the spectral line density of the estimated FRFs directly affects the quality of the 1st peak more than others due to its steepness. This effect will be analysed later on in this chapter.

Another phenomenon that affects the 1st modes damping extraction accuracy is the numerical fitting in the RFP-z process. Increasing the model order in already accurate cases result in the extraction of 2 separate modes in place of the 1st mode. This effect paradoxically occurs when the noise is not very high and the results of low model orders are fairly accurate. This gives higher noise content an advantage with regards to the first mode's extraction accuracy.

Last but not least, 1st modes vicinity to the lower limit of the analysis band causes some information loss and effects the modal parameter extraction in a bad way.

Due to these three mentioned reason the first mode's accuracy should not be taken as the deciding factor of this comparison. Instead, the damping ratios of the twin modes, being the hardest ones to extract accurately, stand to be the values to examine for a healthy comparison.

At a first glance the accuracy does not seem to fall steeply as the noise content increases. This observation is justified considering that as the noise content increases so does the model order with the best least squares fitting. The twin modes accuracies are too sensitive to noise and the model order threshold in this simulation (80) was not enough to retain their extraction in an accurate fashion. Including 10% noise even only in output signals pushes the extracted parameters into the unacceptable zone. As the same noise is included also in the input signal, it is evident that the model order threshold is not enough also for the well separated modes.

Another interesting finding correlates different noise types to accuracy of different mode types. To elaborate, increasing the noise content in the output signals seems to decrease the accuracy of the twin modes harshly, while adding a mirror noise to the input signal does not only moderately decreases the twin mode accuracy, but also hinders the accuracy of the extraction of well separated modes.

It is as if increasing the noise content in the output renders the twin modes undetectable and thus makes the algorithm "focus more" on the detected modes while creating a best fit line, resulting in a slight increase in the accuracy of well separated modes.

It is useful to elaborate how to select the best model order. The problem of selecting that with the minimum error between FRFs it favours the first mode, because it is the highest and the widest peak. The same mode is the most inaccurate one for the reasons mentioned above, and in chapter 7.4 its accuracy will be improved by tweaking the spectral line density, and it usually follows an opposite trend with the rest of the modes. Therefore, the best model order is selected manually focusing on the other modes, especially the 4th and the 5th ones. The plot of extracted damping ratio vs. model order is utilized to facilitate the selection.

7.3 Force Typology

Force typology is one of the most important characteristics in modal analysis because the FRF estimation methods involved assume that the excitation covers a wide frequency band. Several force typologies that will be compared in this chapter are s following:

- Purely random excitation
- Purely harmonic excitation
- Hybrid excitation with low random contribution (random part's std. deviation is 1% of the harmonic part's)
- Hybrid excitation with moderate random contribution (random part's std. deviation is 10% of the harmonic part's)
- Hybrid excitation with high random contribution (random part's std. deviation is same as the harmonic part's)

It has been observed previously that the excitation frequency of the harmonic contribution is a very critical factor and its effect will be analysed thoroughly in the following subchapter. For the force typology comparison, the excitation frequency is 35.32 Hz, which corresponds the 3rd mode's natural frequency. This value is selected because it is neither the best case nor the worst case so the comparison can focus more on the random-harmonic balance of the force signal.

Again, EMA is applied to estimate the FRF with a spectral line amount of 2^{14}. A noise of 3% is considered to be present in both input and output signals. The comparison can be examined in table 7.3.

mode	1	2	3	4	5	6	7
fn (analytical) [Hz]	8.09	24.7	35.3	45.0	47.5	53.4	65.9
ζ (analytical)	0.22%	1.44%	1.43%	1.15%	1.38%	1.61%	1.97%
ζ (Purely Random) model order 32	0.38%	1.56%	1.50%	0.92%	1.29%	1.71%	2.08%
damping error	72.7%	8.3%	4.9%	20.0%	6.5%	6.2%	5.6%
ζ (High Random Hybrid) model order 19	0.39%	1.57%	1.48%	0.62%	1.20%	1.71%	2.09%
damping error	77.3%	9.0%	3.5%	46.1%	13.0%	6.2%	6.1%
ζ (Moderate Random Hybrid) model order 78	0.31%	1.58%	1.44%	0.69%	1.05%	1.65%	1.96%
damping error	40.9%	9.7%	0.7%	40.0%	23.9%	2.5%	0.5%
ζ (Low Random Hybrid) model order 69	0.19%	-	-	-	-	-	-
damping error	13.6%	-	-	-	-	-	-
ζ (Purely Harmonic) model order -	-	-	-	-	-	-	-
damping error	-	-	-	-	-	-	-

Table 7.3: Comparison between varying force typologies with the presence of noise in input & output.

Again, focusing on the accuracy of the twin modes rather than the first mode makes it possible to see that as harmonic contribution gets dominant over the random contribution, the accuracy falls steeply and the number of detected modes is simply pathetic. Repeating the same simulations without noise in the input yields the results in Table 7.4.

mode	1	2	3	4	5	6	7
fn (analytical) [Hz]	8.09	24.7	35.3	45.0	47.5	53.4	65.9
ζ (analytical)	0.22%	1.44%	1.43%	1.15%	1.38%	1.61%	1.97%
ζ (Purely Random) model order 51	0.42%	1.57%	1.50%	1.01%	1.34%	1.71%	2.09%
damping error	90.9%	9.0%	4.9%	12.2%	2.9%	6.2%	6.1%
ζ (High Random Hybrid) model order 55	0.38%	1.57%	1.51%	1.03%	1.36%	1.71%	2.10%
damping error	72.7%	9.0%	5.6%	10.4%	1.4%	6.2%	6.6%
ζ (Moderate Random Hybrid) model order 60	0.31%	1.57%	1.43%	0.60%	1.09%	1.67%	2.01%
damping error	40.9%	9.0%	0.0%	47.8%	21.0%	3.7%	2.0%
ζ (Low Random Hybrid) model order 80	0.40%	1.20%	-	-	-	-	-
damping error	81.8%	16.7%	-	-	-	-	-
ζ (Purely Harmonic) model order -	-	-	-	-	-	-	-
damping error	-	-	-	-	-	-	-

Table 7.4: Comparison between varying force typologies with the presence of noise in output.

There is only a slight difference between two different noise cases. This difference is negligible because it can be attributed to generating a random force and response behaviour in every trial. The non-negligible pattern is clear, as the excitation becomes less random and more harmonic, the performance of RFP-z decreases.

7.4 Harmonic Excitation Frequency

From the previous subchapter it is confirmed that loads with relatively high harmonic content are not suitable for RFP-z while those that contain at least a moderate amount of randomness can yield results to some extent. Regardless of this typology, whenever an excitation has a harmonic nature, its frequency affects the accuracy greatly. This is because it can correspond to either resonant or anti-resonant frequencies.

In chapter 6.3.1 a thorough analysis of different frequency values is performed. The analysis is repeated because to get more realistic conclusion values minimum frequency of the analysis band is set to 2 Hz, while in the previous chapter it was 0 Hz.

The analysis is carried out by utilizing EMA, with an excitation of moderate amount of randomness with respect to the harmonic content. 3% noise is included in the output signals. The results are as follows:

mode	1	2	3	4	5	6	7
fn (analytical) [Hz]	8.09	24.7	35.3	45.0	47.5	53.4	65.9
ζ (analytical)	0.22%	1.44%	1.43%	1.15%	1.38%	1.61%	1.97%
ζ (8.1 Hz) model order -	-	-	-	-	-	-	-
damping error	-	-	-	-	-	-	-
ζ (24.7 Hz) model order 32	0.27%	1.54%	0.82%	-	-	1.18%	1.24%
damping error	22.7%	6.9%	42.7%	-	-	26.7%	37.1%
ζ (35.3 Hz) model order 44	0.33%	1.57%	1.48%	0.61%	1.05%	1.66%	2.00%
damping error	50.0%	9.0%	3.5%	47.0%	23.9%	3.1%	1.5%
ζ (40.5 Hz) model order 79	0.34%	1.57%	1.50%	0.92%	1.28%	1.69%	2.06%
damping error	54.5%	9.0%	4.9%	20.0%	7.2%	5.0%	4.6%
ζ (45.0 Hz) model order 54	0.38%	1.57%	1.51%	1.00%	1.32%	1.71%	2.08%
damping error	72.7%	9.0%	5.6%	13.0%	4.3%	6.2%	5.6%
ζ (47.6 Hz) model order 54	0.39%	1.57%	1.50%	0.92%	1.28%	1.70%	2.08%
damping error	77.3%	9.0%	4.9%	20.0%	7.2%	5.6%	5.6%
ζ (53.5 Hz) model order 79	0.36%	1.56%	1.42%	0.50%	0.98%	1.69%	1.97%
damping error	63.6%	8.3%	0.7%	56.5%	29.0%	5.0%	0.0%
ζ (66.0 Hz) model order 68	0.36%	1.57%	1.46%	0.69%	1.12%	1.65%	1.99%
damping error	63.6%	9.0%	2.1%	40.0%	18.8%	2.5%	1.0%

Table 7.5: Comparison between varying excitation frequencies.

RFP-z detects two different modes at the 1st peak after a certain model order for each case. 1st mode's accuracy decreases as we get closer to that specific model order while the other mode's accuracies generally increase. For this reason, the first accuracy should not be focused on in this analysis. Since the other separate mode accuracies do not change significantly, twin modes' accuracies can be taken as references in a general sense.

The first obvious observation is that the excitation frequency should not be close to the analysis band's lower limit.

Generally speaking, as the excitation frequency approaches a mode's natural frequency, extraction of that frequency improves. This is observed to an extent, but there are lots of exceptions in the results above. This can be attributed to the randomness of the excitation and noise in every case, since the code generates a new random vector for every excitation, small changes should not determine the derived results.

Around 40-50 Hz there is a significant improvement in the accuracy. This range includes the anti-resonance point and twin modes, whose peaks are not as strong as the separate modes.

Overall, this subchapter can be concluded by saying that in case of utilizing EMA to a structure whose FRF has not well-separated modes, the excitation applied by the shakers should have a frequency in the appropriate range.

In fact, to avoid this problem a single frequency excitation is never applied in EMA. Instead, a random input or a sine sweep, where the excitation frequency varies in a large frequency range. Loads with single excitation frequencies (and their harmonics) are not usually there for testing purposes but rather come from rotating machinery which introduce an unmeasured excitation.

7.5 Spectral Line Density

Spectral line density, i.e. frequency resolution plays crucial role in the accuracy of the extraction of narrow and steep modes, as they require a good resolution to encompass their data in the FRF. The importance of this parameter is explained in chapter 5.4. Also, all the previous subchapters do have an inaccurate 1st mode extraction. This is due to having set an inappropriate spectral line density. This decision was done to be able to increase the model order up to 80, which would be computationally a very inefficient task with more spectral lines. In this subchapter the maximum model order is reduced to 30 in order to increase the SLD.

If we consider the simple case of a random force and a 3% noise in the output signal, utilizing EMA, the effect of SLD can be seen in table 7.6.

mode	1	2	3	4	5	6	7
fn (analytical) [Hz]	8.09	24.7	35.3	45.0	47.5	53.4	65.9
ζ (analytical)	0.22%	1.44%	1.43%	1.15%	1.38%	1.61%	1.97%
ζ (2^12 Spectral Lines) model order 19	0.81%	1.61%	1.53%	1.10%	1.43%	1.73%	2.16%
damping error	268.2%	11.8%	7.0%	4.3%	3.6%	7.5%	9.6%
ζ (2^13 Spectral Lines) model order 18	0.56%	1.57%	1.50%	0.91%	1.32%	1.72%	2.12%
damping error	154.5%	9.0%	4.9%	20.9%	4.3%	6.8%	7.6%
ζ (2^14 Spectral Lines) model order 26	0.36%	1.56%	1.49%	0.93%	1.32%	1.70%	2.09%
damping error	63.6%	8.3%	4.2%	19.1%	4.3%	5.6%	6.1%
ζ (2^15 Spectral Lines) model order 30	0.31%	1.56%	1.46%	0.70%	1.18%	1.68%	2.04%
damping error	40.9%	8.3%	2.1%	39.1%	14.5%	4.3%	3.6%
ζ (2^16 Spectral Lines) model order 30	0.30%	1.53%	1.23%	-	0.42%	1.55%	1.74%
damping error	36.4%	6.3%	14.0%	-	69.6%	3.7%	11.7%

Table 7.6: Comparison between varying spectral line densities.

These results are very interesting. Increasing the spectral line amount definitely improves the accuracy of the 1st mode. The other side of the coin is that as the spectral resolution increases the required model order increases, and the accuracy of other modes are compromised. The reason of this is better seen than explained, increasing the SLD harshly decreases the smoothness of the estimated FRF.FRFs of the cases in table 7.6 can be seen in fig. 7.1.

Unless there is an exceptional case like the 1st mode, spectral line density should not be kept high. In the other hand keeping that value low greatly affects the extracted damping ratio too. As seen in the first case (2^{12} lines), the damping ratios are all overestimated. This

overestimation actually improves the accuracy of the 4th mode's extraction, which is always underestimated and is balanced out in this particular case.

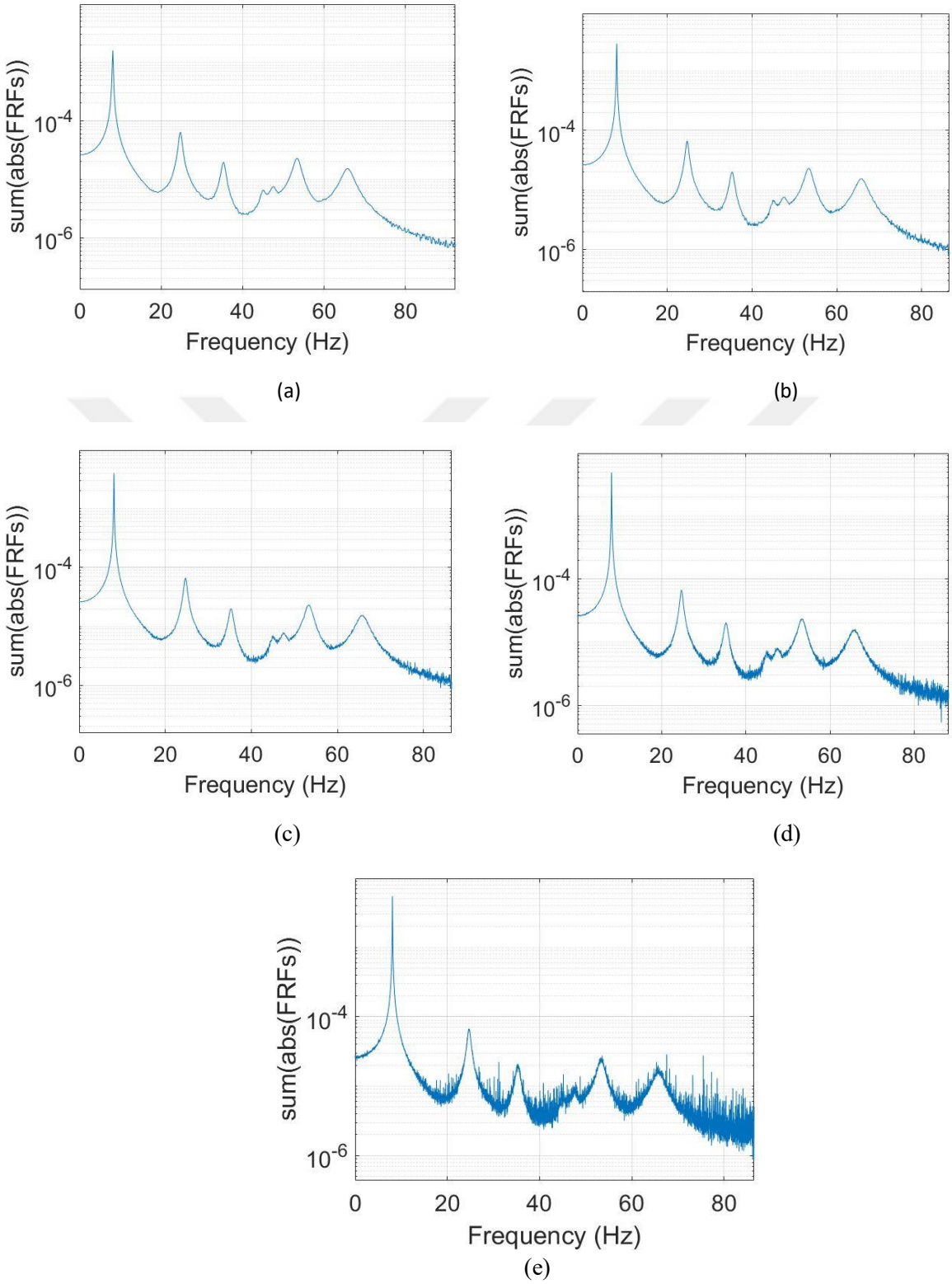

Figure 7.1: Effect of SLD on FRF smoothness. The number of spectral lines are respectively (a) 2^{12}, (b) 2^{13}, (c) 2^{14}, (d) 2^{15} and (e) 2^{16}.

7.6 Utilizing Automatic Selection Algorithm

In all the cases studied this far there was a significant constraint: Parameters extracted from different model orders cannot be used simultaneously, i.e. the best model order is selected and only its associated parameters are used to evaluate the accuracy. Although in the selection of the model order least squares approximation and damping-model order trend plots are used as a guide, the process itself is manual to focus on the appropriate parameter. This is because different modal parameters might exhibit their best extraction accuracy in different model orders, resulting in that there is not actually a universally best model order.

In practice, fortunately there is no reason to adhere to this constraint. Instead, there are algorithms built for detecting the most accurate extraction of every modal parameter within the matrix of parameters including the results of every model order. They can differentiate spurious and non-spurious modes, and seek consistently detected modes, or in other words stable modes.

While sticking to our original constraint gives valuable insights such as the correlation between the noise level and the required minimum model order, utilizing automatic combination algorithms definitely underlines what to expect in a real practical case. It also eliminates the errors caused by the manual selection of the best model order, as observing the data of nearly a hundred model orders quickly can naturally end with erratic conclusions. But unfortunately, this does not guarantee a better accuracy, as the algorithm does not know the analytical modal parameters and select the best extractions based on consistency.

In this chapter an algorithm designed to detect the optimal extraction parameters specifically for RFP-z will be utilized (see [8]). Since EMA is undoubtedly superior to OMA, given that it is feasible, their comparison with this algorithm is skipped and the first simulation characteristic to be analysed is the noise level. Repeating the simulations carried out for table 7.2 yields the results in table 7.7. Control characteristics of the simulation (like the model order, spectral line density...) are conserved.

mode	1	1*	2	3	4	5	6	7
fn (analytical) [Hz]	8.09	8.09*	24.7	35.3	45.0	47.5	53.4	65.9
ζ (analytical)	0.22%	0.22%*	1.44%	1.43%	1.15%	1.38%	1.61%	1.97%
ζ (No Noise)	0.43%	0.46%	1.56%	1.53%	1.23%	1.48%	1.75%	2.25%
damping error	95.5%	95.5%	8.3%	7.0%	7.0%	7.2%	8.7%	14.2%
ζ (3% Output Noise)	0.35%	-	1.56%	1.49%	0.89%	1.27%	1.71%	2.09%
damping error	59.1%	-	8.3%	4.2%	22.6%	8.0%	6.2%	6.1%
ζ (3% I/O Noise)	0.37%	-	1.57%	1.51%	1.05%	1.38%	1.71%	2.10%
damping error	68.2%	-	9.0%	5.6%	8.7%	0.0%	6.2%	6.6%
ζ (10% Output Noise)	0.32%	-	1.54%	1.39%	0.21%	0.75%	1.62%	1.90%
damping error	45.5%	-	6.9%	2.8%	81.7%	45.7%	0.6%	3.6%
ζ (10% I/O Noise)	0.34%	-	1.53%	1.32%	-	0.59%	1.58%	1.79%
damping error	54.5%	-	6.3%	7.7%	-	57.2%	1.9%	9.1%

Table 7.7: Comparison between varying noise presence utilizing automatic selection algorithm.

The first mode is detected twice in the case with no noise. This due to numerical reasons related to absence of the noise, increasing it even to 0.2% eliminates this problem. It is better to ignore the accuracies of the first mode until the spectral line density is adjusted later on.

The twin modes' accuracy significantly falls with respect to manual picking. This is natural since those two modes were taken as reference for handpicking the best model order. Also, especially 4th mode's extracting damping ratio generally increases with the model order and does not converge before the 80th model order, so it is harder to detect a consistent damping ratio for that specific mode.

The well separated modes do not exhibit a significant change in accuracy.

Analysis of the force typology's effect will be done under two different conditions like the previous instance, the first of which is the presence of both input and output noise (table 7.8). In the second case the input noise is assumed to be negligible (table 7.9). Note that the harmonic contributions of the excitations below are applied at a frequency of $35.32\,Hz$ which corresponds to the 3rd mode.

mode	1	2	3	4	5	6	7
fn (analytical) [Hz]	8.09	24.7	35.3	45.0	47.5	53.4	65.9
ζ (analytical)	0.22%	1.44%	1.43%	1.15%	1.38%	1.61%	1.97%
ζ (Purely Random)	0.37%	1.57%	1.51%	1.05%	1.38%	1.71%	2.10%
damping error	68.2%	9.0%	5.6%	8.7%	0.0%	6.2%	6.6%
ζ (High Random Hybrid)	0.38%	1.56%	1.51%	0.98%	1.34%	1.71%	2.09%
damping error	73.6%	8.6%	5.7%	15.1%	2.6%	6.5%	6.3%
ζ (Moderate Random Hybrid)	0.38%	1.49%	1.41%	0.53%	0.97%	1.62%	1.97%
damping error	72.1%	3.4%	1.2%	54.1%	29.7%	0.3%	0.2%
ζ (Low Random Hybrid)	-	-	-	-	-	-	-
damping error	-	-	-	-	-	-	-
ζ (Purely Harmonic)	-	-	-	-	-	-	-
damping error	-	-	-	-	-	-	-

Table 7.8: Comparison between varying force typologies with the presence of noise in input & output utilizing automatic selection algorithm.

mode	1	2	3	4	5	6	7
fn (analytical) [Hz]	8.09	24.7	35.3	45.0	47.5	53.4	65.9
ζ (analytical)	0.22%	1.44%	1.43%	1.15%	1.38%	1.61%	1.97%
ζ (Purely Random)	0.38%	1.57%	1.50%	1.02%	1.35%	1.72%	2.10%
damping error	73.1%	8.8%	4.9%	11.5%	2.5%	6.8%	6.5%
ζ (High Random Hybrid)	0.37%	1.56%	1.47%	0.73%	1.18%	1.69%	2.06%
damping error	69.8%	8.5%	3.1%	36.2%	14.8%	5.2%	4.4%
ζ (Moderate Random Hybrid)	0.36%	1.55%	1.42%	0.45%	0.97%	1.65%	1.98%
damping error	63.4%	7.8%	0.6%	60.5%	29.8%	2.2%	0.3%
ζ (Low Random Hybrid)	0.38%	1.06%	-	-	-	-	-
damping error	73.0%	26.7%	-	-	-	-	-
ζ (Purely Harmonic)	-	-	-	-	-	-	-
damping error	-	-	-	-	-	-	-

Table 7.9: Comparison between varying force typologies with the presence of noise only in output utilizing automatic selection algorithm.

From the data above it is observed that increasing the harmonic contribution of the excitation results in an improvement of the extraction accuracy of well separated modes, up to a point. Increasing the harmonic contribution further has a sudden adverse effect, rendering almost all modes undetectable by RFP-z. The twin modes on the other hand have their extraction accuracy fall steeply with increasing harmonic contribution. Since they count as the bottleneck of the overall accuracy, it can be derived that more random a signal is, more accurate its extraction gets. This confirms with the fact that in practice 2 major methods of performing experimental modal analysis is either supplying a random excitation or performing a sine sweep. The latter is justified by the fact that a moderate amount of harmonic excitation contribution actually improves the extraction of that specific frequency. It is clear that the 3rd mode's extraction gets better by shifting the forces typology to harmonic, up to a point.

The next batch of simulations is dedicated to see the effect of the harmonic excitation frequency. The excitation also includes a moderate amount of random contribution to guarantee some level of accuracy. Only a 3% noise in the output is included.

mode	1	2	3	4	5	6	7
fn (analytical) [Hz]	8.09	24.7	35.3	45.0	47.5	53.4	65.9
ζ (analytical)	0.22%	1.44%	1.43%	1.15%	1.38%	1.61%	1.97%
ζ (8.1 Hz)	-	-	-	-	-	-	-
damping error	-	-	-	-	-	-	-
ζ (24.7 Hz)	0.34%	1.51%	0.76%	-	-	1.15%	1.26%
damping error	54.8%	4.6%	46.7%	-	-	28.5%	35.8%
ζ (35.3 Hz)	0.36%	1.55%	1.42%	0.45%	0.97%	1.65%	1.98%
damping error	63.4%	7.8%	0.6%	60.5%	29.8%	2.2%	0.3%
ζ (40.5 Hz)	0.39%	1.56%	1.49%	0.95%	1.30%	1.71%	2.08%
damping error	75.1%	8.3%	4.2%	17.2%	5.7%	6.2%	5.5%
ζ (45.0 Hz)	0.36%	1.56%	1.48%	0.84%	1.26%	1.71%	2.07%
damping error	65.9%	8.5%	3.4%	26.6%	8.8%	6.1%	5.2%
ζ (47.6 Hz)	0.37%	1.57%	1.48%	0.90%	1.28%	1.70%	2.08%
damping error	70.1%	9.0%	3.5%	21.3%	7.4%	5.8%	5.4%
ζ (53.5 Hz)	0.32%	1.56%	1.38%	0.13%	0.77%	1.61%	1.94%
damping error	47.5%	8.2%	3.4%	88.7%	44.3%	0.2%	1.6%
ζ (66.0 Hz)	0.37%	1.56%	1.44%	0.55%	1.06%	1.68%	1.99%
damping error	68.8%	8.0%	1.0%	52.2%	23.2%	4.1%	0.9%

Table 7.10: Comparison between varying excitation frequencies utilizing automatic selection algorithm.

Data above resonates with the conclusions drawn in chapter 7.4. Frequency range of 40-50 Hz represent the band with most accurate result. This is because it corresponds to the range of anti-resonance and the twin modes. Also, it is very clear that every well-separated mode is extracted most accurately when an excitation with a frequency that correspond to their natural frequency is applied. Additionally, it is evident that applying an excitation close to the limits of the analysis band should be avoided.

To focus on the 1st mode's extraction accuracy, spectral line density should be tweaked. Table 7.11 contains the accuracy results of different frequency resolution values. The excitation is random in nature and a noise of 3% is included in the output channels.

mode	1	2	3	4	5	6	7
fn (analytical) [Hz]	8.09	24.7	35.3	45.0	47.5	53.4	65.9
ζ (analytical)	0.22%	1.44%	1.43%	1.15%	1.38%	1.61%	1.97%
ζ (2^12 Spectral Lines)	0.72%	1.60%	1.53%	0.42%	1.00%	1.74%	2.15%
damping error	226.0%	10.8%	7.2%	63.5%	27.4%	7.9%	9.3%
ζ (2^13 Spectral Lines)	0.55%	1.58%	1.51%	0.96%	1.35%	1.73%	2.13%
damping error	151.6%	9.5%	5.9%	16.2%	2.5%	7.4%	8.3%
ζ (2^14 Spectral Lines)	0.34%	1.57%	1.50%	1.05%	1.37%	1.72%	2.10%
damping error	55.8%	8.9%	5.2%	9.0%	0.8%	6.9%	6.8%
ζ (2^15 Spectral Lines)	0.30%	1.56%	1.48%	0.89%	1.25%	1.70%	2.07%
damping error	37.7%	8.6%	3.5%	22.9%	9.4%	5.7%	4.8%
ζ (2^16 Spectral Lines)	0.26%	1.56%	1.34%	0.03%	0.61%	1.60%	1.85%
damping error	18.5%	8.1%	6.4%	97.8%	56.0%	0.4%	5.9%

Table 7.11: Comparison between varying spectral line densities utilizing automatic selection algorithm.

The results are more accurate than the case with manual selection of the best mode. It is interesting to see that every mode follows a different trend when increasing frequency resolution. A general conclusion can be drawn: If a mode peak is high and close to the analysis band limit, then it is a necessity to increase the spectral line amount. The first mode's increase in accuracy clearly underlines this. Also, the 1st , 2nd and the 5th mode peaks, which are the highest among all peaks, share the trend of increasing accuracy vs. the frequency resolution. Lower mode peaks actually do have a sweet spot, 2^{15} for well separated modes and 2^{14} for the twin modes, which are especially sensitive to the change in the spectral line density.

While the results in the table above clearly show the effects of increasing the frequency resolution, it does not reflect the expected RFP-z accuracy in a practical case because there are ways to improve it. Simply narrowing the analysis band to encompass only modes which are hard to detect, 4 and 5 in our case, improves the result as seen in table 7.12. This prevents the algorithm to not see the majority of the twin modes as the contribution of other modes.

mode	4	5
fn (analytical) [Hz]	45.0	47.5
ζ (analytical)	1.15%	1.38%
ζ (2-80)	0.03%	0.61%
damping error	97.8%	56.0%
ζ (38-50)	0.57%	1.81%
damping error	50.6%	31.5%
ζ (39-49)	0.77%	1.54%
damping error	33.2%	11.8%
ζ (40-49)	0.97%	1.81%
damping error	15.4%	31.3%

Table 7.12: Effect of narrowing down the analysis band on hard-to-detect modes.

It should be noted that the automatic selection algorithm functions only when at least two modes are detected by RFP-z (in order to have a MAC 'matrix'). Due to this reason analysis band cannot be narrowed down on individual peaks. Also, appropriate amount of margin needs to be present to not crop the peaks and thus lose information. As it can be examined, analysis band's final limits are kept at 40 and 49 Hz, narrowing the band further results in RFP-z not detecting 2 distinct modes.

APPENDIX A - Calculation of Unknown Vectors

Eq. 2.10 can be simplified into Eq. 2.11 by utilizing some properties of matrix calculus. The starting point is:

$$\begin{bmatrix} \boldsymbol{A}_1 \\ \vdots \\ \boldsymbol{A}_{NFRF} \end{bmatrix} \boldsymbol{a} + \begin{bmatrix} -\boldsymbol{B} & \cdots & 0 \\ \vdots & \ddots & \vdots \\ 0 & \cdots & -\boldsymbol{B} \end{bmatrix} \begin{Bmatrix} \boldsymbol{b}_1 \\ \vdots \\ \boldsymbol{b}_{NFRF} \end{Bmatrix} = \begin{Bmatrix} \boldsymbol{w}_1 \\ \vdots \\ \boldsymbol{w}_{NFRF} \end{Bmatrix} \tag{A.1}$$

This linear system can be opened up for an m-th generic FRF as:

$$\boldsymbol{A}_m \boldsymbol{a} - \boldsymbol{B}\boldsymbol{b}_m - \boldsymbol{w}_{\boldsymbol{m}} = \boldsymbol{e}_m \tag{A.2}$$

Where $\boldsymbol{e}_m$ is the vector that considers the error between the measured FRF and the assumed model. To find the best fitting $\boldsymbol{a}$ and $\boldsymbol{b}_m$ vectors, the algorithm minimizes the sum of errors present in every spectral line of m FRFs, defined as $E_m = \boldsymbol{e}_m^H \boldsymbol{e}_m$. The global error is thus defined as:

$$E = \sum_{m=1}^{NFRF} E_m = \sum_{m=1}^{NFRF} \boldsymbol{e}_m^H \boldsymbol{e}_m = \mathrm{Re} \sum_{m=1}^{NFRF} [(\boldsymbol{A}_m \boldsymbol{a} - \boldsymbol{B}\boldsymbol{b}_m - \boldsymbol{w}_{\boldsymbol{m}})(\boldsymbol{A}_m \boldsymbol{a} - \boldsymbol{B}\boldsymbol{b}_m - \boldsymbol{w}_{\boldsymbol{m}})^H] \tag{A.3}$$

To find the optimum values in which E is minimum, we should find when its derivative with respect to those vectors correspond to 0. Matrix Calculus rules state for generic **x**, **z** and **Y**:

$$\frac{\partial(\boldsymbol{x}^T \boldsymbol{Y} \boldsymbol{z})}{\partial \boldsymbol{x}} = \boldsymbol{Y}\boldsymbol{z}$$

$$\frac{\partial(\boldsymbol{x}^T \boldsymbol{Y} \boldsymbol{z})}{\partial \boldsymbol{z}} = \boldsymbol{Y}\boldsymbol{x} \tag{A.4}$$

Expanding (A.3) and applying rules in (A.4) yields:

$$\frac{\partial E}{\partial \boldsymbol{a}} = 2 \sum_{m=1}^{NFRF} (\mathrm{Re}[\boldsymbol{A}_m^H \boldsymbol{A}_m]\boldsymbol{a} - \mathrm{Re}[\boldsymbol{A}_m^H \boldsymbol{B}]\boldsymbol{b}_m - \mathrm{Re}[\boldsymbol{A}_m^H \boldsymbol{w}_m]) = 0 \tag{A.5}$$

$$\frac{\partial E}{\partial \boldsymbol{b}_m} = -2\mathrm{Re}[\boldsymbol{B}^H \boldsymbol{A}_m]\boldsymbol{a} + 2\mathrm{Re}[\boldsymbol{B}^H \boldsymbol{B}]\boldsymbol{b}_m + 2\mathrm{Re}[\boldsymbol{B}^H \boldsymbol{w}_m]) = 0 \tag{A.6}$$

Note that the sum is not present because vectors $\boldsymbol{b}_m$ are all independent from each other. Eq. (A.6) yields:

$$\boldsymbol{b}_m = (\mathrm{Re}[\boldsymbol{B}^H \boldsymbol{B}])^{-1} (\mathrm{Re}[\boldsymbol{B}^H \boldsymbol{A}_m]\boldsymbol{a} - \mathrm{Re}[\boldsymbol{B}^H \boldsymbol{w}_m]) \tag{A.7}$$

Efficient way of taking the inverse of $(\mathrm{Re}[\boldsymbol{B}^H \boldsymbol{B}])^{-1}$ is explained in the original paper. Substituting (A.7) into (A.6) and simplifying it result as:

$$\boldsymbol{R}\boldsymbol{a} = \boldsymbol{r} \tag{A.8}$$

APPENDIX B - Calculation of Normalized Residues

Calculation of the normalized residues in Eq. (2.19) is derived from the definitions of the responses H_k in Eq. (2.5) and Eq. (2.8). Placing two definitions in the same equation yields:

$$H_k = \frac{b_1 z_k + \cdots + b_{2n} z_k^{2n}}{a_0 + a_1 z_k + \cdots + a_{2n-1} z_k^{2n-1} + z_k^{2n}} = \sum_{r=1}^{2n} \bar{A}_r \frac{z_k}{z_k - z_r} \qquad (B.1)$$

By multiplying both sides with $(z_k - z_s)$ where $z_s \neq z_r$ we get:

$$\frac{b_1 z_k + \cdots + b_{2n} z_k^{2n}}{(z_k - z_1) * \ldots * (z_k - z_s) * \ldots * (z_k - z_{2n})} (z_k - z_s) = \sum_{r=1}^{2n} \bar{A}_r \frac{z_k}{z_k - z_r} (z_k - z_s) \qquad (B.2)$$

This can be rewritten as:

$$\frac{b_1 z_k + \cdots + b_{2n} z_k^{2n}}{\prod_{r \neq s} (z_k - z_r)} = \bar{A}_s z_k + \sum_{r \neq s} \bar{A}_r z_k \frac{(z_k - z_s)}{(z_k - z_r)} \qquad (B.3)$$

Calculating in $z_k = z_s$ gives:

$$\bar{A}_s z_s = \frac{b_1 z_k + \cdots + b_{2n} z_k^{2n}}{\prod_{r \neq s} (z_s - z_r)} \qquad (B.4)$$

And thus:

$$\overline{A_s} = \frac{b_1 z_s + \cdots + b_{2n} z_s^{2n}}{z_s * \prod_{r \neq s} (z_s - z_r)} \qquad (B.5)$$

With this formula the normalized residues $\overline{A_s}$ can be easily calculated, remembering that vectors $\boldsymbol{b}_m$ are defined as:

$$\boldsymbol{b}_m = (\mathrm{Re}[\boldsymbol{B}^H \boldsymbol{B}])^{-1} (\mathrm{Re}[\boldsymbol{B}^H \boldsymbol{A}_m] \boldsymbol{a} - \mathrm{Re}[\boldsymbol{B}^H \boldsymbol{w}_m]) \qquad (B.6)$$

APPENDIX C - Main MATLAB Verification Code

```
%Building the numerical FRF with extracted poles and zeros
clear all
close all hidden

dir_exe= 'C:\Users\Batuhan\SIMOMIMO\TEZ\'; % .m files
dir_resu='C:\Users\Batuhan\SIMOMIMO\TEZ\Resu\';% Folder containing results
dir_data='C:\Users\Batuhan\SIMOMIMO\TEZ\Data\';% Folder containing true data
dir_alpha='C:\Users\Batuhan\SIMOMIMO\TEZ\Alpha\';%Folder containing FRF_rec.m FRFs
fmin=2;   % Lower limit of the frequency band to analyse (7 dof case)
fmax=80.0;   % Upper limit of the frequency band to analyse (fmax<Fs/2) (7 dof
case)
resol=8192;        %resolution of True FRF (DO NOT CHANGE)
SIMOinp = 3;            %Dof in which the force is applied
analyzeMO = 10; %Model order to be graphed and MAC
anmorange_from = 10; %model order to be analyzed from
anmorange_to = 30; %model order to analyze to


str=['cd ' dir_resu ';'];
eval(str);
load matmodi
load modi_modello
str=['cd ' dir_exe ';'];
eval(str);

n = size(matmodi, 2);       %model order
temp = size(matmodi ,1);
MAXFRF = (temp/n)-2;        %number of output channels
minvec = zeros(n,1);        %for error calculation later
clear temp

str=['cd ' dir_data ';'];
eval(str);
load check
str=['cd ' dir_exe ';'];
eval(str);

%diagonal elements a & b
a = (conj(teta))'*AA*teta;
a = diag(a);
b = (conj(teta))'*BB*teta;
b = diag(b);

%True numerical FRF
DofTrue = size(fr,1);
omegaTrue = 2*pi*fr;
ff=linspace(fmin,Fs/2,resol);
step=(fmax-Fs/2)/(resol-1);
FRF = zeros(DofTrue, DofTrue, length(ff));
tic
for ii=1:DofTrue
    for j=1:DofTrue
        for fff=1:resol
            %FRF(ii,j,fff) = FRF_NUMinv(M, K, C0, fff, ii, j, ff);
            FRF(ii,j,fff) =FRF_NUM(teta, lam, fff, ii, j, ff, DofTrue, a, b);
        end
```

```
    end
end
toc

%set plotband
delta=abs(ff - fmin);
[xxx inmin] = min(delta);
fmin=ff(inmin);
delta=abs(ff - fmax);
[xxx inmax] = min(delta);
fmax=ff(inmax);
clear xxx
plotband = ff(inmin:inmax);

FRFNUMSUM=zeros(resol,1);
figure
for ii=1:DofTrue
    forplot=zeros(1,resol);
    forplot=squeeze(FRF(ii,SIMOinp,:));
    semilogy(plotband,abs(forplot(inmin:inmax)))
    xlabel('Frequency (Hz)')
    ylabel('ANALYTICAL FRF')
    grid on
    zoom on
    hold on
    FRFNUMSUM = FRFNUMSUM + abs(forplot);
end
figure
semilogy(plotband,abs(FRFNUMSUM(inmin:inmax)))
xlabel('Frequency (Hz)')
ylabel('SUM OF ANALYTICAL FRF')
grid on
zoom on
hold on

%ANALYTICAL VALUES

fana = abs(lam)/(2*pi);
zana = real(lam)./abs(lam);

%Obtaining the results of FRF_rec.m

str=['cd ' dir_alpha ';'];
eval(str);
for k=1:7
    str=['load FRF_' num2str(k) '.mat FRF_' num2str(k) ';'];
    eval(str);
end
load FRFSum.mat FRFSum
FRFSum = DofTrue * FRFSum;

%str=['Experimental FRF'];
%figure('Name', str)
%semilogy(plotband, abs(FRFSum(inmin:inmax))) %Because in FRF_rec.m FRFSum =
TxySum/ndof;
%xlabel('Frequency (Hz)')
%ylabel('SUM OF EXPERIMENTAL FRF')
%grid on
%zoom on
%hold on

str=['cd ' dir_resu ';'];
eval(str);
load matmodi
str=['cd ' dir_exe ';'];
eval(str);
```

```
for k=anmorange_from:anmorange_to  %k=5:n     %cycle on model order
   %initialisation
   resir = zeros(k, MAXFRF);     %residues
   freqr = zeros(k,1);           %frequency
   omegr = zeros(k,1);           %frequency in rad/s
   zetar = zeros(k,1);           %damping ratio
   polir = zeros(k,1);           %poles
   for j=1:k                  %cycle to get values from matmodi
       freqr(j,1) = matmodi((k-1)*(2+MAXFRF)+1,j);
       zetar(j,1) = -matmodi((k-1)*(2+MAXFRF)+2,j);    %- because in matmodi zr
values are negative
       for ii=1:MAXFRF
           resir(j,ii) = matmodi((k-1)*(2+MAXFRF)+(2+ii),j);
           resir(j,ii) = Fs .* resir(j,ii) ./ ((Fs/2)/(fmax-fmin)); %We multiply
residues with sampling freq.
       end
   end
   omegr = 2*pi*freqr;
   for ii=1:k           %Cycle to build poles vector
       polir(ii,1) = (-zetar(ii,1)*omegr(ii,1) + i*omegr(ii,1)*sqrt(1-
zetar(ii,1)^2));
   end
   FRFEXC = zeros(DofTrue, DofTrue, length(ff));    %initialise extracted FRF
matrix
   for ii=1:DofTrue
       for fff=1:resol
           %fff is only the index, ff is the vector  from 0 to Fs/2
           FRFEXC(ii,SIMOinp,fff) = FRF_EXC(resir, polir, ii, fff, k, ff);
%SIMOinp=3, we are only interested in that column
       end
   end
   str = ['Model Order' num2str(k)];
   FRFEXCSUM = zeros(resol,1);
   for ii=1:DofTrue %Cycle to compute som of all FRFs
       forplot=zeros(1,resol);
       forplot=squeeze(FRFEXC(ii,SIMOinp,:));
       FRFEXCSUM = FRFEXCSUM + abs(forplot);
   end
   if k == analyzeMO %manually set to avoid a lot of windows
    figure('Name', str)
    semilogy(plotband,abs(FRFEXCSUM(inmin:inmax))) %I can probably omit abs()
    xlabel('Frequency (Hz)')
    ylabel('SUM OF EXTRACTED FRF')
    grid on
    zoom on
    hold on
   end

%BEST MODEL ORDER IS SELECTED IN LEAST SQUARES SENSE
ERROR = zeros(resol,1);
ERROR = (FRFNUMSUM(inmin:inmax) - FRFEXCSUM(inmin:inmax)).^2;
SUMERROR = sum(ERROR);
str = ['Error of model order ' num2str(k) ' is ' num2str(SUMERROR)];
disp(str);
minvec(k,1) = SUMERROR;


end

minvec = minvec(anmorange_from:anmorange_to);
[minerr, index] = min(minvec);
BMO = index+anmorange_from-1; %Best Model Order
str = ['model of order ' num2str(BMO) ' has the minimum total error, which is '
num2str(minerr)];
disp(str);
```

```
BMO = analyzeMO;  %To manually set model order to examine
%MAC
resir = zeros(DofTrue);
for j=1:DofTrue                  %cycle to get values from matmodi
     for ii=1:MAXFRF
           resir(j,ii) = matmodi((BMO-1)*(2+MAXFRF)+(2+ii),j);
           resir(j,ii) = Fs .* resir(j,ii) ./ ((Fs/2)/(fmax-fmin)); %We multiply
residues with sampling freq.
     end
end

MAC = zeros(DofTrue);
for i=1:DofTrue
    for j=1:DofTrue
        A1 = squeeze(resir(i,:));
        T1 = squeeze(modes(:,j));
        A2 = A1';
        T2 = T1';
        %dot product
        nom = 0;
        for k=1:DofTrue
            temp = A2(k)*T1(k);
            nom = nom+temp;
        end
        nom = abs(nom)^2;
        denom1 = 0;
        for k=1:DofTrue
            temp = A2(k)*A1(k);
            denom1 = denom1+temp;
        end
        denom2 = 0;
        for k=1:DofTrue
            temp = T2(k)*T1(k);
            denom2 = denom2+temp;
        end
        MAC(i,j) = nom / (denom1*denom2);
    end
end
xlswrite('MAC.xls',MAC);
```

APPENDIX D - Auxiliary MATLAB functions

```
function [res] = FRF_NUMinv(M, K, C0, fff, ii, jj, ff)


om = ff(1,fff)*2*pi;
temp= K - (om^2) * M + i*om*C0;
temp=inv(temp);
res=temp(ii,jj);

end
```

```
function [SUM] = FRF_NUM(teta, lam, fff, ii, j, ff, DofTrue, a, b)

SUM = 0;
om = ff(1,fff)*2*pi;
for k=1:2*DofTrue
    den=b(k)+i*om*a(k);
    A = teta(ii,k)*teta(j,k)./den;
    SUM = SUM + A;

end
```

```
function [SUM] = FRF_EXC(resir,polir,ii,fff, n, ff)

SUM = 0;
om = ff(1,fff)*2*pi;
for k=1:n
    if polir(k,1) ~= 0
        temp=resir(k,ii)/((i*om)-polir(k,1));
        tempcon = conj(resir(k,ii))/((i*om)-conj(polir(k,1)));
    else
        temp = 0;
        tempcon =0;
    end
        SUM = SUM + temp + tempcon;
end
end
```

Bibliographic References

[1] Maia, Nuno M.M. and Silva, Julio M.M. (1997), Theoretical and Experimental Modal Analysis, Chapter 1.

[2] Ewins, David J. (1984), Modal Testing.

[3] Fasana, A. (2008), Modal Parameters Estimation in the Z-domain, Mechanical Systems & Signal Processing 23 (2009) 217-225.

[4] Richardson, M.H. and Formenti, D.L. (1982), Parameter Estimation from Frequency Response Measurements Using Rational Fraction Polynomials.

[5] Richardson, M.H. and Formenti, D.L. (2002), Parameter Estimation from Frequency Response Measurements Using Rational Fraction Polynomials (Twenty Years of Progress).

[6] Cauberghe, B., (2004) Applied Frequency-Domain System Identification in the Field of Experimental and Operational Modal Analysis, PhD thesis, Vrije Universiteit Brussels, Brussels.

[7] Shannon, C. (1940), Communication in the Presence of Noise, Proceedings of the I.R.E (January 1949)

[8] Petrillo, L.P., (2021) Analisi Modale Sperimentale. Ricerca Automatica delle Soluzioni. Masters' thesis, Politecnico di Torino, Torino.

[9] Genta, G., (2009) Vibration Dynamics and Control, Chapter 1.6

[10] Duncan, W.J., (1938) Elementary Matrices. Cambridge University Press.

[11] Schwarz, B. and Richardson, M., (2004) Measurements Required for Displaying Operating Deflection Shapes.

[12] Brehm, M. et. al., (2013) Optimal Reference Sensor Positions Using Output-only Vibration Test Data.

[13] Welch, P.D., (1967) The Use of Fast Fourier Transform for the Estimation of Power Spectra: A Method Based on Time Averaging Over Short, Modified Periodograms, IEEE Transactions on Audio and Electroacoustics, Vol AU-15, No. 2, June 1967

[14] Shin, K. and Hammond, J.K., (2008) Fundamentals of Signal Processing for Sound and Vibration Engineers, Wiley, p.293

[15] Allemang, R.J., (2003) The Modal Assurance Criterion: Twenty Years of Use and Abuse. Sound Vib 37:14-23.

[16] Jalali, P. *et al.,* (2019) Noise Effects of Modal Parameters Extraction of Horizontal Airplane by Singular Value Decomposition Method Based on Output Only Modal Analysis, Journal of Solid Mechanics.

[17] Masjedian M.H. and Keshmiri M., A Review on Operational Modal Analysis Researches: Classification of Methods and Applications. Proc of the 3rd IOMAC. 2009.

[18] Asia, M. *et al.,* (2018) Operational Modal Identification in Presence of Harmonic Excitation.